A statistical approach to analyse the efficiency of BNS damping and correction algorithms in linear colliders

Stéphane Fartoukh

January 31, 1997

Abstract

This paper presents a new and general method, capable of analysing, in a purely statistical way, the dipole wakefield effects on a high–energy charged–particle beam in a linac. More precisely, starting from a given set of input beam parameters and a given linac layout (focusing lattice, accelerating gradient, ...), given a probabilistic model describing the transverse misalignments of the beam line components (result of the pre–alignment strategy), and a trajectory correction scheme, it becomes possible to convert these informations into statistical results concerning the transverse behaviour of the beam at the line output (offset, emittance, ...). In a first step, we will report in detail the different features of this new approach. Then, we will review the advantages and inconveniences of the two possible implementations of the BNS damping (RFQs or energy spread) in linacs where the transverse wakefields are strong, and we will pursue the following idea. Given a certain magnitude of the transverse wakefields, can we select a focusing lattice in such a way that the simple use of the natural energy spread generated by beam-loading (longitudinal wakefields) remains sufficient to perform BNS damping? It is what we will call the "self–BNS–damping" condition. Lastly, we will apply the new method to the study of the transverse single–bunch emittance control in the CLIC main linac, and will propose a new linac layout without RFQs.

Contents

List of Figures

List of Tables

Introduction

For the studies carried on the CLIC beam dynamics which led to the LC95 main linac parameters [1], classical tracking programs based on the products of 2×2 or 4×4 transfer matrices, transporting the beam matrix and coordinate vectors of the beam, have been used intensively. The basic program or family of codes, grounded on thin elements and continuous variation of the focusing properties with energy, including wakefields, misalignments and correction schemes is called `MTRACK` [2]. Another code, similar in its principles, but based on thick elements and using improved methods of trajectory correction, is named `CALICO` [3]. They both require several runs with different misalignment realisations in the linac in order to produce statistical results on the beam characteristics and do not make it possible, without modifications, to deal with long–range correlation effects. The method proposed in this report and described in Chapter 1, allows a direct statistical approach. For instance, it gives an estimate of the distribution of the beam emittance, noted $\rho_\epsilon(\epsilon)$, where the quantity $\rho_\epsilon d\epsilon$ represents the probability of obtaining a beam with a final emittance between ϵ and $\epsilon + d\epsilon$. As a consequence, the power of this new approach lies in the fact that it can generate, in one passage once all the response coefficients have been calculated (Paragraph 1.1.3), statistical results concerning the beam parameters at the linac output, and possibly including the long–distance correlation effects.
The new code `CORREC` based on this approach has first been used with the idea to reproduce the results previously obtained for the old lattice [4] with `CALICO` and `MTRACK`, in order to validate the method. Once this was done and since the results obtained in the same conditions were in good agreement with those of the other codes mentioned, the method has been applied to a new linac without microwave quadrupoles, with a reinforced optics and satisfying the so–called "self–BNS–damping" condition. Lack of time did not allow the study of the long–range correlations yet.

Chapter 1

Detailed description of the method

The first principles of the method have already been presented in a previous report [6] (generalised R–matrix in the presence of wakefields and computation of the response coefficients of the line according to unit–displacements and unit–rotations of its components), but, in order to make this chapter as complete as possible, we prefer to recall them hereafter. That will form the first section of the chapter, while, the two other sections will deal with the statistical response of the beam travelling through a linac, the different components of which are misaligned (Section 3 & 4), such a response depending on the choice of the correction algorithm (Section 2).

1.1 Response coefficients to unit–displacements of the line components

1.1.1 Equation of motion

We consider an electron beam travelling along a line containing magnetic quadrupoles, microwave quadrupoles (RFQ) and RF structures. We note s the longitudinal coordinate along the line, and z, the relative position within the bunch, with the centre of the bunch for the origin and $z > 0$ at the bunch tail. We will always suppose that the beam is fully relativistic so that, on the one hand, the longitudinal distribution of particles $\rho(z)$ is completely rigid along the $\hat{s}$ axis ($\int \rho_(z)\, dz = N_b$: number of particles within the bunch), and, on the other hand, the particle energy depends only on s and z.
Now, we can derive the single–bunch equation of motion. For a slice of charge at a relative position z inside the bunch, we note $\delta x(s,z)$ the transverse position (horizontal or vertical) of its centre of gravity; we call $x(s,z) = \delta x(s,z) + \tilde{x}(s,z)$ the position of any particle within the slice, and $\gamma(s,z) m_e c^2$ its energy (thus, $\tilde{x}$ describes the betatron motion in the presence of acceleration). Then, the fundamental dynamics relation, projected on the transverse

and longitudinal planes, gives (see Ref. [8]) [1]:

$$\begin{cases} x''(s,z) + \gamma'(s,z)/\gamma(s,z)\, x'(s,z) + k(s,z)\, x(s,z) = \\ \qquad \dfrac{e^2/m_e c^2}{\gamma(s,z)} \displaystyle\int_{-\infty}^{z} W_T^{\delta}(s, z-z^*)\, \rho(z^*)\, \delta x(z^*)\, dz^* \end{cases} \tag{1.1}$$

$$\gamma'(s,z) = e/m_e c^2 G_{RF}(s,z) \; - e^2/m_e c^2 \int_{-\infty}^{z} \rho(z^*)\, W_L^{\delta}(s, z-z^*) \tag{1.2}$$

Here, $k(s,z)$ ([m^{-2}]) is the quadrupole strength seen by the z slice,

$$k(s,z) = \begin{cases} \dfrac{G_q\, e}{\gamma(s,z) m_e c} \text{ in magnetic quads } (G_q \text{ being the quadrupole gradient in [T/m]}) \\ \dfrac{\alpha_{RFQ} G_q\, e}{\gamma(s,z) m_e c} \sin\Big(\omega_{RF} z/c - \phi_{RFQ}\Big) \text{ in RFQs (by definition, } \alpha_{RFQ} G_q \text{ is the peak} \\ \text{effective magnetic gradient and, } \phi_{RFQ}\text{, the RFQ phase angle)} \\ 0 \text{ in RF structures} \end{cases}$$

and $G_{RF}(s,z)$ ([V/m]) represents the accelerating field all along the line,

$$G_{RF}(s,z) = \begin{cases} 0 \text{ in magnetic quadrupoles} \\ G_{RFQ} \cos\Big(\omega_{RF} z/c - \phi_{RFQ}\Big) \text{ in RFQs } [2] \\ G_{RF} \cos\Big(\omega_{RF} z/c - \phi_{RF}\Big) \text{ in RF structures} \end{cases}$$

Lastly, W_L^{δ} and W_T^{δ} are the longitudinal and transverse delta–function wake potentials, active all along the line (in RF structures as well as in drifts: see Appendix A for more details).
Summing equation (1.1) over all the particles of the considered slice, we deduce the following equations for $\delta x(s,z)$ and $\tilde{x}(s,z)$:

$$\begin{cases} \delta x''(s,z) + \gamma'(s,z)/\gamma(s,z)\, \delta x'(s,z) + k(s,z)\, \delta x(s,z) = \\ \qquad \dfrac{e^2/m_e c^2}{\gamma(s,z)} \displaystyle\int_{-\infty}^{z} W_T^{\delta}(s, z-z^*)\, \rho(z^*)\, \delta x(z^*)\, dz^* \end{cases} \tag{1.3}$$

$$\tilde{x}''(s,z) + \gamma'(s,z)/\gamma(s,z)\, \tilde{x}'(s,z) + k(s,z)\, \tilde{x}(s,z) = 0 \tag{1.4}$$

Eq. (1.3) has no general analytical solution, except in some particular cases that we cannot use here: smooth focusing, uniform charge distribution, transverse wakefield W_T^{δ} varying linearly with z [8], [9]. The numerical treatment of this equation will be explained in the

[1] Compared to Ref. [6], the following equations do not take into account the fact that each mode ω of the wakes possesses a finite group velocity, $v_g(\omega) = \beta_g(\omega) c \neq 0$. Nevertheless, this effect is insignificant for what concerns the single–bunch mode.

[2] Following Ref. [7], we have $G_{RFQ} = c\,\lambda_{RF}/\pi \dfrac{\alpha_{RFQ} G_q}{\eta_{RFQ}}$, where η_{RFQ} ($\simeq 85\%$ for the actual CLIC microwave quadrupoles) is linked to the structure geometry.

next paragraph.
Eq. (1.4) is the the well–known Hill equation and the classical theory of the beam matrix, not reported here, can be applied in order to track the "$\tilde{x}$–envelope" of each slice all along the line[3]. We will simply recall that analytical solutions of equation (1.4) exist in the three following particular cases; they are reported in Appendix B, in term of classical R matrix:

- $k(s) = Cst$, $\gamma' = 0$: "quadrupole case"
- $k(s) = 0$, $\gamma' = Cst$: "RF case"
- $k(s) = Cst$, $\gamma' = Cst$: "RFQ case " embracing the last two cases mentioned.

1.1.2 Generalised R–matrix in the presence of wakefields

We note $X(s,z)$ the two dimensional vector $\Big[\delta x(s,z), \delta x'(s,z)\Big]$. Using Eq. (1.3), we see that $X(s,z)$ verifies the following linear integro–differential equation:

$$X'(s,z) = A_0(s,z)\, X(s,z) \; + \; \int_{-\infty}^{z} A_w(s,z,z^*)\, X(s,z^*)\, dz^* \tag{1.5}$$

$$\text{where } A_0(s,z) = \begin{pmatrix} 0 & 1 \\ -k(s,z) & -\gamma'(s,z)/\gamma(s,z) \end{pmatrix} \text{ and}$$

$$A_w(s,z,z^*) = \frac{e^2/m_e c^2}{\gamma(s,z)} \begin{pmatrix} 0 & 0 \\ W_T^{\delta}(s, z-z^*)\rho(z^*) & 0 \end{pmatrix} \; .$$

The linear equation (1.5) is deterministic and has the following formal solution (it can be identified to a infinite system of linear differential equations):

$$X(s,z) = R_0(s,z)\, X(0,z) + \int_{-\infty}^{z} R_w(s,z,z^*)\, X(0,z^*)\, dz^* \tag{1.6}$$

Finally, using Eq. (1.5), we can write the differential equations verified by the two matrices R_0 and R_w:

$$\begin{aligned} R_0'(s,z) \quad &= \quad A_0(s,z)\, R_0(s,z) \text{ : it is the matricial Hill equation} \\ R_w'(s,z,z^*) \quad &= \quad A_0(s,z)\, R_w(s,z,z^*) + A_w(s,z,z^*)\, R_0(s,z^*) \\ &\qquad + \int_{z^*}^{z} A_w(s,z,z^{**})\, R_w(s,z^{**},z^*) \Big)\, dz^{**} \end{aligned} \tag{1.7}$$

To go further in the computation, we have to discretise equations (1.6) and (1.7) by splitting the bunch into n_s slices of constant thickness $\triangle z$. So, we note $\mathcal{R}$(s) the following

[3]In this model, we see that the motion of $\tilde{x}$ is totally independent of the one of δx, and that it is not perturbed by the wakefield dipole mode; this would not be the case anymore if, for instance, we had taken into account the quadrupole mode of the wakes or the fact that the longitudinal wake seen by a particle may also change according to its transverse position.

$2n_s \times 2n_s$ square matrix:

$$\mathcal{R}(s) = \begin{pmatrix} R_0(s,z_1) & 0 & \dots & 0 \\ \triangle z\, R_w(s,z_2,z_1) & R_0(s,z_2) & \dots & 0 \\ \vdots & \vdots & \ddots & \vdots \\ \triangle z\, R_w(s,z_{n_s},z_1) & \triangle z\, R_w(s,z_{n_s},z_2) & \dots & R_0(s,z_{n_s}) \end{pmatrix}$$

$\mathcal{R}$ is what we call the generalised R matrix in the presence of wakefield. It is a lower triangular 2×2 block matrix because of the causality principle; the diagonal block $R_0(s,z_i)$ is the usual R matrix describing the motion of the slice z_i without any wakefields, whereas the lower block $R_w(s,z_i,z_j)$ describes the interaction between the slices z_i and z_j due to the transverse wake. Using equation (1.7), $\mathcal{R}$ verifies the following matricial differential equation:

$$\begin{cases} \mathcal{R}'(s) = \mathcal{A}(s)\,\mathcal{R}(s) \;\text{ with }\; \mathcal{A}(s) = \begin{pmatrix} A_0(s,z_1) & 0 & \dots & 0 \\ A_w(s,z_2,z_1) & A_0(s,z_2) & \dots & 0 \\ \vdots & \vdots & \ddots & \vdots \\ A_w(s,z_{n_s},z_1) & A_w(s,z_{n_s},z_2) & \dots & A_0(s,z_{n_s}) \end{pmatrix} \\ \mathcal{R}(0) = \mathbf{Id} \end{cases} \tag{1.8}$$

which can be solved numerically by a classical fourth–order Runge–Kutta type method. Certainly more complicated than a classical tracking, this method has nevertheless two great advantages:

- For any initial conditions $\mathcal{X}(0) = \big[\delta x(0,z_1), \delta x'(0,z_1), \dots, \delta x'(0,z_{n_s})\big]$, and any coordinate s along the line, we have: $\mathcal{X}(s) = \mathcal{R}(0\to s)\,\mathcal{X}(0)$; thus, for any abscissas s_1, s_2 and s_3, the matrix $\mathcal{R}(s_1\to s_3)$ is just the matricial multiplication of $\mathcal{R}(s_2\to s_3)$ by $\mathcal{R}(s_1\to s_2)$.

- The second advantage is a very practical computation of the response coefficients to unit–displacements of beam line components (see next paragraph) which are the starting point for the statistical method developed in Section 3.

1.1.3 Computation of the beam line sensitivity

Here, we are interested in the effects of transverse misalignments of the beam line components. If we suppose that the elements are totally rigid objects, their position along the beam line, as well as their orientation according to a reference straight line, can be defined by six parameters (see Fig. 1.1); first, we execute a global translation of the component, then, three rotations, leaving invariant the middle point of the displaced entry face of the component (I'_{in} in Fig. 1.1):

- the horizontal displacement dx.

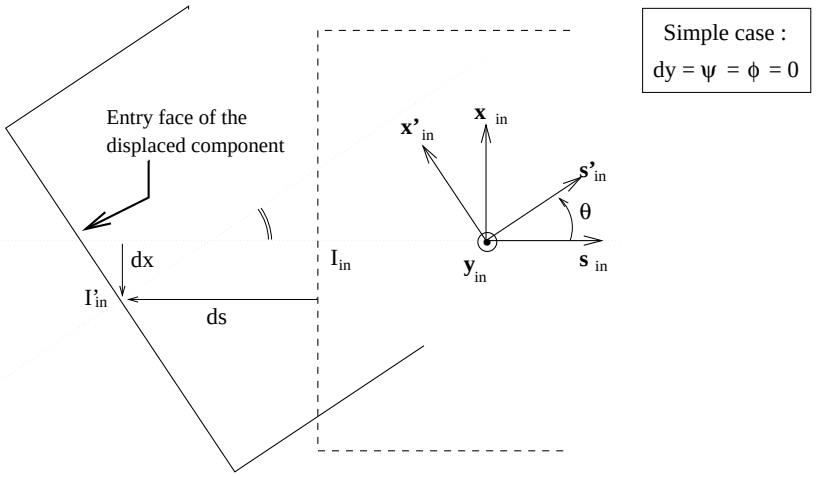

Figure 1.1: A simple scheme to describe the alignment defaults of the beam line components

- the vertical displacement dy.
- the longitudinal displacement ds according to an ideal location along the line.
- the rotation θ around the actual vertical axis, $\hat{y}_{\rm in}$ in Fig. 1.1, or yaw angle.
- the rotation ϕ around the newly defined horizontal axis, $\hat{x}'_{\rm in}$ in Fig. 1.1, or pitch angle.
- the rotation ψ around the newly defined longitudinal axis or roll angle.

For what we are concerned, we forget the "longitudinal alignment errors", ds and ψ, which do not create any transverse offset when the beam travels through the line [4].
Then, we consider a component of length L with the alignment defaults dx and θ, and we suppose that the beam goes into the component (abscissa s_0) with an horizontal offset described by the vector $\mathcal{X}(s_0)$; so, using the formalism developed in the previous paragraph, we can compute the beam offset at the exit of the component (abscissa $s_1 = s_0 + L$) in the following way [5]:

$$\mathcal{X}(s_1) = \mathcal{R}(s_0 \rightarrow s_1)\left(\mathcal{X}(s_1) + \mathcal{X}_{\rm in}(dx,\theta)\right) \; + \; \mathcal{X}_{\rm out}(dx,\theta)$$

where $\mathcal{X}_{\rm in}(dx,\theta) = \Big[-dx, -\theta, \ldots, -dx, -\theta\Big]$ refers to the change of coordinate at the component entry, and $\mathcal{X}_{\rm out}(dx,\theta) = \Big[dx + L\theta, \theta, \ldots, dx + L\theta, \theta\Big]$ refers to the one at the component exit.
Thus, at any abscissa s_f, we can estimate the line sensitivity relative to the misalignments

[4] For what concerns flat beams, the roll angle ψ, coupling both transverse planes, may become critical for the emittance growth in the plane where the beam dimension is the smallest, but, actually, it is not yet implemented in the method.

[5] The argument in the vertical plane is exactly the same, changing (dx, θ) into (dy, ϕ).

of any of its components; for instance, for a yaw angle θ_i of the element number i, we obtain:

$$\partial_{\theta_i}\mathcal{X}(s_f) = \mathcal{R}(s_i + L_i \rightarrow s_f)\Big(\Theta_{\text{out}}(L_i) + \mathcal{R}(s_i \rightarrow s_i + L_i)\,\Theta_{\text{in}}\Big)$$

where $\Theta_{\text{in}} = [0, -1, 0, -1, \ldots, 0, -1]$ and $\Theta_{\text{out}}(L_i) = [L_i, 1, \ldots, L_i, 1]$.
Finally, in the same way, we can obtain all the response coefficients of the line, concerning the initial offset or jitter (angle or position) of the bunch.

1.2 Correction algorithms

1.2.1 Recall about beam–based alignments methods

The most simple alignment methods consist in a correction of the bunch centre–of–charge deviation $< \delta X_{meas} >$ measured at one or several beam position monitors (BPM) within the line, using kickers, option I, or moving transversely the quadrupoles, option II. For what concerns the CLIC main linac, the quadrupole support remains independent of the one of the vacuum chamber (as it is the case for the majority of the other linac designs); thus, option II is applicable and was preferred to option I for evident reasons (no supplementary correctors and weak tolerances on the quadrupoles misalignments during the linac pre–alignment since they are realigned by the correction).
The idea is then the following:

- select a given region at the linac input containing a given number, N_q, of quadrupoles (bin) and a given number, N_{BPM}, of BPMs between each quadrupole.

- minimise the following function Φ, $\Phi = \sum_{i=1}^{N_q} \sum_{j_i=1}^{N_{BPM}} < \delta X_{meas} >_{j_i}^2$
  where $< \delta X_{meas} >_{j_i}$ is the measurement, on the BPM number j_i, of the bunch centre–of–charge deviation after correction:

$$< \delta X_{meas} >_{j_i} = \underbrace{< \delta x >_{j_i}}_{\substack{\text{exact bunch centre–of–charge} \\ \text{deviation before correction}}} + \underbrace{\sum_{i_q=1}^{i} m_{i_q,j_i}\, dx_{i_q}}_{\text{correction}} - \xi_{d,j_i} - \xi_{r,j_i}$$

  where m_{i_q,j_i} is the response coefficient to the displacement of quadrupole i_q at the BPM j_i, and where ξ_{d,j_i} and ξ_{r,i_j} are the misalignment and the resolution of the BPM i_j, respectively.

- repeat the operation for the following bin, starting from the quadrupole $N_q + 1$ or from another quadrupole ahead of it (bin overlapping).

The case $N_q = N_{BPM} = 1$ corresponds to the well–known "one–to–one" correction scheme. When the number of BPMs between two quadrupoles becomes greater than one, it is question of, either the "one–to–few" correction scheme (more BPMs than quadrupoles), or the "few–to–few" correction scheme when $N_q > 1$ (the quality of the correction increasing with N_q and N_{BPM}).
More recently, new methods of correction have been proposed, based on the simultaneous minimisation of trajectory deviations and trajectory differences linked to variable quadrupole settings (Dispersion–free, DF, and Wake–free, WF, correction [10]), or linked to variable bunch charge N_b or bunch length σ_z (Measured-wake, MW, algorithm [11]). Finally, a combination of these two ideas was investigated with success for the study of the single–bunch emittance preservation in the CLIC main linac ("so–called" Dispersion–wake, DW, correction [12]).
Finally, all these correction techniques comes down to the minimisation of the general following function:

$$\begin{aligned}
\Phi \;= \sum_{i=1}^{N_q} \sum_{j_i=1}^{N_{BPM}} \Big\{ \;& w_t \left(< \delta x(N_b;\sigma_z;p_0) >_{j_i} - \xi_{d,j_i} - \xi_{r,j_i} \right)^2 \\
+ \;& w_{d1} \left(< \delta x(N_b;\sigma_z;p_0) >_{j_i} - < \delta x(N'_b;\sigma'_z;p_0+\delta) >_{j_i} - 2\,\xi_{r,j_i} \right)^2 \\
+ \;& w_{d1} \left(< \delta x(N_b;\sigma_z;p_0) >_{j_i} - < \delta x(N'_b;\sigma'_z;p_0-\delta) >_{j_i} - 2\,\xi_{r,j_i} \right)^2 \\
+ \;& w_{d2} \left(< \delta x(N_b;\sigma_z;p_0) >_{j_i} - < \delta x(N'_b;\sigma'_z;p_0\pm\delta) >_{j_i} - 2\,\xi_{r,j_i} \right)^2 \\
+ \;& w_{d2} \left(< \delta x(N_b;\sigma_z;p_0) >_{j_i} - < \delta x(N'_b;\sigma'_z;p_0\mp\delta) >_{j_i} - 2\,\xi_{r,j_i} \right)^2 \Big\}
\end{aligned} \tag{1.9}$$

where

- $< \delta x(N_b;\sigma_z;p_0) >_{j_i}$ represents the deviation of the nominal trajectory (charge N_b and bunch length σ_z) at BPM i_j.

- $< \delta x(N'_b;\sigma'_z;p_0+\delta) >_{j_i}$ (resp. $< \delta x(N'_b;\sigma'_z;p_0-\delta) >_{j_i}$) denotes the offset, at BPM i_j, of a bunch of length, σ'_z, and of charge, N'_b, tracked in a line where the nominal strengths of the quadrupoles has been divided by the factor $1+\delta$ (resp. $1-\delta$).

- the quantity $< \delta x(N'_b;\sigma'_z;p_0\pm\delta) >_{j_i}$ (resp. $< \delta x(N'_b;\sigma'_z;p_0\mp\delta) >_{j_i}$) has the same definition as the previous one, except that, the focusing quadrupole strengths are divided by a factor $1+\delta$ (resp. $1-\delta$), and the defocusing quadrupole strengths, by a factor $1-\delta$ (resp. $1+\delta$)[6].

[6] We have to be aware that such a re-matching of the machine, when tracking the non–nominal trajectories, requires, on the one hand, the division of the quadrupole gradient by the factor $1 \pm \delta$; but, on the other hand, it requires also a rescaling of these gradients which takes into accounts the following fact: two bunches of different length or of different charge do not lose the same amount of energy in the structures by beam-loading, and then, have not the same energy all along the line. Consequently, the resetting of the focusing has to be, $G_q = G_{q,0}/(1 \pm \delta)\, E(N'_b;\sigma'_z;s_q)/E_0(s_q)$, where $G_{q,0}$ indicates the nominal quadrupole gradient, and where $E_0(s_q)$ (resp. $E(N'_b;\sigma'_z;s_q)$) represents the mean energy of the nominal (resp. non–nominal) trajectory at the location s_q of the considered quadrupole.

When the weights w_{d1} and w_{d2} are set to zero, we retrieve the "one–to–one", "one–to–few", or "few–to–few" correction schemes; the case $N_b' = N_b$, $\sigma_z' = \sigma_z$ and $\delta \neq 0$ defines the DF algorithm when $w_{d2} = 0$, and the WF algorithm when $w_{d1} = 0$. The case $\delta = 0$, with different bunch length or different bunch charge refers to the so–called MW algorithm. Lastly, when $w_{d2} = 0$, the general case is called DW algorithm (combination of DF and MW), and WW algorithm when $w_{d1} = 0$ (combination of WF and MW).

1.2.2 Redefinition of the quadrupole displacements after correction

Since the theory is linear[7], and since the dependence of the function Φ in Eq. (1.9) is quadratic according to the average offsets of the different trajectories, and according to the BPM misalignments and to their resolution of the BPMs, we can rewrite Eq. (1.9) in the formal following manner:

$$\begin{aligned} \Phi \;=\; & {}^{\mathrm{T}}dX_{q,n}\, A_n\, dX_{q,n} \;+\; {}^{\mathrm{T}}dX_{q,n} \Big\{ \sum_{i=1}^{n-1} B_{n,i}\, (dX_{q,i} + \Xi_{\,q,i}) \\ & +\; C_n\, \Xi_{\,d,n} + \widetilde{C_n}\, \Xi_{\,r,n} \;+\; D_n\, dX_{c,n} + E_n \delta X_0 + \mathbf{Cst} \Big\} \end{aligned} \tag{1.10}$$

where

- n indicates the number of the considered quadrupole bin; N_q is the number of quadrupoles per bin; $(dX_{q,i}\,, 1 \leq i \leq n)$ (resp. $(\Xi_{q,i}\,, 1 \leq i \leq n)$), is a N_q–dimensional stochastic vector containing the transverse displacements, after a "perfect correction", of the N_q quadrupoles belonging to the bin number i (resp. the residual misalignments of these quadrupoles after having achieved the correction for the bin number i, i.e the resolution of the correction).

- A_n is a symmetric positive–definite $N_q \star N_q$ square matrix (positive–definite because the quadratic polynomial Φ is positive).

- $(B_{n,i}, 1 \leq i \leq n)$ are $N_q \star N_q$ square matrices.

- $\Xi_{\,d,n}$ (resp. $\Xi_{\,r,n}$) is a stochastic vector of dimension $N_{BPM}^{tot} = N_q\, N_{BPM}$, which is the total number of BPMs in the bin number n, containing the displacement errors (resp. the resolution) of each of these BPMs; C_n and $\widetilde{C_n}$ are two $N_q \star N_{BPM}^{tot}$ rectangular matrices.

- $dX_{c,n}$ is a stochastic vector containing the misalignments and angles of the $N_{c,n}$ cavities, located between the beginning of the line and the end of the bin number n, and D_n is a $N_q \star 2N_{c,n}$ rectangular matrix.

[7] $\delta x(\ldots)$ in Eq. (1.9) depends linearly on the transverse displacements of the beam line components via the response coefficients.

- δX_0 is a vector referring to the N_0 initial conditions (offset and angle) of each of the considered trajectories, while E_n is a $N_q \star N_0$ rectangular matrix.
- Finally **Cst** is a scalar independent of $dX_{q,n}$.

All these matrices are computed with the help of the response coefficients defined in the previous section; they depend obviously on the choice of the parameters w_t, w_{d1}, w_{d2}, δ, ... (see Eq. (1.9)), and then, on the choice of the correction algorithm.
Now, the minimisation condition leads to:

$$\begin{aligned} dX_{q,n} = \; & \Xi_{q,n} - \frac{1}{2} A_n^{-1} \Big\{ \sum_{i=1}^{n-1} B_{n,i} \, (dX_{q,i} + \Xi_{q,i}) \\ & + C_n \, \Xi_{\,d,n} + \widetilde{C_n} \, \Xi_{\,r,n} + D_n \, dX_{c,n} + E_n \delta X_0 \Big\} \end{aligned} \tag{1.11}$$

which redefines by recursion the displacement of the quadrupoles all along the line.
Consequently, since this relation is linear, we easily see that for any correction scheme, provided that Φ remains quadratic, the quadrupole displacements, after correction, become linear combinations of the structure and BPM misalignments, of the BPM resolution, of the resolution of the correction, and lastly, of the initial conditions of the different trajectories considered in the algorithm. Then, we transcribe this result in the following formal way:

$$dX_q^{tot} = M_q \, dX_{err} \tag{1.12}$$

where dX_q^{tot} is a vector containing the transverse displacement of all the N_q^{tot} quadrupoles within the line, where dX_{err} is a generic vector of N_{err} dimensions pointing out all the "error sources" present in the line, and where M_q is a $N_q^{tot} \star N_{err}$ rectangular matrix depending on the focusing lattice (via the response coefficients) and on the choice of the correction algorithm (via the definition of Φ in Eq. (1.9)).
Finally, by reconsidering the formalism developed in Paragraph 1.1.2, the vector $\mathcal{X}(s_f)$ (containing the positions and angles of the n_s slices at the line output) becomes also linearly dependent of the vector dX_{err}, and do not depends anymore directly on the transverse displacements of the quadrupoles required by the correction (vector dX_q^{tot} in the previous equation), what we write in the following manner:

$$\mathcal{X}(s_f) \stackrel{def}{=} M_{err} \, dX_{err} \tag{1.13}$$

where M_{err} is a $2n_s \star N_{err}$ rectangular matrix.

1.3 Statistical response of the line

1.3.1 Statistic distribution of the "error sources" in the linac

Here, we will only consider static misalignments of the structures, resulting from the linac pre–alignment scheme; then, we suppose that the characteristic time required to apply

the correction remains very small compared to the characteristic period of the machine vibrations (ground motion).
For all the rest of the paper, the notation $< \mathcal{Q} >_{err}$ will represent the average of the quantity $\mathcal{Q}$ over the statistic distribution of the "errors", compared to the same notation, without suffix, previously used and referring to an average over the longitudinal charge distribution $\rho(z)$. So, we suppose that the vector, $\mathbf{m_{err}} \equiv < dX_{err} >_{err}$, and the covariance matrix, $\Gamma_{err} \equiv < dX_{err}\ {}^{\mathrm{T}}dX_{err} >_{err} - \mathbf{m_{err}}\ {}^{\mathrm{T}}\mathbf{m_{err}}$, are known quantities which depends on the pre–alignment scheme. For instance, the most simple case, referring to a linac with uncorrelated and random misalignments of the structures around a straight line, corresponds to $\mathbf{m_{err}} = 0$ and Γ_{err} diagonal (with, on the diagonal, the RMS value of the structure and BPM misalignments, the BPM resolution, the resolution of the correction and the initial conditions of the different trajectories involved in the correction, i.e. offset, angle, jitters ...).

1.3.2 Statistical estimation of the corrector displacements; illustration by the "one to one" correction scheme

Using the previous notations, and the formal equation (1.12) which links together the vectors dX_q^{tot} and dX_{err}, we can then produce the first statistic results which concerns the transverse displacements of the quadrupoles after correction. More precisely, we have access to the average and to the covariance matrix of these displacements:

$$\begin{aligned} &< dX_q^{tot} >_{err} = M_q\, \mathbf{m_{err}} \\ &< dX_q^{tot}\ {}^{\mathrm{T}}dX_q^{tot} >_{err} - < dX_q^{tot} >_{err} < {}^{\mathrm{T}}dX_q^{tot} >_{err} = M_q\, \Gamma_{err}\ {}^{\mathrm{T}}M_q \end{aligned} \tag{1.14}$$

In order to illustrate this kind of consideration, we pose the problem of a "one–to–one" correction scheme in a pure FODO lattice which is, as we will see, entirely analytically solvable. Then, we consider a succession of pure FODO cells of length $2L$, containing thin quadrupoles of focal length $f = 1/2g$, in such a way that the phase advance per cell is given by $\sin(\mu/2) = gL$. We suppose that, just behind each quadrupole is placed one BPM with the same number as the one of the considered quadrupole (see Fig. 1.2). We note dx_n, the transverse displacement of the quadrupole n, and ξ_n, the alignment default of the BPM number n. Lastly, at the input of the quadrupole n, (x_n, x'_n) represent the transverse position and the angle of the tracked particles. Since we deal with the "one–to–one" method, we have $x_n = \xi_n$, and since the quadrupoles are treated, for this example, in thin lens approximation, we have $x'_n = (x_n - x_{n-1})/L = (\xi_n - \xi_{n-1})/L$.
Now, we write $x_{n+1} = dx_n + R_{1,1}\Big(x_n - dx_n\Big) + R_{1,2}x'_n$, where $R_{1,1}$ and $R_{1,2}$ are the coefficients (1,1) and (1,2) of the usual transfer matrix between the input of quadrupole n and the input of quadrupole $n+1$, given by $R_{1,1} = 1 \mp 2gL$, according as the quadrupole n is focusing or defocusing, and $R_{1,2} = L$.
Finally, using all that has been said so far, we obtain the relation between dx_n, i.e the quadrupole displacements required by the "one–to–one correction", and the BPM mis-

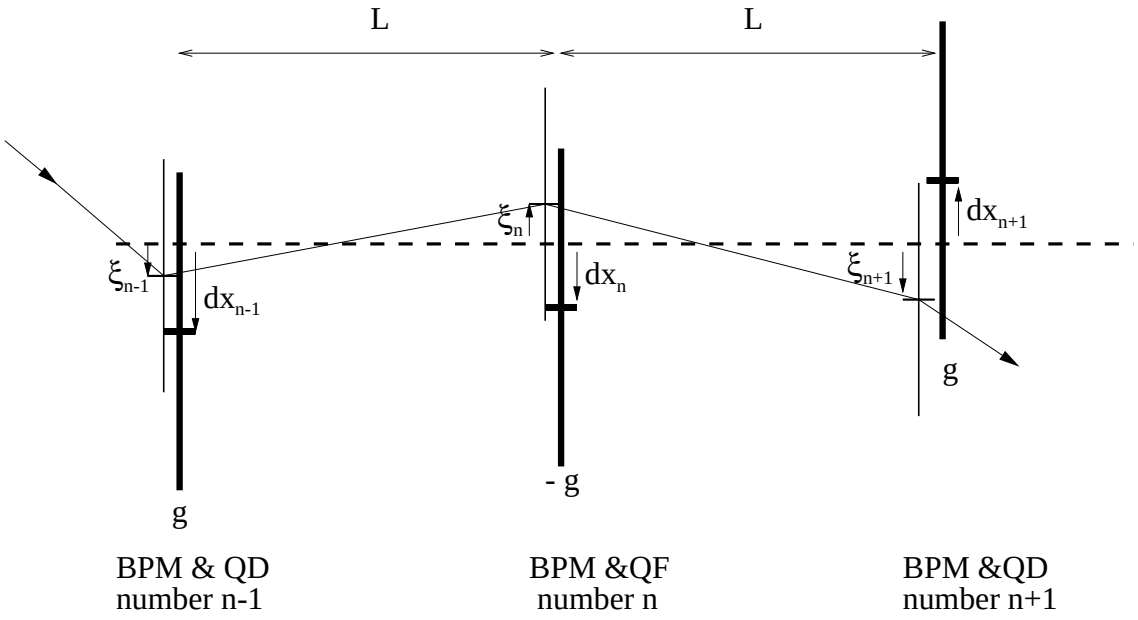

Figure 1.2: One–to–one correction scheme by moving quadrupoles

alignments (ξ_n), i.e. the so–called "error sources all along the line":

$$dx_n = \mp\frac{1}{2gL}\left(2\left(1 \mp gL\right)\xi_n - \xi_{n-1} - \xi_{n+1}\right)$$

which defines the matrix M_q of Eq. (1.12). Lastly, if we suppose that the BPM misalignments are uncorrelated and identically distributed (same statistic distribution), with an RMS value noted σ_p, we can then, for instance, compute the RMS value of the quadrupole displacements after correction:

$$\sigma_{dx_n} = \sigma_p \frac{\sqrt{1 + 2\left(1 \mp \sin(\mu/2)\right)^2}}{\sqrt{2}\sin(\mu/2)} \tag{1.15}$$

which is the coefficient (n, n) of the matrix $< dX_q^{tot\ \mathrm{T}} dX_q^{tot} >_{err}$ previously defined[8] (more precisely the square root of this coefficient).
In view of this simple result, we would like to make the two following remarks before closing the paragraph.

- Firstly, we note that the statistical behaviour, concerning the transverse position of the quadrupoles after correction, is different, according as the considered quad is focusing or defocusing (in Eq. (1.15), the minus sign refers to focusing quads and vice versa). This is a general result observed by simulation for any type of correction scheme (but for random and uncorrelated errors). In a more precise way, as it will be shown in the four examples of Chapter 3, each of these two statistical behaviours

[8]Here we have assumed $\mathbf{m_{err}} = 0$, so that $< dX_q^{tot} >_{err} = 0$.

divides one more time into three new branches, less distinct, which corresponds logically to the three different quadrupole settings involved in the WW correction (i.e. p_0, $p_0 \pm \delta$ and $p_0 \mp \delta$ in Eq. (1.9)).

- A second important point, which appears clearly here and in the equations (1.12) and (1.13), is that the absolute transverse position of the quadrupoles after correction, as well as the particle trajectory, do not depend anymore at all on the initial quad misalignments, but only on the other errors in the line and, of course, on the choice of the correction algorithm. Consequently, the tolerances concerning the quadrupole misalignments before correction become large ($\sim 50\mu$m for CLIC [1]) compared to the ones referring for instance to the structure misalignments ($\sim 10\mu$m for CLIC [1]), the only constraint being that the beam remains inside the beam pipe physical aperture during the stage of the machine pre–alignment; of course, this would not be the case anymore if, for instance, we had decided to choose the "steering option" in order to perform the correction (option I in Paragraph 1.2.1).

1.3.3 A generalised version of the beam matrix

By using Eq. (1.13), and in the same way as for the vector dX_q^{tot}, we can define the average and the covariance matrix of the vector $\mathcal{X}(s_f)$ at a certain location s_f in the line, say, at the line output:

$$\begin{array}{rcl} \widetilde{\mathbf{m}} \stackrel{def}{=} < \mathcal{X}(s_f) >_{err} & = & M_{err}\,\mathbf{m_{err}} \\ \widetilde{\Gamma} \stackrel{def}{=} < \mathcal{X}(s_f)\,{}^{\mathrm{T}}\mathcal{X}(s_f) >_{err} - \widetilde{\mathbf{m}}\,{}^{\mathrm{T}}\widetilde{\mathbf{m}} & = & M_{err}\,\Gamma_{err}\,{}^{\mathrm{T}}M_{err} \end{array} \tag{1.16}$$

For reasons which will appear in the next section, we prefer to define the two following objects:

$$\mathbf{m} = \begin{pmatrix} \sqrt{\triangle z\,\rho(z_1)}\left\langle \delta x(z_1) - < \delta x > \right\rangle_{err} \\ \sqrt{\triangle z\,\rho(z_1)}\left\langle \delta x'(z_1) - < \delta x' > \right\rangle_{err} \\ \vdots \\ \sqrt{\triangle z\,\rho(z_{n_s})}\left\langle \delta x(z_{n_s}) - < \delta x > \right\rangle_{err} \\ \sqrt{\triangle z\,\rho(z_{n_s})}\left\langle \delta x'(z_{n_s}) - < \delta x' > \right\rangle_{err} \end{pmatrix} \text{ where}^{9} \begin{cases} < \delta x > = \sum_{n=1}^{n_s} \triangle z\,\rho(z_n)\delta x(z_n) \\ < \delta x' > = \sum_{n=1}^{ns} \triangle z\,\rho(z_n)\delta x'(z_n) \end{cases} \tag{1.17}$$

and $\Gamma_{\substack{1 \le i \le 2n_s \\ 1 \le j \le 2n_s}}$, the symmetric matrix defined by

[9] For the rest of the paper, we will omit s_f in the notations.

$$\begin{cases} \Gamma_{2i-1,2j-1} = \triangle z\sqrt{\rho(z_i)\rho(z_j)}\Big\langle(\delta x(z_i) - <\delta x>)(\delta x(z_j) - <\delta x>)\Big\rangle_{err} \\ \qquad\qquad -\mathbf{m}_{2i-1}\mathbf{m}_{2j-1}\ ,\ 1 \leq i \leq n_s\ ,\ 1 \leq j \leq n_s \\ \Gamma_{2i,2j} = \quad \triangle z\sqrt{\rho(z_i)\rho(z_j)}\Big\langle(\delta x'(z_i) - <\delta x'>)(\delta x'(z_j) - <\delta x'>)\Big\rangle_{err} \\ \qquad\qquad -\mathbf{m}_{2i}\mathbf{m}_{2j}\ ,\ 1 \leq i \leq n_s\ ,\ 1 \leq j \leq n_s \\ \Gamma_{2i-1,2j} = \quad \triangle z\sqrt{\rho(z_i)\rho(z_j)}\Big\langle(\delta x(z_i) - <\delta x>)(\delta x'(z_j) - <\delta x'>)\Big\rangle_{err} \\ \qquad\qquad -\mathbf{m}_{2i-1}\mathbf{m}_{2j}\ ,\ 1 \leq i \leq n_s\ ,\ 1 \leq j \leq n_s \end{cases} \tag{1.18}$$

The coefficients of the vector $\mathbf{m}$, as well as the ones of the matrix Γ can then be easily computed from $\widetilde{\mathbf{m}}$ and $\widetilde{\Gamma}$ defined in Eq. (1.16), and from the longitudinal distribution $\rho(z)$. The symmetric matrix Γ is what we will call the generalised beam matrix, which refers to a statistic over the error sources within the line, compared to the usual 2×2 beam matrix with refers to a statistic related to the beam itself.

1.4 Statistical beam response in terms of emittance growth

1.4.1 The emittance as a function of the coordinates of the slice positions

We note $\mathcal{S}$ the usual beam matrix of the whole bunch at the line output, i.e:

$$\mathcal{S} = \begin{pmatrix} < x^2 > & < xx' > \\ < xx' > & < x'^2 > \end{pmatrix}$$

where the used notations are explained hereafter.

- $< x^2 >$ is the RMS value of the transverse beam extension at the line output. Since the betatron motion is not affected by the dipole wakefields (no correlation between $\tilde{x}(z)$ and $\delta x(z)$: see Paragraph 1.1.1), we have:

$$< x^2 > = \int dz\, \rho(z)[(\sigma_x^2(z) + (\delta x(z) - <\delta x>)^2]$$

  where $\sigma_x(z)$ represents the transverse size (RMS value) of the z–slice at the line output.

- In a same way, and with evident notations, we have:

$$< x'^2 > = \int dz\, \rho(z)[\sigma_{x'}^2(z) + (\delta x'(z) - <\delta x'>)^2]$$

$$< xx' > = \int dz\, \rho(z)[\sigma_{xx'}(z) + (\delta x(z) - <\delta x>)\,(\delta x'(z) - <\delta x'>)]$$

Thus, by coming back to the formalism developed in Paragraph 1.1.2, we can write:

$$\mathcal{S} = \sum_{n=1}^{n_s} \rho(z_n) \triangle z \left[\Sigma_{out}(z_n) + \begin{pmatrix} (\delta x(z_n) - <\delta x>)^2 & (\delta x(z_n) - <\delta x>)(\delta x'(z_n) - <\delta x'>) \\ (\delta x(z_n) - <\delta x>)(\delta x'(z_n) - <\delta x'>) & (\delta x'(z_n) - <\delta x'>)^2 \end{pmatrix} \right]$$

where $\Sigma_{out}(z_n)$ represents the usual beam matrix of the slice z_n at the line output. If now, we note $\Sigma_{in}(z_n)$ the beam matrix of the slice z_n at the line input, $\Sigma_{out}(z_n)$ can be computed by the usual formula:

$$\Sigma_{out}(z_n) = \mathcal{R}_{n,n}\, \Sigma_{in}(z_n)\, {}^{\mathrm{T}}\mathcal{R}_{n,n}$$

where $\mathcal{R}_{n,n}$ is the diagonal block (n,n) of the generalised R–matrix (from the beginning to the end of the line), which is also the classical 2×2 transfer matrix describing the motion of the slice z_n without any wakefields (see Paragraph 1.1.2).
Thus, we can write the matrix $\mathcal{S}$ in the following manner:

$$\mathcal{S} = \Sigma_0 + \begin{pmatrix} \sum_{n=1}^{n_s} X_{2n-1}^2 & \sum_{n=1}^{n_s} X_{2n-1} X_{2n} \\ \sum_{n=1}^{n_s} X_{2n-1} X_{2n} & \sum_{n=1}^{n_s} X_{2n}^2 \end{pmatrix} \tag{1.19}$$

where, with the previous notations,

$$\Sigma_0 \stackrel{def}{=} \sum_{n=1}^{n_s} \rho(z_n) \triangle z\, \mathcal{R}_{n,n}\, \Sigma_{in}(z_n)\, {}^{\mathrm{T}}\mathcal{R}_{n,n} \tag{1.20}$$

describes the usual beam matrix of the whole bunch without any errors within the line[10], and where X is the $2n_s$–dimensional vector defined by:

$$\begin{cases} X_{2n-1} &= \sqrt{\triangle z \rho(z_n)} \Big(\delta x(z_n) - <\delta x> \Big), \quad 1 \le n \le n_s \\ X_{2n} &= \sqrt{\triangle z \rho(z_n)} \Big(\delta x'(z_n) - <\delta x'> \Big), \quad 1 \le n \le n_s \end{cases} \tag{1.21}$$

Thus, the average, $<X>_{err}$, and the covariance matrix, $<X\, {}^{\mathrm{T}}X>_{err} - <X>_{err} <{}^{\mathrm{T}}X>_{err}$, are exactly the vector $\mathbf{m}$ and the symmetric matrix Γ defined in the previous paragraph by Eq. (1.17) and Eq. (1.18).
Finally, the RMS emittance is defined in the usual manner:

$$\epsilon\Big(X\Big) \stackrel{def}{=} \sqrt{\det\Big(\mathcal{S}\Big)} =$$

$$\sqrt{\det\Big(\Sigma_0\Big) + \Sigma_{0_{2,2}} \sum_{i=1}^{n_s} X_{2i-1}^2 + \Sigma_{0_{1,1}} \sum_{i=1}^{n_s} X_{2i}^2 - 2\Sigma_{0_{1,2}} \sum_{i=1}^{n_s} X_{2i-1} X_{2i} + \sum_{i=1}^{n_s} X_{2i-1}^2 \sum_{i=1}^{n_s} X_{2i}^2 - \left(\sum_{i=1}^{n_s} X_{2i-1} X_{2i} \right)^2} \tag{1.22}$$

[10]Note that the quantity, $<\gamma> (\det(\Sigma_0))^{1/2}$, obtained at the line output, is not equal to the normalised emittance of the bunch at the line input, due to the so–called "butterfly effect" (because of RFQs in the line or/and because of the intra–bunch energy spread). Nevertheless, we will see in Example 4 of Chapter 3 that this effect remains small in the CLIC main linac compared to the one generated by the wakefields.

Consequently, we consider here the final single–bunch emittance, as a function of the slice positions at the line output (vector X). Thus, since we have gathered some information referring to the statistic of the vector X (via the vector $\mathbf{m}$ and the matrix Γ), we are now able to convert these data into statistical results concerning the emittance. That will form the subject of the last two paragraphs of this chapter.

1.4.2 Exact computation of the first and second moments of the emittance distribution

In order to go further in the computations, we are forced to make the following assumption: we assume the vector X_{err} to be Gaussian, so that the vector X becomes also Gaussian[11]. Hence, the knowledge of $\mathbf{m}$ and Γ is sufficient to describe completely the statistical distribution, ρ_X, related to the vector X:

$$\rho_X\Big(X\Big) = \frac{1}{(2\pi)^{n_s}\sqrt{\det(\Gamma)}}\exp\Big(-\frac{1}{2}{}^{\mathrm{T}}(X-\mathbf{m})\,\Gamma^{-1}\,(X-\mathbf{m})\Big) \tag{1.23}$$

We are interested here in the computation of the first and second moment of the emittance distribution, i.e:

$$\begin{aligned} <\epsilon>_{err} &= \int_{\mathbf{R}^{2n_s}} \epsilon(X)\,\rho_X(X)\,d^{2n_s}X \\ <\epsilon^2>_{err} &= \int_{\mathbf{R}^{2n_s}} \epsilon^2(X)\,\rho_X(X)\,d^{2n_s}X \end{aligned} \tag{1.24}$$

where the function $\epsilon(X)$ is given by Eq. (1.22).
The second moment is easy to compute, since the function $\epsilon^2(X)$ is a polynomial in X of degree 4. Indeed, for a Gaussian vector X of average $\mathbf{m}$ and of covariance matrix Γ, the following moments are given by:

$$\begin{aligned} <X_iX_j> &= \Gamma_{i,j} + \mathbf{m}_i\mathbf{m}_j \\ <X_iX_jX_kX_l> &= \Big(\Gamma_{i,j}+\mathbf{m}_i\mathbf{m}_j\Big)\Big(\Gamma_{k,l}+\mathbf{m}_k\mathbf{m}_l\Big) + \Big(\Gamma_{i,k}+\mathbf{m}_i\mathbf{m}_k\Big)\Big(\Gamma_{j,l}+\mathbf{m}_j\mathbf{m}_l\Big) \\ &+ \Big(\Gamma_{i,l}+\mathbf{m}_i\mathbf{m}_l\Big)\Big(\Gamma_{j,k}+\mathbf{m}_j\mathbf{m}_k\Big) - 2\mathbf{m}_i\mathbf{m}_j\mathbf{m}_k\mathbf{m}_l \end{aligned} \tag{1.25}$$

The situation is quite more complicated for what concerns the computation the first moment. A direct estimation, by numerical integration, of the $2n_s$–dimensional integral which defines $<\epsilon>_{err}$, is of course out of question (the computation time growing exponentially with $2n_s$). In fact, we are able to reduce this integral to a 2–dimensional integral (independently of n_s) and, under these conditions, we can compute it numerically.

- Firstly, we rewrite Eq. (1.22) in the following manner:

$$\epsilon(X) = \sqrt{\det\Big(\mathcal{S}\Big)} = \frac{\det\Big(\mathcal{S}\Big)}{\sqrt{\det\Big(\mathcal{S}\Big)}} = \det\Big(\mathcal{S}\Big)\frac{1}{2\pi}\int_{\mathbf{R}^2} d^2\mathbf{u}\,\exp(-\frac{1}{2}{}^{\mathrm{T}}\mathbf{u}\mathcal{S}\,\mathbf{u})$$

[11] X depends linearly on the vector $\mathcal{X}$, Eq. (1.21), which depends linearly on the vector X_{err}, Eq. (1.13).

- Then, using Eq. (1.19), we note that the quantity ${}^{\mathrm{T}}\mathbf{u}\mathcal{S}\,\mathbf{u}$ is given by:

$${}^{\mathrm{T}}\mathbf{u}\mathcal{S}\,\mathbf{u} = {}^{\mathrm{T}}\mathbf{u}\Sigma_0\mathbf{u} + {}^{\mathrm{T}}X\Gamma^*(\mathbf{u})X \text{ where } \Gamma^*(\mathbf{u}) = \begin{pmatrix} \begin{pmatrix} u_1^2 & u_1u_2 \\ u_1u_2 & u_2^2 \end{pmatrix} & 0 & \dots & 0 \\ 0 & \begin{pmatrix} u_1^2 & u_1u_2 \\ u_1u_2 & u_2^2 \end{pmatrix} & \dots & 0 \\ \vdots & \vdots & \ddots & \vdots \\ 0 & 0 & \dots & \begin{pmatrix} u_1^2 & u_1u_2 \\ u_1u_2 & u_2^2 \end{pmatrix} \end{pmatrix}$$

- Lastly, we write:

$$\begin{aligned} &{}^{\mathrm{T}}(X-\mathbf{m})\,\Gamma^{-1}\,(X-\mathbf{m}) + {}^{\mathrm{T}}X\Gamma^*(\mathbf{u})X = \\ &\quad {}^{\mathrm{T}}\mathbf{m}\Gamma^{-1}\mathbf{m} - {}^{\mathrm{T}}\mathbf{m}(\mathbf{u})\Gamma^{-1}(\mathbf{u})\mathbf{m}(\mathbf{u}) + {}^{\mathrm{T}}\Big(X-\mathbf{m}(\mathbf{u})\Big)\Gamma^{-1}(\mathbf{u})\Big(X-\mathbf{m}(\mathbf{u})\Big) \end{aligned}$$

$$\text{where} \begin{cases} \mathbf{m}(\mathbf{u}) & \stackrel{def}{=} & \Big(\mathbf{1} + \Gamma\,\Gamma^*(\mathbf{u})\Big)^{-1}\mathbf{m} \\ \Gamma(\mathbf{u}) & \stackrel{def}{=} & \Big(\Gamma^{-1} + \Gamma^*(\mathbf{u})\Big)^{-1} = \Big(\mathbf{1} + \Gamma\,\Gamma^*(\mathbf{u})\Big)^{-1}\Gamma \end{cases}$$

- Finally, the integration over X can be achieved analytically, and it remains to compute numerically the 2–dimensional integration over $\mathbf{u}$:

$$<\epsilon>_{err} = \frac{\exp(-\frac{1}{2}{}^{\mathrm{T}}\mathbf{m}\Gamma^{-1}\mathbf{m})}{2\pi}\int_{\mathbf{R}^2}\frac{\exp(-\frac{1}{2}{}^{\mathrm{T}}\mathbf{u}\Sigma_0\mathbf{u})\,\exp\Big(\frac{1}{2}{}^{\mathrm{T}}\mathbf{m}(\mathbf{u})\,\Gamma^{-1}(\mathbf{u})\,\mathbf{m}(\mathbf{u})\Big)}{\sqrt{\det\left(\mathbf{1}+\Gamma\,\Gamma^*(\mathbf{u})\right)}}\;<\epsilon^2>(\mathbf{u})\,d^2\mathbf{u}$$

  where $<\epsilon^2>(\mathbf{u})$ is the average of the function $\epsilon^2(X)$ over the $2n_s$–dimensional Gaussian distribution of average $\mathbf{m}(\mathbf{u})$ and of covariance matrix $\Gamma(\mathbf{u})$, i.e.:

$$<\epsilon^2>(\mathbf{u}) \stackrel{def}{=} \frac{1}{(2\pi)^{n_s}\sqrt{\det\Big(\Gamma(\mathbf{u})\Big)}}\int_{\mathbf{R}^{2n_s}} d^{2n_s}X\,\epsilon^2(X)\,\exp\Big(-\frac{1}{2}{}^{\mathrm{T}}(X-\mathbf{m}(\mathbf{u}))\Gamma^{-1}(\mathbf{u})(X-\mathbf{m}(\mathbf{u}))\Big)$$

  which can be easily computed by using the formulae given in Eq. (1.25).

1.4.3 Derivation of the emittance distribution in a perturbation regime

Unfortunately, it was not found any solution permitting to estimate, in the most general case, the emittance distribution, ρ_ϵ. As shown hereafter, some approximations are needed in order to perform this computation. If we note $N(\epsilon)$, the percentage of machines which give, at the line output, a single–bunch emittance lower than ϵ, we have:

$$N(\epsilon) = \int_{\epsilon(X)\le\epsilon}\rho_X(X)\,d^{2n_s}X = \int_{\mathbf{R}^{2n_s}}\Theta\Big((\epsilon-\epsilon(X)\Big)\rho_X(X)\,d^{2n_s}X$$

where the function $\epsilon(X)$ and the density $\rho_X(X)$ are defined by Eq. (1.22) and Eq. (1.23), respectively, and where Θ represents the Heaviside step function. Now, we write the definition of the density ρ_ϵ:

$$\rho_\epsilon(\epsilon) \stackrel{def}{=} \frac{dN}{d\epsilon}(\epsilon) = \int_{\mathbf{R}^{2n_s}} \delta\Big(\epsilon - \epsilon(X)\Big)\rho_X(X)\, d^{2n_s}X = \frac{1}{2\pi}\int_{-\infty}^{\infty} dk\, e^{ik\epsilon}\left[\int_{\mathbf{R}^{2n_s}} d^{2n_s}X\, e^{-ik\epsilon(X)}\rho_X(X)\right] \tag{1.26}$$

where δ is the Dirac's distribution.
Then, in order to go further in the computations, we have to approximate the function $\epsilon(X)$ (Eq. (1.22)) by its development at the second order in the coefficients of the vector X. In other words, we assume to have reached a perturbation regime, for which the non–constant part of the function $\epsilon(X)$ becomes small, when averaging over the distribution of the beam line errors, in such a way that the moments of order greater than two can be neglected. Thus, we obtain:

$$\begin{aligned}\epsilon(X) &\approx \sqrt{\det(\Sigma_0)}\Big[1 + \frac{1}{2\det(\Sigma_0)}\Big(\Sigma_{0_{2,2}}\sum_{n=1}^{n_s} X_{2n-1}^2 + \Sigma_{0_{1,1}}\sum_{n=1}^{n_s} X_{2n}^2 - 2\Sigma_{0_{1,2}}\sum_{n=1}^{n_s} X_{2n-1}X_{2n}\Big)\Big] \\ &= \sqrt{\det(\Sigma_0)}\Big[1 + \frac{1}{2}{}^{\mathrm{T}}X\Gamma_0^{-1}X\Big]\end{aligned} \tag{1.27}$$

where Γ_0 is the 2×2 block diagonal following matrix,

$$\Gamma_0 \stackrel{def}{=} \begin{pmatrix} \Sigma_0 & 0 & \dots & 0 \\ 0 & \Sigma_0 & \dots & 0 \\ \vdots & \vdots & \ddots & \vdots \\ 0 & 0 & \dots & \Sigma_0 \end{pmatrix} \tag{1.28}$$

which is a $2n_s$–dimensional version of the beam matrix without any correlations between the different "bunch slices".
For a short while, we would like to stop here our investigations in order to make the following remark. By using Eq. (1.27), the computation of $<\epsilon>_{err}$ (defined by Eq. (1.24)) becomes quite simple in this regime. Indeed, we can easily show that:

$$<\epsilon>_{err} \stackrel{12}{\approx} \sqrt{<\epsilon^2>_{err}} \stackrel{13}{\approx} \sqrt{\det(\Sigma_0)}\Big(1 + \frac{1}{2}\,\mathbf{tr}(\Gamma\Gamma_0^{-1})\Big) \tag{1.29}$$

Thus, equation (1.29) gives its whole physical meaning to the "generalised beam matrix", Γ, defined in Paragraph 2.3.3 (Eq.(1.18)). Indeed, just by computing the trace of the matrix

[12] In the computation of $<\epsilon^2>_{err}$, we neglect the terms containing four order moments.

[13] Here, we have assumed $\mathbf{m} = 0$ in order to simplify the notations (what means that the errors are distributed within the linac around a straight line); if it is not the case, the considered equation has to be:

$$<\epsilon>_{err} \approx \sqrt{\det(\Sigma_0)}\Big(1 + \frac{1}{2}\,\mathbf{tr}\big(\Gamma\Gamma_0^{-1}\big) + \frac{1}{2}\,{}^{\mathrm{T}}\mathbf{m}\Gamma_0^{-1}\mathbf{m}\Big)\ .$$

$\Gamma\Gamma_0^{-1}$, that is, by comparing the matrix Γ with the matrix Γ_0, the definition of which is more intuitive, we can estimate the statistical average of the relative emittance growth at the line output (assuming that the "butterfly effect" is small, i.e. $<\gamma_f> \sqrt{\det(\Sigma_0)} \approx \gamma_0\epsilon_0$). Moreover, another interesting result appears clearly in this same equation, which is that the "emittance spread from machine to machine", i.e. the relative standard deviation $(<\epsilon^2>_{err} - <\epsilon>_{err}^2)/ <\epsilon>_{err}^2$, goes to zero when the perturbation regime is reached (see the four examples given in Chapter 3, and compare the "emittance spread" concerning the horizontal and the vertical planes).
Having said this, we come back to the computation of the function ρ_ϵ. Starting from Eq. (1.26), making the change of variable $k \longrightarrow \sqrt{\det(\Sigma_0)}\, k$, and using Eq. (1.27) which approximates the function $\epsilon(X)$ in the perturbation regime, we obtain after some algebraic manipulations (similar to the ones used for the computation of $<\epsilon>_{err}$ in the previous paragraph):

$$\begin{aligned}\rho_\epsilon(\epsilon) = & \frac{\exp(-\frac{1}{2}{}^{\mathrm{T}}\mathbf{m}\Gamma^{-1}\mathbf{m})}{2\pi\sqrt{\det(\Sigma_0)}} \int_{-\infty}^{\infty} dk \exp\Big(ik(\triangle\epsilon/\epsilon)\Big) \frac{\exp\Big(\frac{1}{2}{}^{\mathrm{T}}\mathbf{m}(k)\,\Gamma^{-1}(k)\,\mathbf{m}(k)\Big)}{\sqrt{\prod_{p=1}^{2n_s}(1+ik\lambda_p)}} \\ \stackrel{def}{=} & \frac{1}{\sqrt{\det(\Sigma_0)}} \rho_{(\triangle\epsilon/\epsilon)}(\triangle\epsilon/\epsilon)\end{aligned} \tag{1.30}$$

where the notations are the following.

- $(\triangle\epsilon/\epsilon) \stackrel{def}{=} \dfrac{\epsilon - \sqrt{\det(\Sigma_0)}}{\sqrt{\det(\Sigma_0)}}$

- λ_p, $1 \leq p \leq 2n_s$, are the $2n_s$ eigenvalues of the matrix $\Gamma\Gamma_0^{-1}$. They are all real and positive[14], in such a way that:

$$\sqrt{1+ik\lambda_p} \stackrel{def}{=} \sqrt[4]{1+k^2\lambda_p^2}\exp\Big(+\frac{i}{2}\arctan(k\lambda_p)\Big)$$

- $\Gamma(k) \stackrel{def}{=} \Big(\Gamma^{-1} + ik\Gamma_0^{-1}\Big)^{-1} = \Big(\mathbf{Id} + ik\Gamma\Gamma_0^{-1}\Big)^{-1}\Gamma$[15] and $\mathbf{m}(k) \stackrel{def}{=} \Big(\mathbf{Id} + ik\Gamma\Gamma_0^{-1}\Big)^{-1}\mathbf{m}$

Before studying the particular case, $\mathbf{m} = 0$ (the linac structures are organised around a straight line), which is the case resulting from the actual pre–alignment scheme of the CLIC

[14] Indeed, if A and B are any two matrices, it can be shown that both matrices, $\mathbf{AB}$ and $\mathbf{BA}$, have the same characteristic polynomial, i.e. $\det(\mathbf{AB} - \lambda\mathbf{I}) = \det(\mathbf{BA} - \lambda\mathbf{I})$, and then, the same eigenvalues (but not the same eigenvectors). Consequently, we see that the eigenvalues of the matrix $\Gamma\Gamma_0^{-1}$ are the same as the ones of the matrix $\Gamma_0^{-1/2}\,\Gamma\,\Gamma_0^{-1/2}$ ($\Gamma_0^{1/2}$ being the square root of the symmetric positive–definite matrix Γ_0), which is real symmetric, then $\mathbf{R}$–diagonalisable, and positive since Γ_0 and the covariance matrix Γ are both positive.

[15] The matrix $\left(\mathbf{Id} + ik\Gamma\Gamma_0^{-1}\right)$ is regular, since, as said before, the eigenvalues of $\Gamma\Gamma_0^{-1}$ are real.

main linac, we would like to make the following remark concerning Eq. (1.30). Indeed, in order to make sure of its validity, we should at least verify that no machine is able to deliver a bunch with a final emittance strictly lower than $\sqrt{\det(\Sigma_0)}$; hence, we have to verify that $\rho_\epsilon(\epsilon) = 0$ when $\triangle\epsilon/\epsilon < 0$. It is the case as shown hereafter. The integrand in Eq. (1.30) is an analytic function, $\mathbf{F}(z)$, in the complex half–plane, $\{z,\, \Im z \leq 0\}$, since we have seen that the eigenvalues (λ_p, $1 \leq p \leq 2n_s$) are real positive numbers. Then, we consider the contour $\mathcal{C}(\mathcal{R})$, included in this half–plane, and defined by

$$\mathcal{C}(R) = [-R, R] \cup \{R\, e^{i\theta} : -\pi \leq \theta \leq 0\} \stackrel{def}{=} \mathcal{C}_1(R) \cup \mathcal{C}_2(R)\,.$$

After that, we use the Cauchy formulae: $\displaystyle\int_{\mathcal{C}(R)} \mathbf{F}(z)\, dz = 0 = \int_{\mathcal{C}_1(R)} (\ldots) + \int_{\mathcal{C}_2(R)} (\ldots)$. Finally, we consider the limit, $R \to \infty$, in the previous equality: the first term goes to $\rho_\epsilon(\epsilon)$ and the second one to zero, since $\triangle\epsilon/\epsilon < 0$.

Case $\mathbf{m} = 0$

Now, we will finish this section by studying the particular case $\mathbf{m} = 0$. Eq. (1.30) gives in this case:

$$\rho_{(\triangle\epsilon/\epsilon)}(\triangle\epsilon/\epsilon) = \frac{1}{2\pi} \int_{-\infty}^{\infty} \exp\Big(ik(\triangle\epsilon/\epsilon)\Big) \frac{dk}{\sqrt{\displaystyle\prod_{p=1}^{2n_s} (1 + ik\lambda_p)}} \tag{1.31}$$

The author has not found any solution in order to compute analytically this integral in the most general case. Nevertheless, for one or two non zero eigenvalues, analytic solution can be derived (see Appendix C) and are reported hereafter:

- Case 1: one single non zero eigenvalue

$$\mathcal{I}_1(\lambda; \epsilon) \stackrel{def}{=} \frac{1}{2\pi} \int_{-\infty}^{\infty} \frac{e^{ik\epsilon}\, dk}{\sqrt{1 + i\lambda k}} = \begin{cases} \dfrac{e^{-\epsilon/\lambda}}{\sqrt{\pi\lambda\epsilon}} & \lambda > 0,\, \epsilon > 0 \\ 0 & \lambda > 0,\, \epsilon < 0 \end{cases}$$

  which corresponds, as expected, to a Chi–Square distribution of one degree of freedom (i.e the distribution related to the square of one Gaussian variable).

- Case 2: two non zero eigenvalues[16]:

$$\begin{aligned} \mathcal{I}_2(\lambda; \mu; \epsilon) &\stackrel{def}{=} \frac{1}{2\pi} \int_{-\infty}^{\infty} \frac{e^{ik\epsilon}\, dk}{\sqrt{(1 + i\lambda k)(1 + i\mu k)}} \\ &= \begin{cases} \dfrac{1}{\sqrt{\lambda\mu}} \exp\left[-\epsilon(\dfrac{1}{2\lambda} + \dfrac{1}{2\mu})\right]\; I_0\left[\epsilon(\dfrac{1}{2\lambda} - \dfrac{1}{2\mu})\right] & \lambda > 0,\, \mu > 0,\, \epsilon > 0 \\ 0 & \lambda > 0,\, \mu > 0,\, \epsilon < 0 \end{cases} \end{aligned} \tag{1.32}$$

The case number one is irrelevant to the computation of ρ_ϵ, since we intuitively see that this problem has at least two degrees of freedom (angle and transverse positions of the slices). In fact, we are going to show that only two degrees of freedom emerge naturally from the perturbation regime, or, more precisely, that the matrix $\Gamma\Gamma_0^{-1}$ possesses only two non zero eigenvalues in this regime. Indeed, if we consider a slice of charge z, its offset at the line output is given by:

$$\delta x(z) = \sum_{n=1}^{N_q^{tot}} a_{q,n}(z)\, dx_{q,n} + \sum_{n=1}^{N_c^{tot}} b_{c,n}(z)\, dx_{c,n}$$

where $a_{q,n}(z)$ (resp. $b_{c,n}(z)$) is the response coefficient of the slice z to the displacement $dx_{q,n}$ (resp. $dx_{c,n}$) of the quadrupole (resp. the cavity) number n. In a perturbation regime, and in thin lens approximation (for the quads as well as for the dipole kicks in the structures), these response coefficients are simply given by:

$$a_{q,n}(z) \approx k_{q,n}L_{q,n}\left[(1+f(z))R_{1,2}(s_{q,n};s_f) - \sum_{\substack{\text{cavities} \\ s_{c,n} > s_{q,n}}} \frac{e^2 W_T(z)}{\gamma(s_{c,n};z)mc^2}\, L_c\, R_{1,2}(s_{q,n};s_{c,n})\, R_{1,2}(s_{c,n};s_f)\right]$$

$$\text{and } b_{c,n}(z) \approx \frac{e^2 W_T(z)}{\gamma(s_{c,n};z)mc^2} L_c R_{1,2}(s_{c,n};s_f)$$

where $k_{q,n}L_{q,n}$ is the integrated strength of the quad number n, and L_c, the effective length of the structures, where $R_{1,2}(s_{q,n};s_f)$ (resp. $R_{1,2}(s_{c,n};s_f)$) is the element (1,2) of the usual R–matrix from the location $s_{q,n}$ (resp.$s_{c,n}$) of the quadrupole n (resp. the cavity n) to the end of the line, and where $W_T(z)$ is the transverse delta–function wake potential convoluted with the longitudinal distribution (see Appendix A, Eq. (A.4)). Then, we use the fact that the transverse positions of the quadrupoles after correction depends linearly on the errors within the line (cavity misalignments, BPM misalignments, ...: vector X_{err} in Paragraph 1.2.2), and that the BNS damping condition requires a modulation, $f(z)$, of the quadrupole gradients which is proportional to $W_T(z)$ (see next Chapter). As a consequence, neglecting the intra–bunch energy spread in the previous equation (i.e. $\gamma(s_{c,n};z) \approx \gamma(s_{c,n},0)$), we obtain the following result:

$$\begin{aligned} \delta x(z) - <\delta x> &= (W_T(z) - <W_T>)\chi_1 \text{ and, in a same way,} \\ \delta x'(z) - <\delta x'> &= (W_T(z) - <W_T>)\chi_2 \end{aligned}$$

[16]The distribution $\mathcal{I}_2$ does not refer to a classical distribution. If X is a two–dimensional Gaussian vector of covariance matrix Γ, and if $\epsilon(X)$ is any positive quadratic form of associated matrix Γ_0 (Γ_0 plays here the same role as Γ_0^{-1}), we have shown that the density of probability, $\rho_\epsilon(\epsilon)$, corresponds exactly to the distribution $\mathcal{I}_2(\lambda;\mu;\epsilon)$, where λ and μ are the two eigenvalues of the matrix $\Gamma\Gamma_0$. In the case where $\Gamma = \Gamma_0^{-1}$, or, in a more general way, in the case where $\Gamma\Gamma_0$ is a homotethie, these two eigenvalues are equal, and $\mathcal{I}_2$ becomes the exponential distribution, $1/\lambda\, e^{-\epsilon/\lambda}$, which is also a so–called Chi–Square distribution of two degrees of freedom (i.e the distribution related to the sum of squares of two Gaussian variables, independent and identically distributed).

where χ_1 and χ_2 depend linearly on the vector X_{err}, and then, are two Gaussian variables (independent of z) with the following covariance matrix:

$$\mathbf{S}_{err} = \begin{pmatrix} < {\chi 1}^2 >_{err} & < \chi 1 \chi 2 >_{err} \\ < \chi 1 \chi 2 >_{err} & < {\chi 2}^2 >_{err} \end{pmatrix} = \sigma_1^2 \begin{bmatrix} \alpha_1 \\ \beta_1 \end{bmatrix} [\alpha_1 \ \beta_1] + \sigma_2^2 \begin{bmatrix} \alpha_2 \\ \beta_2 \end{bmatrix} [\alpha_2 \ \beta_2]$$ [17]

where $(\sigma_i^2,\ i = 1, 2)$ are the two positive eigenvalues of the matrix $\mathbf{S}_{err}$, and $([\alpha_i \ \beta_i],\ i = 1, 2)$, the two associated eigenvectors: they are orthogonal, since $\mathbf{S}_{err}$ is symmetric, and normalised to unity, i.e $\alpha_1\alpha_2 + \beta_1\beta_2 = 0$ and $\alpha_i^2 + \beta_i^2 = 1$, $i = 1, 2$. Using these notations, the matrix Γ (Paragraph 1.3.3, Eq. (1.18)) can be written in the following manner:

$$\Gamma = \triangle z \Big[{X_1}^{\mathrm{T}} X_1 + {X_2}^{\mathrm{T}} X_2 \Big] \quad \text{with} \quad X_i = \sigma_i \begin{pmatrix} \sqrt{\rho(z_1)}(W_T(z_1) - < W_T >)\alpha_i \\ \sqrt{\rho(z_1)}(W_T(z_1) - < W_T >)\beta_i \\ \vdots \\ \sqrt{\rho(z_{n_s})}(W_T(z_{n_s}) - < W_T >)\alpha_i \\ \sqrt{\rho(z_{n_s})}(W_T(z_{n_s}) - < W_T >)\beta_i \end{pmatrix},\ i = 1, 2$$

We can verify, that these two vectors are also orthogonal, i.e. ${}^{\mathrm{T}}X_1 X_2 = 0$, in such a way that the matrix Γ has only two non zero eigenvalues $(\tilde{\lambda},\ \tilde{\mu})$ which correspond to the two vectors X_1 and X_2. We have:

$$\begin{cases} \tilde{\lambda} \ = \ \triangle z {}^{\mathrm{T}}X_1 X_1 \ = \ \triangle z \sigma_1^2 \displaystyle\sum_{n=1}^{n_s} \rho(z_n) \Big(W_T(z_n) - < W_T > \Big)^2 \ = \ \sigma_1^2 (< W_T^2 > - < W_T >^2) \\ \tilde{\mu} \ = \ \triangle z {}^{\mathrm{T}}X_2 X_2 \ = \ \triangle z \sigma_2^2 \displaystyle\sum_{n=1}^{n_s} \rho(z_n) \Big(W_T(z_n) - < W_T > \Big)^2 \ = \ \sigma_2^2 (< W_T^2 > - < W_T >^2) \end{cases}$$

Finally, the matrix $\Gamma\Gamma_0^{-1}$ has also two non–zero eigenvalues, $(\lambda,\ \mu)$[18].
In all the simulations which give a small emittance dilution at the linac output, we always observe that the matrix $\Gamma\Gamma_0^{-1}$ possesses effectively two eigenvalues, λ and μ, at least one order of magnitude greater than the others, in such a way that we have approximately: $< \triangle\epsilon/\epsilon >_{err} = 1/2\,(\lambda + \mu)$, as announced by Eq. (1.29). Thus, in the fourth example of Chapter 3, we will see that the function $\mathcal{I}_2(\lambda; \mu; \triangle\epsilon/\epsilon)$ fits extremely well the distribution $\rho_{(\triangle\epsilon/\epsilon)}(\triangle\epsilon/\epsilon)$, except perhaps, when $\triangle\epsilon/\epsilon$ is close to zero (where the smallest eigenvalues have some importance), since $\rho_{(\triangle\epsilon/\epsilon)}(0) = 0$ and $\mathcal{I}_2(\lambda; \mu; 0) = 1/\sqrt{\lambda\mu} \neq 0$.
Finally, using $\mathcal{I}_2$ instead of $\rho_{(\triangle\epsilon/\epsilon)}$, we have estimated numerically that the 95% confidence level corresponds to a final emittance dilution between zero (forgetting the butterfly effect) and two or three times the average dilution, i.e. the quantity $1/2\,(\lambda + \mu)$.

[17] Here, we write, in a different manner, the matricial equality, $\mathbf{S}_{err} = P\,\mathrm{Diag}(\sigma_1^2, \sigma_2^2)\,{}^{\mathrm{T}}P$, where P is the orthogonal matrix which diagonalises the symmetric matrix $\mathbf{S}_{err}$.

[18] Since Γ_0^{-1} is regular, the rank of the matrix $\Gamma\Gamma_0^{-1}$, then the number of its non–zero eigenvalues, is also the one of the matrix Γ, then equal to two.

Chapter 2

BNS damping

2.1 BNS damping in a strong focusing system

It is well–known that correction algorithms, as sophisticated as they can be, remain insufficient to preserve the transverse single–bunch emittance in a linac where the dipole wakefields are relatively strong. Indeed, in addition to powerful alignment methods, we have to resort to the so–called BNS damping [13], the principle of which is reported hereafter in a simplified way. Due to the short–range dipole wakefields, the bunch is subjected to "inhomogeneous kicks" (i.e. depending on the relative position of the particles inside the bunch) within the structures, that tends to increase the projected RMS beam emittance all along the linac. In order to fight against this "head–tail effect", the BNS damping principle consists in modulating the quadrupole strength seen by the different particles within the bunch, so that the tail particles are more focused than the head ones.
Theoretical illustrations of this principle are generally formulated in the so–called "smooth focusing approximation", for which the betatron focusing is provided by a smooth function, $k^2(s;z) = k_0^2(s)(1+f(z))$[1], rather than from a series of lumped quadrupoles (see for instance Ref. [14]). Then, starting from initial conditions, assumed to be the same ones for all the particles within the bunch, the bunch oscillates coherently, in spite of the transverse wakefields, if and only if the function $f(z)$ verifies [14]:

$$f(z) = \frac{e^2}{mc^2\gamma(s)k_0^2(s)} \int_{-\infty}^{z} \rho(z^*) W_T^{\delta}(z-z^*)\, dz^* \stackrel{def}{=} \frac{e^2}{mc^2\gamma(s)k_0^2(s)}\, W_T(z)$$

leading also to the fact that the quantity $\gamma(s)k_0^2(s)$ has to remain constant all along the linac.
Here, we prefer to study the problem in the more realistic model of a strong focusing lattice, and then use, in a concrete way, the generalised R matrix introduced previously. So, we come back to the notations of Paragraph 1.1.2. Let us consider the two–dimensional vector $X(0,z)$ referring to the initial conditions of the slice z. At any abscissa s within the line,

[1] $k_0(s) = 2\pi/\lambda_\beta(s)$, where $\lambda_\beta(s)$ is the instantaneous betatron wave length a the position s.

the vector $X(s,z)$ is given by (see Eq. (1.6)):

$$X(s,z) = R_0(s,z)\,X(0,z) + \int_{-\infty}^{z} R_w(s,z,z^*)\,X(0,z^*)\,dz^* \tag{2.1}$$

We note, $k(s,z) = k_0(s)(1+f(z))$, the quadrupole strength seen by the slice z, and rewrite, in the following manner, the coupled differential equations verified by the two matrices R_0 and R_w (see Eq. (1.7))[2]:

$$\left\{\begin{array}{lcl} R_0'(s,z) & = & \Big(A_0(s) + \delta A_0(s,z)\Big)\,R_0(s,z) \\ R_w'(s,z,z^*) & = & \Big(A_0(s) + \delta A_0(s,z)\Big)\,R_w(s,z,z^*) + A_w(s,z,z^*)\,R_0(s,z^*) \\ & & + \displaystyle\int_{z^*}^{z} A_w(s,z,z^{**})\,R_w(s,z^{**},z^*)\Big)\,dz^{**} \end{array}\right. \tag{2.2}$$

$$\begin{array}{ll} \text{where} & A_0(s) = \left(\begin{array}{cc} 0 & 1 \\ -k_0(s) & -\gamma'(s)/\gamma(s) \end{array}\right)\ ,\ \delta A_0(s,z) = \left(\begin{array}{cc} 0 & 0 \\ -k_0(s)f(z) & 0 \end{array}\right) \\ \text{and} & A_w(s,z,z^*) = \dfrac{e^2/m_ec^2}{\gamma(s)}\left(\begin{array}{cc} 0 & 0 \\ W_T^\delta(z-z^*)\rho(z^*) & 0 \end{array}\right)\ . \end{array} \tag{2.3}$$

Then, assuming the functions $f(z)$ and $W_T^\delta(z)$ to be small, we make the following perturbative expansion: $R_0(s,z) = R_0^{(0)}(s) + R_0^{(1)}(s,z) + \ldots$ and $R_w(s,z,z^*) = R_w^{(1)}(s,z,z^*) + \ldots$. Using Eq. (2.2), we obtain the differential equations verified by the three matrices $R_0^{(0)}(s)$, $R_0^{(1)}(s;z)$ and $R_w^{(1)}(s,z,z^*)$:

$$\left\{\begin{array}{lcll} R_0^{(0)\prime}(s) & = & A_0(s)\,R_0^{(0)}(s) & R_0^{(0)}(0) = \mathbf{Id} \\ R_0^{(1)\prime}(s,z) & = & A_0(s)\,R_0^{(1)}(s,z) + \delta A_0(s,z)\,R_0^{(0)}(s) & R_0^{(1)}(0,z) = 0 \\ R_w^{(1)\prime}(s,z,z^*) & = & A_0(s)\,R_w^{(1)}(s,z,z^*) + A_w(s,z,z^*)\,R_0^{(0)}(s) & R_w^{(1)}(0,z,z^*) = 0 \end{array}\right.$$

Consequently, the matrix $R_0^{(0)}$ is the usual R matrix, describing the motion of accelerated particles in the focusing lattice defined by the step function $k_0(s)$. Now, supposing that the matrix $R_0^{(0)}$ is known, and using the previous equations, we can verify that the two matrices $R_0^{(1)}$ and $R_w^{(1)}$ are given by:

$$\left\{\begin{array}{lcl} R_0^{(1)}(s,z) & = & R_0^{(0)}(s)\displaystyle\int_0^s R_0^{(0)^{-1}}(s')\,\delta A_0(s',z)\,R_0^{(0)}(s')\,ds' \\ R_w^{(1)}(s,z,z^*) & = & R_0^{(0)}(s)\displaystyle\int_0^s R_0^{(0)^{-1}}(s')\,A_w(s',z,z^*)\,R_0^{(0)}(s')\,ds' \end{array}\right. \tag{2.4}$$

Finally, if the vector $X(0,z)$ in Eq. (2.1) does not depend on z (same initial conditions for all the particles within the bunch), we can use Eq. (2.4) to obtain $X(s,z)$ at any location s

[2]Here, we neglect all the terms relative to the intra–bunch energy spread which appears explicitly in the considered equations; in other words, we write $\gamma'(s;z)/\gamma(s;z) \approx \gamma'(s)/\gamma(s)$ and $W_T^\delta(z-z^*)/\gamma(s;z) \approx W_T^\delta(z-z^*)/\gamma(s)$.

within the line:

$$\begin{aligned} X(s,z) &= R_0^{(0)}(s)[\mathbf{Id} + \delta R(s,z)]\, X(0) \\ \text{where } \delta R(s,z) &= \int_0^s R_0^{(0)^{-1}}(s')\Big[\delta A_0(s',z) + \int_{-\infty}^{z} A_w(s',z,z^*)\, dz^*\Big]\, R_0^{(0)}(s')\, ds' \\ &= \int_0^s \Big[-k_0(s')f(z) + \frac{e^2}{mc^2\gamma(s')} W_T(z)\Big] \begin{pmatrix} -R_{11}^{(0)}R_{12}^{(0)} & -R_{12}^{(0)^2} \\ R_{11}^{(0)^2} & R_{11}^{(0)}R_{12}^{(0)} \end{pmatrix} \frac{\gamma(s')}{\gamma_0}\, ds' \end{aligned} \tag{2.5}$$

Here, $R_{11}^{(0)}$ and $R_{12}^{(0)}$ represents the elements (1,1) and (1,2) of the matrix $R_0^{(0)}(s')$, which are given by:

$$\begin{cases} R_{11}^{(0)} &= \sqrt{\dfrac{\gamma_0}{\gamma(s')}}\sqrt{\dfrac{\beta(s')}{\beta_0}}\Big(\cos\Psi(s') + \alpha_0 \sin\Psi(s')\Big) \\ R_{12}^{(0)} &= \sqrt{\dfrac{\gamma_0}{\gamma(s')}}\sqrt{\beta_0\beta(s')}\, \sin\Psi(s') \\ \Psi(s') &= \displaystyle\int_0^{s''} \frac{ds''}{\beta(s'')} \end{cases} \tag{2.6}$$

Now, as done in the smooth focusing approximation, we are looking for a condition on $f(z)$ which permits coherent oscillations of the bunch all along the line (assuming same initial conditions for all the bunch slices, i.e. $X(0,z) = X(0)$). This condition corresponds obviously to $\delta R(s,z) = 0$ in Eq. (2.5). Nevertheless, unlike to the smooth focusing case, an exact cancellation of the matrix $\delta R(s,z)$ cannot be obtained for any location s within the line. More precisely, assuming a periodic focusing lattice, and looking at Eq. (2.5) and (2.6), it can be shown, by symmetry and periodicity considerations, that the δR cancellation occurs, if and only if:

- 1. $\mu = \dfrac{m}{n}\pi$, $m < n$, where μ is the phase advance per period. If this condition is satisfied, we have:

$$\begin{aligned}
&\int_0^{nL} R_{11}^{(0)}(s')R_{12}^{(0)}(s')\frac{\gamma(s')}{\gamma_0}\, ds' &&= \int_0^{nL} \beta(s')\sin\Psi(s')\,\Big(\cos\Psi(s') + \alpha_0\sin\Psi(s')\Big)ds' &&= \frac{nL\alpha_0}{2}\overline{\beta} \\
&\int_0^{nL} k_0(s')\, R_{11}^{(0)}(s')R_{12}^{(0)}(s')\frac{\gamma(s')}{\gamma_0}\, ds' &&= \int_0^{nL} k_0(s')\beta(s')\sin\Psi(s')\,\Big(\cos\Psi(s') + \alpha_0\sin\Psi(s')\Big)ds' &&= \frac{nL\alpha_0}{2}\overline{k_0\beta} \\
&\int_0^{nL} R_{12}^{(0)^2}(s')\frac{\gamma(s')}{\gamma_0}\, ds' &&= \int_0^{nL} \beta_0\beta(s')\sin^2\Psi(s')\, ds' &&= \frac{nL\beta_0}{2}\overline{\beta} \\
&\int_0^{nL} k_0(s')\, R_{12}^{(0)^2}(s')\frac{\gamma(s')}{\gamma_0}\, ds' &&= \int_0^{nL} k_0(s')\,\beta_0\beta(s')\sin^2\Psi(s')\, ds' &&= \frac{nL\beta_0}{2}\overline{k_0\beta} \\
&\int_0^{nL} R_{11}^{(0)^2}(s')\frac{\gamma(s')}{\gamma_0}\, ds' &&= \int_0^{nL} \frac{\beta(s')}{\beta_0}\Big(\cos\Psi(s') + \alpha_0\sin\Psi(s')\Big)^2 ds' &&= \frac{nL(1+\alpha_0^2)}{2\beta_0}\overline{\beta} \\
&\int_0^{nL} k_0(s')\, R_{11}^{(0)^2}(s')\frac{\gamma(s')}{\gamma_0}\, ds' &&= \int_0^{nL} k_0(s')\,\frac{\beta(s')}{\beta_0}\Big(\cos\Psi(s') + \alpha_0\sin\Psi(s')\Big)^2 ds' &&= \frac{nL(1+\alpha_0^2)}{2\beta_0}\overline{k_0\beta}
\end{aligned}$$

  where L is the lattice period, and where the over-lined quantities are referring to averages over one period.

- 2. The location s, where the matrix $\delta R(s,z)$ is equal to zero, is then an integer multiple of nL.

- 3. Finally, the function $f(z)$ has to be[3]:

$$f(z) = \frac{\overline{\beta}}{\overline{k_0\beta}} \frac{e^2}{<\gamma> mc^2} W_T(z) \tag{2.7}$$

  where $<\gamma> mc^2$ represents the average energy of the bunch, that we have assumed constant along the n periods of the focusing lattice (frozen beam).

The quantity $\overline{\beta}/\overline{k_0\beta}$ can be easily estimated in thin length approximation, in the case of a FODO lattice; after computation, we find:

$$f(z) = \frac{L^2}{24} \frac{2+\cos^2(\mu/2)}{\sin^2(\mu/2)} \frac{e^2}{<\gamma> mc^2} W_T(z) \tag{2.8}$$

Consequently, we have to be aware of the fact that the BNS damping is not so efficient in the strong focusing case as it is in the smooth focusing one, since, on the one hand, the bunch does not oscillate, strictly speaking, in a coherent way, and, on the other hand, since Eq. (2.7) or Eq. (2.8) are valid for just a perturbation regime, which then corresponds approximately to:

$$\overline{\beta}^2(\gamma) \frac{e^2 < W_T >}{\gamma\, mc^2} \ll 1 \ [4] \tag{2.9}$$

Starting from initial conditions which are identical for all the bunch slices, Eq. (2.8) has always been checked by simulation, after minimisation of the final emittance dilution. Unfortunately, when the structures are misaligned ("inhomogeneous kicks" are given to the bunch all along the linac), or when different correction algorithms are considered, the theoretical development previously presented cannot stick to reality anymore, and the author remains actually without hope, concerning the elaboration of an analytical model able to describe such a situation.
Nevertheless, the numerical values obtained for $f(z)$ by simulation are of the same order of magnitude as the theoretical ones given by Eq. (2.8) (a factor like 1/2 has to multiply the second side of Eq. (2.8)), and the scaling of $f(z)$ with $W_T(z)$ and L^2 (or $\overline{\beta}^2$ when μ is kept constant) remains rigorously correct [15]. In conclusion, we will then remember the following scaling law:

$$\frac{1}{k_0} < \frac{\partial k}{\partial z} > \propto \frac{\overline{\beta}^2(\gamma)}{\gamma} < \frac{\partial W_T}{\partial z} > \propto \frac{L^2(\gamma)}{\gamma} < \frac{\partial W_T}{\partial z} > \tag{2.10}$$

[3] If condition 1. is not satisfied, the matrix $\delta R(s,z)$ remains bounded all along the line, provided that $f(z)$ is given by Eq. (2.7); nevertheless, its coefficients are never zero in the same time.

[4] Here, we use the fact that $\overline{\beta} \propto L$ when the phase advance μ is constant all along the line.

2.2 Two options to implement BNS damping in a linac

2.2.1 The microwave quadrupole (RFQ) option

There are two main remedies which permit to carry out BNS damping in strong wakefield linacs, either through microwave quadrupoles (RFQ), as it is actually the case for the CLIC main linac [1], or by generating a negative energy spread within the accelerated beam.
We begin here by the first option, which decouples the problem of the minimisation of the beam energy spread at the end of the linac, from the constraint which is imposed by the BNS damping condition (Eq. (2.10)).
Then, we consider a slice z within the bunch, of energy $E(s,z)$, where s is the RFQ location in the line. The quadrupole strength seen by the considered slice is given by:

$$k_{\rm RFQ}(s,z) = \frac{\alpha_{RFQ} k_0(s)}{1-\alpha_{RFQ}\sin\phi_{RF}} \sin\left(\frac{\omega_{RF} z}{c} - \phi_{RF}\right) \frac{E(s,0)}{E(s,z)} \tag{2.11}$$

where the previous notations needs some explanations.

- Firstly, we assume the RF phase to be the same in the microwave quadrupoles and in the accelerating structures ($\phi_{RFQ} = \phi_{RF}$ in Paragraph 1.1.1).
- We start from a linac without any RFQs, where the focusing lattice is defined by the step function $k_0(s)$. Then, by referring to the actual layout of the CLIC main linac, one or several RFQs are arranged after each magnetic quadrupole, in such a way that their total effective length is equal to the one of the quad preceding it. Now, we note, $k_{\rm RFQ}(s,0)$ (resp. $k_{\rm Q}(s,0)$), the magnetic strength seen by the bunch centre, $z=0$, within the RFQs (resp. within the magnetic quad ahead of it). So, we parametrise $k_{\rm RFQ}(s,0)$ by $\dfrac{-\alpha_{RFQ} k_0(s)\sin\phi_{RF}}{1-\alpha_{RFQ}\sin\phi_{RF}}$, which defines completely the parameter α_{RFQ}. Finally, we readjust $k_{\rm Q}(s,0)$, in such a manner that, the quadrupole strength seen by the bunch centre, and averaged over the magnetic quad and the RFQs which are associated to it, is exactly equal to $k_0(s)$; what leads to $k_{\rm Q}(s,0) = k_0(s)/(1-\alpha_{RFQ}\sin\phi_{RF})$. This choice, rather complicated, comes from the fact that, in `MTRACK` [2], RFQs and magnetic quadrupoles were always simulated as if they were completely overlapping each other; in this "combined component", the quadrupole strength was then defined by:

$$k_{\rm I}(s,z) = \frac{k_0(s)}{1-\alpha_{RFQ}\sin\phi_{RF}} \left[1 + \alpha_{RFQ}\sin\left(\frac{\omega_{RF} z}{c} - \phi_{RF}\right)\right] \frac{E(s,0)}{E(s,z)} \tag{2.12}$$

Having clarified this point, the function $E(s,z)$ is easily deduced from Eq. (1.2):

$$E(s,z) = E_0 + eG_{RF}\, s\, \cos\left(\frac{\omega_{RF} z}{c} - \phi_{RF}\right) - e^2 W_L(z)\, s \stackrel{def}{=} E_0 + eG(z)s \tag{2.13}$$

In the previous equality, E_0 represents the input energy, assuming that the energy spread is zero at the line entrance[5] , while $W_L(z)$, given by Eq. (A.4), defines the longitudinal wake potential at a relative position z within the bunch[6].
Now, since the "RFQ option" has been chosen, the intra–bunch energy spread can be controlled all along the linac by using the following strategy. We have to shape the longitudinal distribution of particles, $\rho(z)$, in such a way that, for a judicious choice of the RF phase, the effective accelerating gradient, $G(z)$, defined in Eq. (2.13), may become independent of z. More precisely, we consider the following positive functional:

$$\mathbf{F}(\rho;\phi_{RF};G_{RF};\omega_{RF};W_L^\delta) \stackrel{def}{=} \left\langle \left(G - \langle G \rangle_\rho\right)^2 \right\rangle_\rho = \int_{-\infty}^{\infty} dz^* \rho(z^*) G^2(z^*) - \left[\int_{-\infty}^{\infty} dz^* \rho(z^*) G(z^*)\right]^2$$

$$\text{where } G(z) = G_{RF}\cos\left(\frac{\omega_{RF} z}{c} - \phi_{RF}\right) - e\int_{-\infty}^{z} dz^* \rho(z^*) W_L^\delta(z^*)$$

It has been shown [16] that, for any function $W_L^\delta(z)$ and any values given to G_{RF}, to ω_{RF} and to ϕ_{RF}, it existed an unique solution, $\rho(z)$, to the equation $\mathbf{F} = 0$. The distributions that we obtain are then characterised by sharp truncation of their two extremities, in a more marked way at the head than at the tail [16]. Nevertheless, it seems difficult, in practice, to generate exactly such bunch distributions, and we will discuss truncated Gaussian distributions, already proposed for CLIC [17].
Such a distribution is characterised by 4 parameters: σ_z, the RMS value of the distribution without truncation, σ_h, the head truncation, σ_t, the tail truncation and N_b the total charge of the distribution. Thus, we consider the function $\mathbf{G}$ defined by:

$$\mathbf{G}(\sigma_z;\sigma_h;\sigma_t;\phi_{RF}) = \mathbf{F}(\rho;\phi_{RF};G_{RF};\omega_{RF};W_L^\delta)$$

where the function W_L^δ is fixed, as well as G_{RF} and ω_{RF}, and where ρ is the truncated Gaussian distribution defined above, the total charge of which is also assumed to be constant. Then, varying σ_z, σ_h, σ_t and ϕ_{RF} in a "certain selected region", we search to minimise numerically the function $\mathbf{G}$. For what concerns the CLIC main beam parameters (see Section 3.1), the explored region has been:

- σ_z between 100 μm and 400 μm (in the same range as the other designs, except TESLA, [18]), and σ_h and σ_t greater than 1.3 σ_z and 1.5 σ_z, respectively. A preliminary design of a bunch compressor as a two–stage device has already been investigated [19], showing the possibility to reduce the bunch length from its value at the damping–ring extraction to the range of values previously defined. Nevertheless, no serious solution has been actually proposed in order to solve the truncation problem of the bunch charge distribution.

[5]If the relative input energy spread is not zero, its contribution becomes more and more negligible, when the beam is accelerated.

[6]Here, we neglect the fact that the peak effective accelerating gradient is not equal to G_{RF} in RFQ structures (see Paragraph 1.1.1). Nevertheless, for what concerns the CLIC main linac, RFQs represents only $\sim$ 10% of the total number of accelerating structures, and the considered effect is not of great importance (see example II in Chapter 3).

- ϕ_{RF} lower than 12°. This upper value must be kept reasonably small as we will see in the following, but the choice of the value itself is just historical (by comparison with previous choices [4], [17]).

Then, after minimisation of the function **G**, we can define a positive angle, noted ϕ_W [7], and a truncated Gaussian bunch distribution characterised by σ_z, σ_h and σ_t, so that:

$$\mathbf{G}(\sigma_z;\sigma_h;\sigma_t;\phi_W) \approx 0 \text{ leading to } eW_L(z) \approx G_{RF}\cos\left(\frac{\omega_{RF}z}{c}-\phi_W\right)+\mathbf{Cst}$$

Now, by using the fact that the longitudinal wake is close to zero at the bunch head, we obtain:

$$eW_L(z) \approx G_{RF}\cos\left(\frac{\omega_{RF}z}{c}-\phi_W\right)-G_{RF}\cos\left(\frac{\omega_{RF}\sigma_h}{c}-\phi_W\right) \tag{2.14}$$

Note that, by deriving the previous equation according to z, and by using Eq. (A.6), we obtain the ϕ_W dependence according to the beam and RF parameters. We have roughly:

$$\phi_W \;\approx\; \frac{e<\partial W_L/\partial z>}{G_{RF}\omega_{RF}/c} \;\propto\; \frac{N_b\,\omega_{RF}}{G_{RF}\,\sigma_z} \tag{2.15}$$

Finally, if the RF phase is taken equal to ϕ_W, Eq. (2.11) and (2.12) become:

$$k_{\mathrm{RFQ}}(s,z) = \frac{\alpha_{RFQ}k_0(s)}{1-\alpha_{RFQ}\sin\phi_W}\,\sin\left(\frac{\omega_{RF}z}{c}-\phi_W\right) \tag{2.16}$$

$$k_{\mathrm{I}}(s,z) = \frac{k_0(s)}{1-\alpha_{RFQ}\sin\phi_W}\left[1+\alpha_{RFQ}\sin\left(\frac{\omega_{RF}z}{c}-\phi_W\right)\right] \tag{2.17}$$

so that, by using Eq. (A.6) and the BNS damping condition (Eq. (2.10)), we obtain:

$$\alpha_{RFQ} \;\approx\; \frac{c}{\omega_{RF}}\,\frac{<\partial k_{\mathrm{I}}/\partial z>}{k_0} \;\overset{8}{\propto}\; \frac{\overline{\beta}^2(\gamma)}{\gamma\omega_{RF}} \;<\frac{\partial W_T}{\partial z}> \propto\; N_b\,\frac{\overline{\beta}^2(\gamma)}{\gamma}\,\omega_{RF}^3 \tag{2.18}$$

2.2.2 The "energy spread option"

In this paragraph, we deal with the feasibility of implementing BNS damping by accelerating the beam with a small negative energy spread, and then, for a short while, we will leave the "RFQ option" aside.

[7] With our conventions, ϕ_W is necessarily positive; indeed, due to the longitudinal wakes, the tail particles ($z<0$) lose more energy than the others, and consequently they have to be placed on the negative slope of the RF wave.

[8] Writing Eq. (2.18), we suppose, on the one hand, that the iris aperture scales with ω_{RF}^{-1}, and, on the other hand, that the fundamental frequency of the dipole mode, $\omega_{T,0}$ in Eq. (A.6), is roughly equal to the RF frequency.

So, at the level of the quadrupoles, the magnetic strength seen by the different particles of the bunch is simply given by:

$$k_{\rm II}(s,z) = k_0(s)\frac{E(s,0)}{E(s,z)} \tag{2.19}$$

where the energy $E(s,z)$ is deduced from Eq. (2.13) and (2.14):

$$E(s,z) = E_0 + e\,G_{RF}\,s\,\left(\cos\Big(\frac{\omega_{RF}z}{c} - \phi_{RF}\Big) - \cos\Big(\frac{\omega_{RF}z}{c} - \phi_W\Big) + \cos\Big(\frac{\omega_{RF}\sigma_h}{c} - \phi_W\Big)\right) \tag{2.20}$$

Here, of course, the RF phase has to be taken different from ϕ_W in order to generate the required energy spread within the bunch; more precisely, it has to be lower than ϕ_W (and even negative as we will show it latter), in such a way that the z derivative of the quadrupole strength, $k_{\rm II}(s,z)$ in Eq. (2.11), remains positive all along the bunch (tail particles more focused than the head ones).
Having said this, the problem of the spread compensation arises, and we adopt the following strategy. The linac is then divided into two different regions.

- In a first region, at low energy, where the wakefield effects are strong, the beam is accelerated with an RF phase, $\phi_1 \leq 0$, so that the BNS damping condition can be satisfied; we note L_1 the total effective length of the structures within this region.

- In a second part of the linac, of effective length L_2, at higher energy, we forget the BNS damping condition, and the RF phase is switched to a positive value, ϕ_2, in order to compensate the bunch energy spread generated in the first region.

Consequently, the final energy, $E_f(z)$, has the following profile:

$$\frac{E_f(z)}{e\,G_{RF}} = \underbrace{L_1\,\cos\left(\frac{\omega_{RF}z}{c} - \phi_1\right)}_{\text{region of spread generation}} + \underbrace{L_2\,\cos\left(\frac{\omega_{RF}z}{c} - \phi_2\right)}_{\text{region of spread compensation}} - \underbrace{(L_1+L_2)\,\cos\left(\frac{\omega_{RF}z}{c} - \phi_W\right)}_{\substack{\text{spread generated by beam-loading}\\ \text{all along the line}}} + \mathbf{Cst} \tag{2.21}$$

Now, ϕ_1 being frozen by the BNS damping condition, there exist at least two possibilities for a natural choice of the phase ϕ_2.

- Condition I: by imposing on the tail particles and on the head ones, to have the same final energy, i.e. $E_f(\sigma_t) = E_f(\sigma_h)$.

- Condition II: by cancelling, at the middle of the bunch, the derivative of the function E_f, i.e $E_f'(z_m) = 0$, where $z_m = (\sigma_t + \sigma_h)/2$.

In fact, due to the particular form of the function $E_f(z)$ (any sum of sinusoids), it can be easily verified that these two conditions are identical, and equivalent to[9]:

$$\begin{aligned} &E_f(\sigma_t) = E_f(\sigma_h) \iff E'_f(z_m) = 0 \iff \\ &L_1 \sin\left(\frac{\omega_{RF} z_m}{c} - \phi_1\right) + L_2 \sin\left(\frac{\omega_{RF} z_m}{c} - \phi_2\right) = (L_1 + L_2) \sin\left(\frac{\omega_{RF} z_m}{c} - \phi_W\right) \end{aligned} \tag{2.22}$$

Finally, we will remember the linearised version of the previous equation,

$$\frac{L_1 \phi_1 + L_2 \phi_2}{L_1 + L_2} = \phi_W \tag{2.23}$$

which describes simply the fact that the RF phase, averaged over the whole linac, has to be equal to the phase ϕ_W, defined by the shape of the longitudinal wake potential, by the RF frequency and by the accelerating gradient (Eq. (2.14)).

2.2.3 Equivalence between the two options: formulation of the "self–BNS–damping" condition

Now, rather than use the BNS damping condition (Eq. (2.10)) in order to estimate directly the value required for ϕ_1, we prefer here to choose a roundabout way which consists in searching an equivalence between the "RFQ option" and the "energy spread option". In fact, these two options are completely equivalent if we suppose that RFQs and magnetic quadrupoles can be combined (see Paragraph 2.2.1). In this ideal case, we want $k_{\mathrm{I}}(s,z) = k_{\mathrm{II}}(s,z)$, where k_{I} and k_{II} are given by Eq. (2.17) and Eq. (2.19), respectively. Since these two functions take the same value for $z = 0$, and are quasi–linear in z for short enough bunches, the desired condition is:

$$\begin{aligned} &\left(\frac{\partial k_{\mathrm{I}}}{\partial z}\right)_{z=0} = \left(\frac{\partial k_{\mathrm{II}}}{\partial z}\right)_{z=0} \text{ leading to} \\ &\frac{\alpha_{RFQ} \cos\phi_W}{1 - \alpha_{RFQ} \sin\phi_W} = \frac{-\sin\phi_1 + \sin\phi_W}{E_0/(e\,G_{RF}\,s) + \cos\phi_1 - \cos\phi_W + \cos(\omega_{RF}\sigma_h/c - \phi_W)} \end{aligned} \tag{2.24}$$

Now, if we suppose that $e\,G_{RF}\,s \gg E_0$, and that the considered angles are small, we obtain the linearised version of the previous equation:

$$-\phi_1 = \alpha_{RFQ} - \phi_W \tag{2.25}$$

which illustrates simply the following situation: the modulation of the quadrupole strength, required by the BNS damping condition, and completely described by the parameter α_{RFQ}

[9] Do not forget that the function E_f can be written as a sum of sinusoids, uniquely because of the special choice of the longitudinal bunch distribution (see the previous paragraph). Hence, here also, the shaping of the charge distribution remains completely justified, otherwise the conditions I and II would not be equivalent anymore, and, as a result, a large energy spread would be obtained at the end of the linac (even after having fixed ϕ_2 by the one or the other of the two conditions).

(see Eq. (2.18)), has to be produced by a negative energy spread within the bunch, which is the result of the positive slope of the RF wave ($\phi_1 < 0$) during the beam acceleration, combined with the beam–loading effect.
Then, in order to minimise the RF power loss in the first part of the linac (region of spread generation), it seems feasible to choose $\phi_1 \simeq 0$ without transgressing the BNS damping condition, which leads to:

$$\phi_W = \alpha_{RFQ} \tag{2.26}$$

It is what we call, for evident reasons, the "self–BNS–damping" condition. Actually, for what concerns the CLIC main linac, the beam parameters, as well as the ones concerning the focusing lattice, the RF frequency and the RF gradient, are in a region where $\alpha_{RFQ} > \phi_W$. More precisely, we have, $\alpha_{RFQ} \sim 0.5 \sim 30°$ and $\phi_W = 12°$ [4]. Hence, we can adopt two possible strategies in order to satisfy the "self–BNS–damping" condition.

- Increase ϕ_W by acting essentially on the beam parameters (decrease the bunch length or increase the bunch charge: see Eq. (2.15)). Nevertheless, by coming back to Eq. (2.23), which controls the value of the RF phase ϕ_2 in the second part of the linac, and using Eq. (2.26), we have:

$$\phi_2 = \frac{L_1}{L_2}\,\alpha_{RFQ} + \phi_W = \frac{L}{L_2}\phi_W \tag{2.27}$$

  which imposes on ϕ_W to be as small as possible.

- Decrease α_{RFQ}, leaving the value of ϕ_W unchanged, by decreasing the value of the β–function all along the linac (see Eq. (2.18)).

We will then adopt the second strategy in the CLIC main linac (see example IV of Chapter 3), since actually the "RFQ option" may not be optimum for reasons which will be explained in the next chapter (see example II of Chapter 3). Then, referring to Eq. (2.18), the "self–BNS–damping" condition is reached if the average value of the β function is divided by the factor $(\alpha_{RFQ_{old}}/\phi_W)^{1/2} \sim 1.6$ (i.e if the number of quadrupoles is roughly multiplied by a factor 1.6, keeping constant the phase advance per FODO cell).
Finally, supposing that the focusing has been fixed in order to satisfy the "self–BNS–damping" condition, as well as the other parameters, G_{RF}, ω_{RF}, N_b, and σ_z (also for some other reasons [18]), it only remains for us to choose the length, L_2, of the second part of the linac where the spread has to be compensated (assuming that the total length of the linac to be given by $L = (E_{out} - E_{in})/(G_{RF}\cos\phi_W)$. Using Eq. (2.21) and Eq. (2.22) with $\phi_1 = 0$, the final energy of the bunch is given by[10]:
$E_f(z) \simeq E_f(0) = \mathbf{cst} + G_{RF} L \cos\phi_W\, E_r(x)$, where $x = L_2/L$, $\mathbf{cst} = E_0 - L\, W_L(0)$, and where,

$$E_r(x) = \frac{1 - x + x\sqrt{1 - \sin^2\phi_W/x^2}}{\cos\phi_W} \tag{2.28}$$

which compares, in term of beam acceleration, two different linacs:

[10] In Eq. (2.22), we assume $z_m \approx 0$, which is effectively the case for the CLIC main beam parameters ($\omega_{RF}\, z_m/c \approx 3°$).

- a linac, where the "energy spread option" has been chosen, and where the "self–BNS–damping" condition is satisfied.

- an hypothetical linac (or reference linac), where any kind of BNS damping would be required, and where the RF phase is taken equal to ϕ_W all along the line.

Firstly, we see that Eq. (2.28) fixes a minimum value for the choice of L_2: $L_{2_{min}} = \sin\phi_W\, L$. Secondly, we can verify that the function $E_r(x)$ is strictly increasing, from the value $E_r(\sin\phi_W) = 1-\sin\phi_W$ up to the value $E_r(1) = 1$ which corresponds to a linac where the region of spread generation has disappeared. Consequently, there is no optimum choice for L_2; simply, this length has to be greater than $\sin\phi_W\, L$, in order to have a solution for the energy spread minimisation at the end of the linac, not too large compared to L_1, in order to preserve the bunch emittance growth[11], but also not too small in order to maximise the bunch energy gain (in example IV of Chapter 3, the choice will be "2/3–1/3")

2.3 Some natural scaling laws imposed by the "self–BNS–damping" condition

We will finish here, by the derivation of simple scaling laws linking the optics of the line (β function, number of quadrupoles, quadrupole length and electrical power for the quadrupole supply) to the beam parameters, and resulting from the so–called "self–BNS–damping" condition (Eq. (2.26)). Here, we suppose that the injection energy of the bunch as well as its final energy are fixed quantities, so that the dependences according to γ_{in} and γ_{out} will be deliberately omitted in all the scaling laws which will be derived hereafter. Firstly, using the fact that ϕ_W has to remain relatively small, we obtain directly from Eq. (2.15):

$$\frac{N_b\ \omega_{RF}}{G_{RF}\ \sigma_z} \approx \mathbf{cst} \tag{2.29}$$

Secondly, using Eq. (2.15), (2.18) and (2.26), we have:

$$\overline{\beta}(\gamma) = \beta_0 \left(\frac{\gamma}{\gamma_{in}}\right)^{\alpha_\beta} \text{ where } \beta_0 \propto \frac{1}{\omega_{RF}\ G_{RF}^{1/2}\ \sigma_z^{1/2}} \text{ and } \alpha_\beta = \frac{1}{2} \tag{2.30}$$

in which the bunch charge, N_b, has naturally disappeared[12]. In fact, for the CLIC main linac, the phase advance per cell is not kept constant along the linac (see Paragraph 3.2.2), and therefore the scaling of $\overline{\beta}(\gamma)$ with the square root of the energy is not completely exact anymore; we will then remember $\alpha_\beta \sim 1/2$ (for CLIC $\alpha_\beta \simeq 0.4$ [21]).

[11] Note that even in the second region of the linac, and up to the end of the line, the bunch energy spread remains negative.

[12] We correct the "head–tail" effect which is proportional to the bunch charge, by using the intra–bunch energy spread which is generated by beam–loading, and then, which is also proportional to the bunch charge.

Then, if we neglect the finite quadrupole length, the total number of quadrupoles, N_q, verifies the condition:

$$\sum_{n=1}^{N_q} L_{FODO_n} = \frac{\gamma_{out} - \gamma_{in}}{\gamma'_{RF}} \qquad (mc^2\,\gamma'_{RF} \stackrel{def}{=} e\,G_{RF})$$

where L_{FODO_n} is the distance between the quadrupoles number n and $n+1$. Agreeing a scaling of L_{FODO} with the energy (see Paragraph 3.2.2), $L_{FODO} = L_0(\gamma/\gamma_{in})^{\alpha_L}$ with $L_0 \propto \beta_0$ (and $\alpha_L \sim 0.3$ for CLIC [21]), and referring to Appendix D, we obtain:

$$N_q \simeq \frac{\gamma_{in}(1+(\gamma_{out}-\gamma_{in})/\gamma_{in})^{1-\alpha_L}}{1-\alpha_L}\,\frac{1}{\gamma'_{RF}L_0} \propto \frac{\omega_{RF}\;\sigma_z^{1/2}}{G_{RF}^{1/2}} \tag{2.31}$$

For what concerns, the maximum length, L_q^{max}, of the quadrupoles at the end of the line (high energy), we use the well-known formula: $gL_{FODO} = \sin(\mu/2) = \sin(\mu_0/2)(\gamma/\gamma_{in})^{\alpha_\mu}$ (with $\alpha_\mu \sim -0.1$ for CLIC, see Paragraph 3.2.2, Eq. (3.2)), where $g = B_0/a\,L_q/(mc\gamma/e)$ is the integrated quadrupole strength. Except for super-conducting magnets, the maximum magnetic field, B_0^{max}, which can be obtained at the pole tips, is roughly the same in all the quadrupole designs ($B_0^{max} \sim 1$ T). Hence, using the usual scaling of the beam pipe aperture with the inverse of the RF frequency, we obtain finally:

$$L_q^{max} = \frac{\sin(\mu_0/2)\,mc/e}{B_0^{max}}\,\gamma_{in}\left(\frac{\gamma_{out}}{\gamma_{in}}\right)^{\alpha_\mu-\alpha_L+1}\frac{a}{L_0} \propto G_{RF}^{1/2}\;\sigma_z^{1/2} \propto \omega_{RF}^{1/2}\,N_b^{1/2}\;^{13} \tag{2.32}$$

Moreover, assuming the quadrupole gradient to be equal to B_0^{max}/a all along the linac, we have:

$$L_q(\gamma) = L_{q0}\left(\frac{\gamma}{\gamma_{in}}\right)^{\alpha_\mu-\alpha_L+1} \quad \text{with } L_{q,0} \propto G_{RF}^{1/2}\;\sigma_z^{1/2} \propto \omega_{RF}^{1/2}\,N_b^{1/2} \tag{2.33}$$

Lastly, we note $\mathcal{P}$, the average electrical power required for the quadrupole supply; we have:

$$\mathcal{P} = \frac{1}{2}\sum_{n=1}^{N_q} R_{\omega n}\;I_n^2$$

where $R_{\omega n} \propto L_{q,n}\,n_T/(\sigma S)$ is the electrical resistance of the coils of quadrupole n (S being the section of the copper wires, σ, the copper conductivity, n_T, the number of turns in the quadrupole coils [14], and $L_{q,n}$, the length of the considered quadrupole) and where the current I_n, supplying the quadrupole n, is proportional to $B_{0n}a/n_T$ (see for example Ref. [20]). Thus, keeping the assumption made in Eq. (2.33)[15], we obtain:

$$\mathcal{P} \propto \frac{1}{2}\,\frac{a^2\,B_0^{max^2}\,L_{q0}}{n_T\sigma S}\;\sum_{n=1}^{N_q}\left(\frac{\gamma_n}{\gamma_{in}}\right)^{\alpha_\mu-\alpha_L+1}.$$

[13] We suppose that the initial phase advance μ_0 is quasi–identical for all the linac designs , close to 90°.

[14] We assume n_T and S to be the same for all the quadrupoles of the linac.

[15] $B_0 = B_0^{max}$ for all the quadrupoles within the line, implies that the total quadrupole length is minimum and that the power consumption is maximum.

$$\text{But, } \sum_{n=1}^{N_q} \left(\frac{\gamma_n}{\gamma_{in}}\right)^{\alpha_\mu-\alpha_L+1} = \frac{1}{\gamma'_{RF}L_0} \sum_{n=1}^{N_q} \left\{ \left(\frac{\gamma_n}{\gamma_{in}}\right)^{\alpha_\mu-2\alpha_L+1} \overbrace{\left[\gamma'_{RF}L_0 \left(\frac{\gamma_n}{\gamma_{in}}\right)^{\alpha_L}\right]}^{\gamma_{n+1}-\gamma_n} \right\}$$

$$\simeq \frac{1}{G_{RF}L_0} \int_{\gamma_{in}}^{\gamma_{out}} d\gamma \left(\frac{\gamma}{\gamma_{in}}\right)^{\alpha_\mu-2\alpha_L+1} \propto \frac{1}{G_{RF}L_0}\text{, so that:}$$

$$\mathcal{P} \propto \frac{L_{q0}\, a^2}{L_0\, G_{RF}\, n_T\, S\, \sigma} \propto \frac{\omega_{RF}^{-1}\, \sigma_z}{n_T\, S\, \sigma} \tag{2.34}$$

which surprisingly decreases with the RF frequency, even if stronger wakefields (high frequency) require a stronger focusing, characterised by more quadrupoles, Eq. (2.31), and longer quadrupoles, Eq. (2.32) or (2.33).

Chapter 3

From the "RFQ option" to the "energy spread option" in the CLIC main linac

The statistical method presented in Chapter 1 has been directly applied to the study of the CLIC main linac in single–bunch operation (500 GeV, centre of mass). We will start by recalling the CLIC main beam parameters at the line input, as well as the ones relative to the linac layout and to the focusing lattice (Section 1). After that, the theoretical considerations of Chapter 2 will be numerically investigated, in order to deduce a new focusing lattice for the CLIC main linac, without RFQ, and with a reinforced optics that allows it to satisfy the "self–BNS–damping" condition.

3.1 CLIC main beam parameters

Bunch charge $[10^{10}\, e]$	$N_b = 0.8$	0.8
Bunch length $[\mu$m$]$	$\sigma_z = 195$	165
Head truncation $[\sigma_z]$	$\sigma_h = 1.3$	1.3
Tail truncation $[\sigma_z]$	$\sigma_t = 1.8$	1.7
Injection energy [GeV]	$E_0 = 9$	9
Vertical normalised emittance [mrad]	$< \gamma_0 > \epsilon_y = 5\,10^{-8}$	$5\,10^{-8}$
Emittance ratio (hor./vert.)	$\epsilon_x/\epsilon_y = 29$	29
RF frequency [GHz]	$f_{RF} = 29.9855$	29.9855
Accelerating gradient [MV/m]	$G_{RF} = 80$	100

Table 3.1: Old and new CLIC main beam parameters

The old and updated CLIC main beam parameters [1], [5] are reported in Tab. 3.1 (first and second column, respectively). The main difference between these two sets of parameters lies in an increase by 25 % of the accelerating gradient and in a reduction of the bunch length which satisfies Eq. (2.15), so that the angle ϕ_W defined in Paragraph 2.2.1 remains the same in both cases, and equal to 12°.

3.2 A realistic model for the CLIC main linac

3.2.1 Brief description of the CLIC main linac lattice

The CLIC main linac is made up of a succession of several girders, jointed one to another with the aid of small bellows (for the pre–alignment requirements), and on top of which, the beam line components are fixed (except the quadrupoles, the supports of which being independent of the ones of the girders). Each girder is composed of one BPM, ahead of it [1] [2], and of four sections, which are "filled" by accelerating structures or by quadrupoles. For what concerns the old linac layout (Fig. 3.1), the line was assumed to contain short–size (1 section), medium–size (2 sections) or long–size (3 sections) quadrupoles [4], compared to quadrupoles of two or four sections in the actual design (Fig. 3.2) which are required for a better adaptation of the focusing lattice between the main linac and the drive linac. Lastly, when the linac contains microwave quadrupoles (examples I-II referring to the first column of Tab. 3.1, for what concerns the beam parameters, and to Fig. 3.1, for what concerns the girder layout parameters), these ones are arranged just after each magnetic quadrupoles, and their number is equal to the number of sections substituted by the considered quadrupole.

3.2.2 From a continuous scaling of the focusing with energy to an arrangement in sectors of constant focusing

Now, comes the problem of the quadrupole distribution all along the linac. Considering a beam line with a continuous scaling of the focusing with energy, it has been shown [21] that, rather than use the usual scaling of the β function with the square root of the energy, independent scalings of the cell length and of the focal length gave better results for the emittance dilution at the end of the linac, although leading to a different scaling law for β:

$$\frac{L_c(s)}{L_{c0}} = \left(\frac{\gamma(s)}{\gamma_0}\right)^{\alpha} \quad \text{and} \quad \frac{f(s)}{f_0} = \left(\frac{\gamma(s)}{\gamma_0}\right)^{\beta} \tag{3.1}$$

[1] In the old design (Fig. 3.1), the space for the BPMs were omitted, assumed to be blended with the first component of each girder.

[2] More precisely, the BPMs are assumed to be arranged every two girders, and, by default, ahead of each girder supporting a quadrupole; BPMs are therefore replaced by simple drifts, when the girder number between two quadrupoles is an odd number.

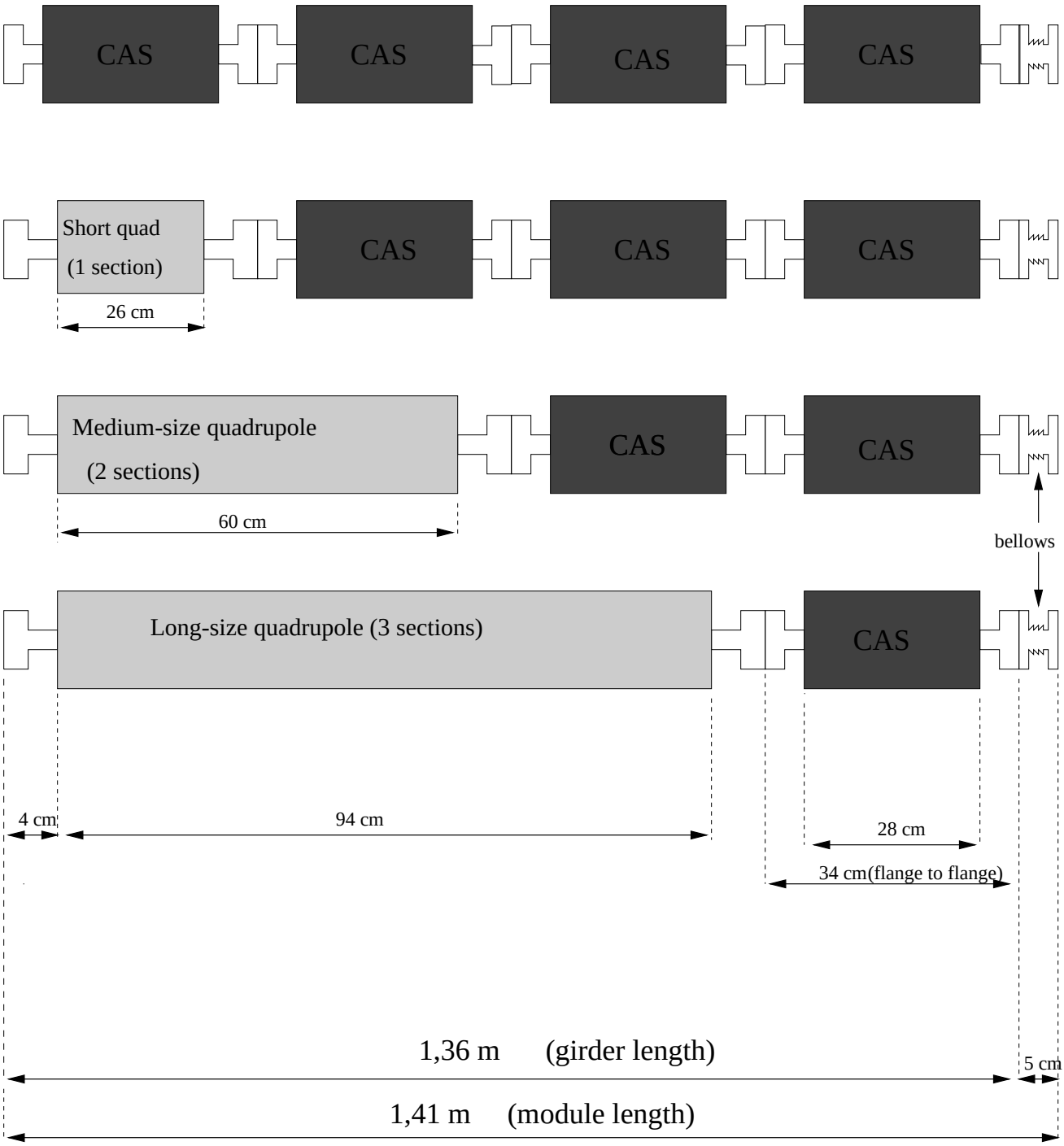

Figure 3.1: Arrangement of the beam line components on the CLIC main linac girders: old lattice

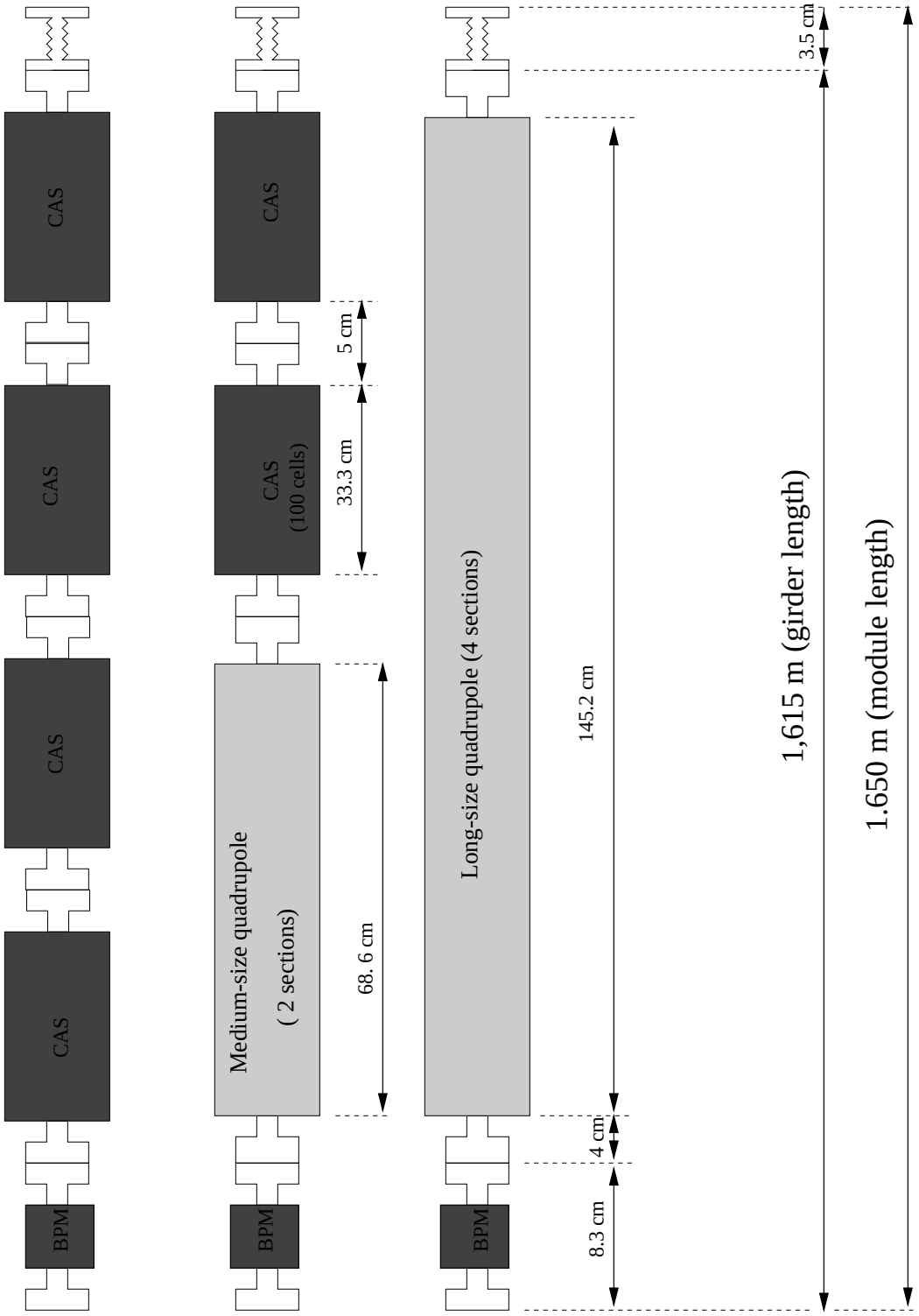

Figure 3.2: Arrangement of the beam lime components on the CLIC main linac girders: new lattice

with $\alpha = 0.3$ and $\beta = 0.4$, leading to $\overline{\beta} \approx \overline{\beta_0}(\gamma/\gamma_0)^{0.4}$.
Nevertheless, if we want to preserve the periodic succession of girders in the CLIC main linac, it becomes difficult, in practice, to implement such a focusing lattice. Then, following Ref. [4], the linac has been divided into a small number of sectors of constant focusing, (i.e constant phase advance per FODO cell and constant FODO cell length equal to an integer number of module length[3]), defining in this way a focusing lattice which approximates, by step functions, the two continuous functions given by Eq. (3.1). The strategy employed is reported hereafter, and has been automated with the help of a small program in order to pass rapidly from the first model of linac to the second one, rather more realistic.
Firstly, we start by choosing the four following parameters which define the lattice scaling:

- $\lambda_{\beta_0} = L_{c_0} 4\pi/\mu_0$, the initial betatron wave length (L_{c_0} being the initial half–cell length), and $\mu_0 = 2\arcsin(L_{c_0}/(2f_0))$, the initial phase advance per cell.

- the parameters α and β, defined by Eq. (3.1), so that the phase advance $\mu(s)$ is given all along the linac by:

$$\sin(\mu(s)/2) = \sin(\mu_0/2)(\gamma(s)/\gamma_0)^{\alpha-\beta} \tag{3.2}$$

  which generally decreases with energy ($\alpha < \beta$ for what we are concerned).

Secondly, the linac is divided, one first time, into n regions of initial and final energy, (γ_{in_i}, γ_{out_i}, $1 \leq i \leq n$), so that the quantities $L_{c_0}(\gamma_{in_i}/\gamma_0)^\alpha$ and $L_{c_0}(\gamma_{out_i}/\gamma_0)^\alpha$ are two consecutive half–integer numbers of the module length L_m, i.e $(p_i - 1/2)L_m$ and $(p_i + 1/2)L_m$, respectively. Therefore, the cell length $L_{c,i}$ is fixed in the region number i and equal to $2p_iL_m$. Then, given $L_{c,i}$ and a certain length, $L_{q,i}$, for the quadrupoles of region number i (1, 2 or 3 sections for the old lattice in Fig. 3.1, and 2 or 4 sections for the new one, Fig. 3.2), the program computes the quadrupole strength, $k_{q,i}$, which corresponds to the phase advance, μ_i, given by Eq. (3.2) with $\gamma(s) = \gamma_{in_i}$. Finally, the higher quadrupole gradient in the region i, i.e $k_{q,i}mc\gamma_{out_i}/e$, has to be lower than a given maximum value, G_q^{max}, imposed by the quadrupole design (typically 100 T/m, for what concerns the CLIC main linac), and the considered region may be subdivided into two new regions, the second one containing longer quadrupoles if the previous condition is not respected. Having done this, the last step consists of a slight modification of the sector layout, in order to minimise the total length of the linac.
The situation relative to the old lattice has been directly taken from Ref. [4] and is illustrated by Fig. 3.3. Then, the linac contains six sectors (500 GeV c.m.), and a total number of 538 quadrupoles, the gradients of which do never exceed 100 T/m (see Tab. 3.2 for a rapid description of the linac layout, and Tab. 3.3 for more details within each sector).
As said before, the new lattice requires a stronger focusing (in order to satisfy the "self–BNS–damping" condition). So, the initial betatron wave length λ_{β_0} has been drastically decreased (the other three scaling parameters remaining almost the same: see Tab. 3.2), and as a result, the number of sectors is now equal to 4 and the total number of quadrupole equal

[3]The definition of the module is one girder plus one bellow.

to 866, having supposed that the quadrupole gradients could be pushed up to 125 T/m (see Fig. 3.4 and Tab. 3.4).
We will note, in Tab. 3.2, 3.3 and 3.4, that we have assumed the RF phase to be set to $\phi_W = 12°$ all along the linac. Hence, we will remember that the values concerning the average beam energy at the linac output, or at the end of each sector, are just reference values (see the hypothetical linac defined at the end of Paragraph 2.2.3), and will become inexact, in examples II, III and IV, for the following reasons.

- In example II, we will take into consideration, among other things, the fact that the microwave quadrupoles produce an accelerating gradient which is generally lower than the one produced in the accelerating structures.

- In examples III and IV, we will try successively to adapt the "energy spread option" to the old and to the new linac.

	Old lattice	New lattice
Initial betatron wave length [m]	$\lambda_{\beta_0} = 32.72$	18.00
Initial phase advance [°]	$\mu_0 = 90.$	100.
Cell length scaling	$\alpha = 0.3$	0.3
Focal length scaling	$\beta = 0.4$	0.43
Number of sectors	6	4
Total number of quadrupoles	$N_q^{tot} = 538$	866
Maximum gradient in quadrupoles [T/m]	$G_q^{max} = 100$	125
Total length of quadrupoles [m]	385.36	952.56
Total number of cavities	$N_c^{tot} = 11420$	7636
Accelerating gradient [MV/m]	$G_{RF} = 80$	100
Total length of RF structures [m]	3197.6	2542.78
Total number of BPMs	$N_{BPM}^{tot} = 1820$	1492
Total number of girders	$N_g^{tot} = 3170$	2576
Module length [m]	$L_m = 1.41$	1.65
Total length of the linac [m]	4469.7	4250.4
Initial energy [GeV]	$E_0 = 9$	9
Final average energy [GeV]	$< E_f >= 249.44$	249.65

Table 3.2: Brief comparison between the old and the new CLIC main linac (500 GeV c.m)

Lastly, matching routines have been implemented in the program in order to adapt the optics of two consecutive sectors. Four conditions (upon α_x, β_x, α_y and β_y) have to be imposed at the sector transition; hence, it is theoretically sufficient to act on the strength of only four quadrupoles (the last two ones and the first two ones of each sector). Nevertheless, in order to make the optics more flexible and to avoid, by this way, large excursions of the function β at the transition, it has been decided [4] to act on the strength

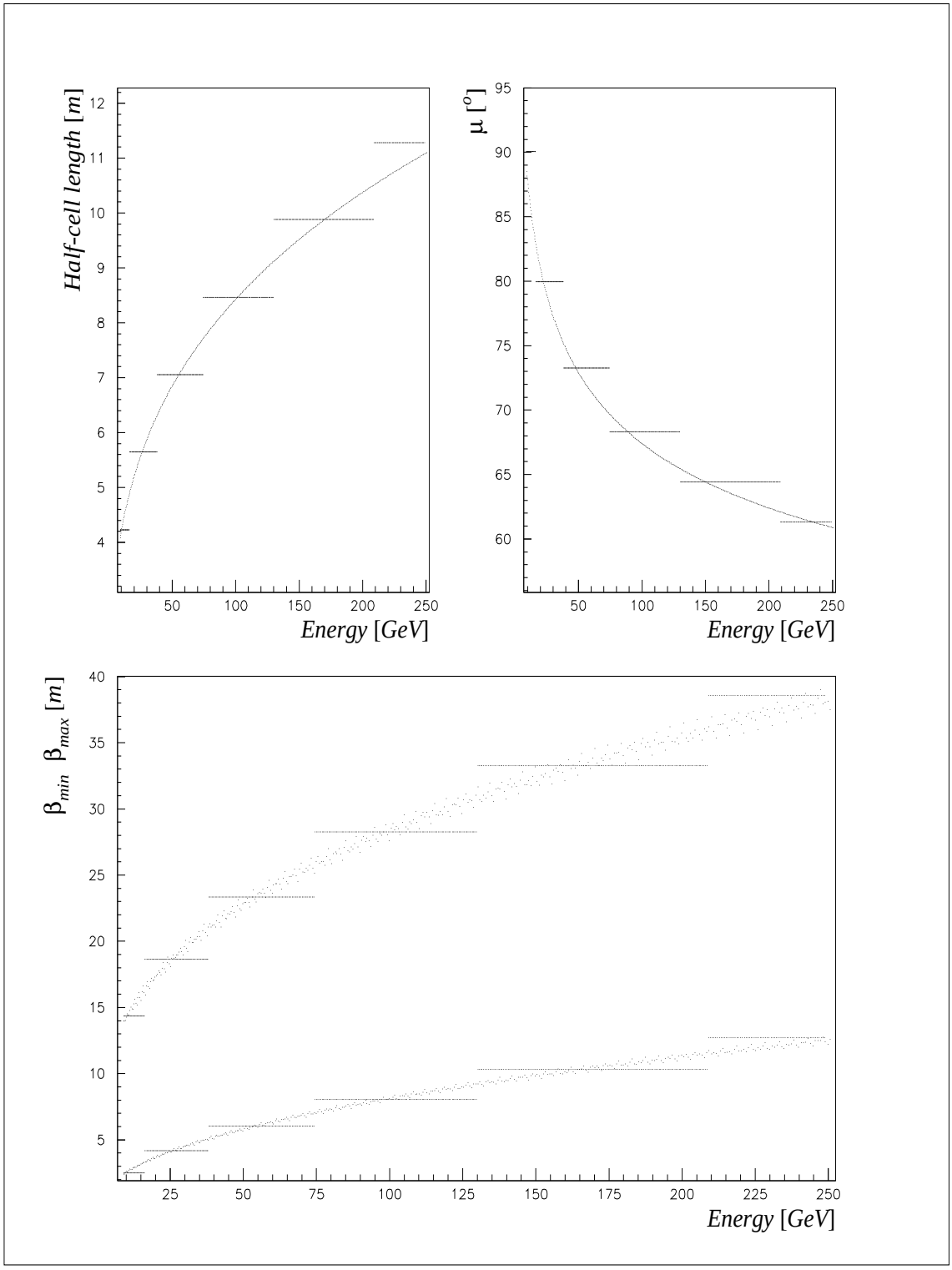

Figure 3.3: Arrangement in sectors of the CLIC main linac focusing: old lattice

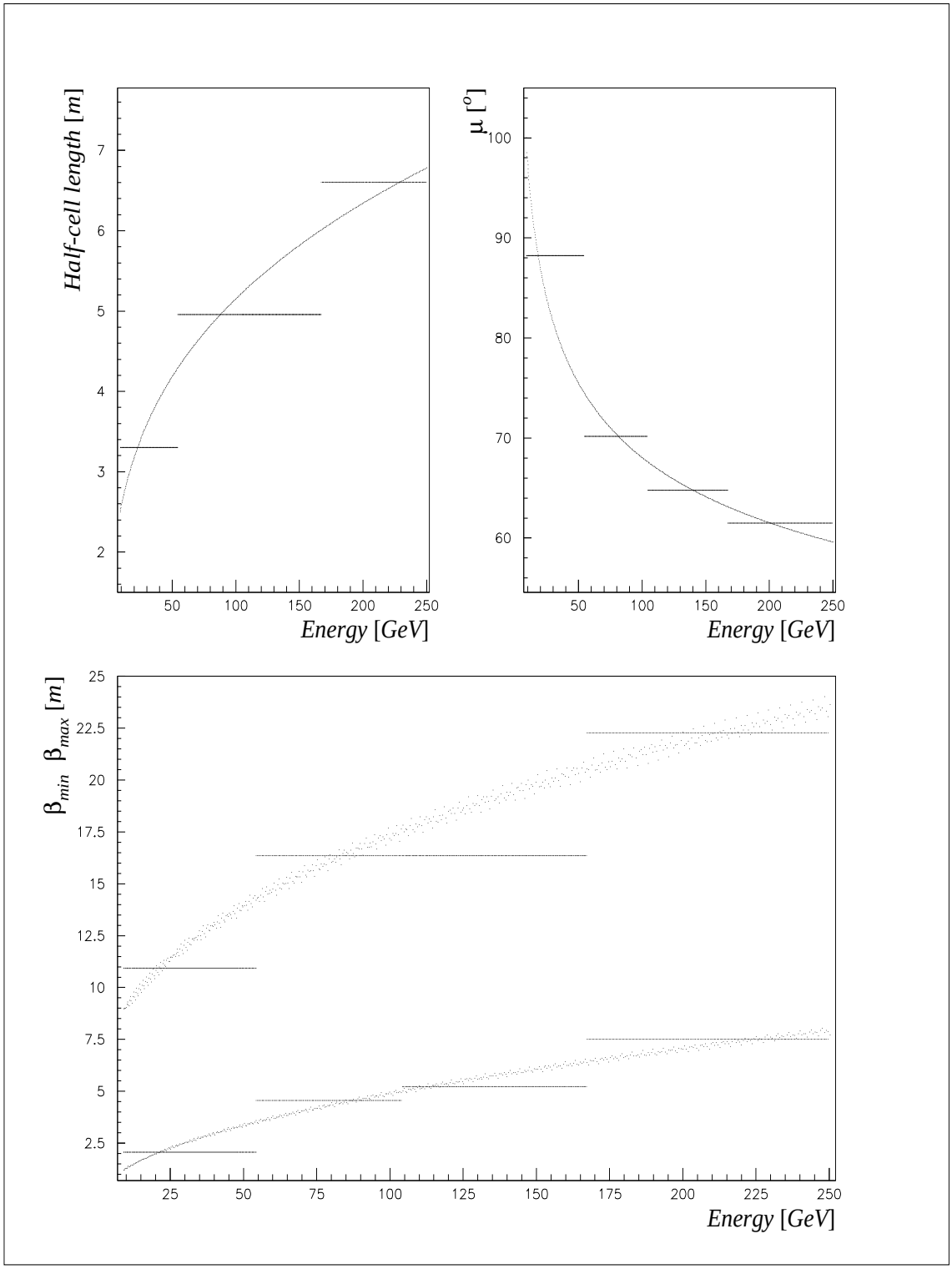

Figure 3.4: Arrangement in sectors of the CLIC main linac focusing: new lattice

of a fifth quadrupole[4] (see Appendix E, for illustration of the three transition zones in the new linac, as well as for the values of the quadrupole strengths at the transition).

	Sect. 1	Sect. 2	Sect. 3	Sect. 4	Sect. 5	Sect. 6
Number of quadrupoles	32	74	96	120	150	66
Quadrupole length [section]	1	2	2	2	3	3
Half–cell length [girder]	3	4	5	6	7	8
Quadrupole strength $[m^{-2}]$	1.3131	0.3940	0.2904	0.2266	0.1188	0.0990
Phase advance [°]	90.00	79.95	73.23	68.28	64.43	61.32
Minimum β function [m]	2.50	4.14	5.99	8.04	10.30	12.69
Maximum β function [m]	14.34	18.60	23.31	28.24	33.26	38.55
Total length [m]	135.36	417.36	676.80	1015.20	1480.50	744.48
Initial average energy [GeV]	9.00	16.41	38.22	74.60	130.19	209.14
Final average energy [GeV]	16.41	38.22	74.60	130.19	209.14	249.44

Table 3.3: Characteristics of each sector in the old linac

	Sect. 1	Sect. 2	Sect. 3	Sect. 4
Number of quadrupoles	240	158	250	218
Quadrupole length [section]	2	2	4	4
Half–cell length [girder]	2	3	3	4
Quadrupole strength $[m^{-2}]$	0.6626	0.3553	0.1662	0.1155
Phase advance [°]	88.18	70.14	64.75	61.50
Minimum β function [m]	2.06	4.54	5.21	7.48
Maximum β function [m]	10.92	16.35	16.36	22.27
Total length [m]	792.00	782.10	1237.50	1438.80
Initial average energy [GeV]	9.00	54.38	104.17	167.20
Final average energy [GeV]	54.38	104.17	167.20	249.65

Table 3.4: Characteristics of each sector in the new linac

3.2.3 A simple statistical model for the misalignments

The strategy adopted for the pre–alignment of the CLIC main linac uses the so-called double stretched wire method [22]. By modelling this pre–alignment scheme, numerical simulations have recently shown [23] that the beam line components were then distributed around a straight line, i.e $\mathbf{m}_{err} = 0$ (see Paragraph 1.3.1), and that the RMS value of the relative transverse position between two different objects depended only on their relative

[4]The matching of two consecutive sectors is then achieved with the help of the last three quadrupoles of the first considered sector and of the first two quadrupoles of the second one.

distance. More precisely, we have:

$$\left\langle \Big(dx(s_j) - dx(s_i)\Big)^2 \right\rangle_{err} = \sigma_{dx}\ |s_j - s_i|^{\alpha} \text{ with } \alpha \approx 1 \text{ and } \sigma_{dx} \approx 9\,10^{-7}\mu\text{m}$$

so that the relative transverse displacement between two components distant by 1 km is about of 30 μm. Therefore, the coefficient (i,j) of the matrix M_{err} (see Paragraph 1.3.1) is simply given by:

$$\begin{aligned}\Gamma_{err_{i,j}} \overset{\text{def}^5}{=} \langle dx(s_i)\, dx(s_i)\rangle_{err} &= \frac{1}{2}\left\langle dx^2(s_i)\right\rangle_{err} + \frac{1}{2}\left\langle dx^2(s_j)\right\rangle_{err} - \frac{1}{2}\left\langle \Big(dx(s_j) - dx(s_i)\Big)^2 \right\rangle_{err} \\ &\overset{6}{=} \frac{\sigma_{dx}}{2}\left(s_i^{\alpha} + s_j^{\alpha} - |s_j - s_i|^{\alpha}\right)\end{aligned}$$

Unfortunately, due to a lack of time, this model of misalignment is not yet implemented in the program, whereas the method presented in Chapter 1 is completely suited to study this problem. Thus, by comparison with the classical tracking method (for what concerns the misalignments of the beam line components), we have supposed that the different error sources within the line could be represented by uncorrelated Gaussian variables (i.e Γ_{err} diagonal) with the following RMS values:

- Structure misalignments : 10 μm [1].
- BPM misalignments : $\xi_d = 10$ μm [1].
- BPM resolution : $\xi_r = 0.1$ μm [24].
- Correction resolution : 0.5 μm [25].

Lastly, in all the simulations presented hereafter, we have chosen to use the WW beam based alignment method (see Paragraph 1.2.1) with the following parameters:

- Number of quadrupoles per bin : $N_q = 12$.
- Bin overlapping : 6 quadrupoles.
- Quadrupole strength resetting : $\delta = 1\%$.
- Bunch length for the non–nominal trajectories : $\sigma_z' = \sigma_z$.
- Bunch charge for the non–nominal trajectories : $N_b' = 6.\,10^8 \approx N_b/12$.
- Weight on the trajectory differences : $w_{d1} = 0$ and $w_{d2} = 1$.
- Weight on the trajectory : $w_t = 0$.

[5] Here, in order to simplify the talk, we only consider the region of the matrix Γ_{err} which contains the transverse misalignments of the beam line components.

[6] The reference straight line defining the absolute displacement of the beam line components is assumed to pass by the fixed point, $s_0 = 0$, so that $dx(s_0) = 0$.

Note that, contrary to the algorithms DF or WF, the correction methods DW or WW seem to be converging , even if no weight is given to the nominal trajectory during the minimisation process ($w_t = 0$) [26]; therefore, the tolerances on the BPM misalignments become obsolete. Nevertheless, we have to remain very cautious about this last assertion, since it is based just on numerical observations which concern the simple statistic model previously defined. Actually, the author has not found any theoretical explanation able to validate this result in the most general case, so that it might strongly depend on the statistic over the structure misalignments which results from the pre–alignment scheme?!

3.3 Example I : BNS damping with RFQs in the case where RFQs and quads are moved together

This first example is referring to the beam parameters and to the RF parameters given in the first column of Tab. 3.1 (old beam parameters [1]). The linac layout is completely defined by Fig. 3.1 and Tab. 3.3 (old linac). Here, we assume the BNS damping to be implemented by microwave quadrupoles ("RFQ option", Paragraph 2.2.1), so that the energy spread of the bunch can be controlled all along the linac choosing the RF phase equal to ϕ_W (see Fig. 3.5). Moreover, we suppose, in this example, that RFQs and magnetic quadrupoles are joint, i.e. misaligned and moved together for correction, and that the peak effective accelerating gradient is equal to G_{RF} in all the RF structures (we forget the fact that the RF gradient is lower in RFQs than in the other structures).
The main results concerning this first example are then reported hereafter:

- The final average energy is $< E_f > = 249.4$ GeV (cf. Tab. 3.3), the total energy spread is $\triangle E/E = (E_{f_{max}} - E_{f_{min}})/ < E_f > = 1.1$ %, and the energy spread RMS value is $\sigma_{\triangle E/E} = 0.22$ % (see Fig. 3.6 for the energy spectrum at the end of the linac).

- The parameters α_{RFQ} which define the RFQ strengths in each of the six sectors (see Paragraph 2.2.1, Eq. (2.11)) and which minimise the vertical emittance dilution at the end of the linac, are:

$$\alpha_{RFQ} = 0.57/0.52/0.48/0.45/0.43/0.41 \ .$$

  The final relative emittance growth is then in both transverse planes:

$$\langle \triangle (\gamma\epsilon_x) / (\gamma\epsilon_x)_0 \rangle_{err} = 3\% \text{ and } \langle \triangle (\gamma\epsilon_y) / (\gamma\epsilon_y)_0 \rangle_{err} = 20\% \ .$$

  In Fig. 3.7, we have plotted the RMS values of the quadrupole displacements imposed by the choice of the correction scheme (first column), the average emittance dilution (second column) as well as the emittance standard deviation (last column) all along the linac.

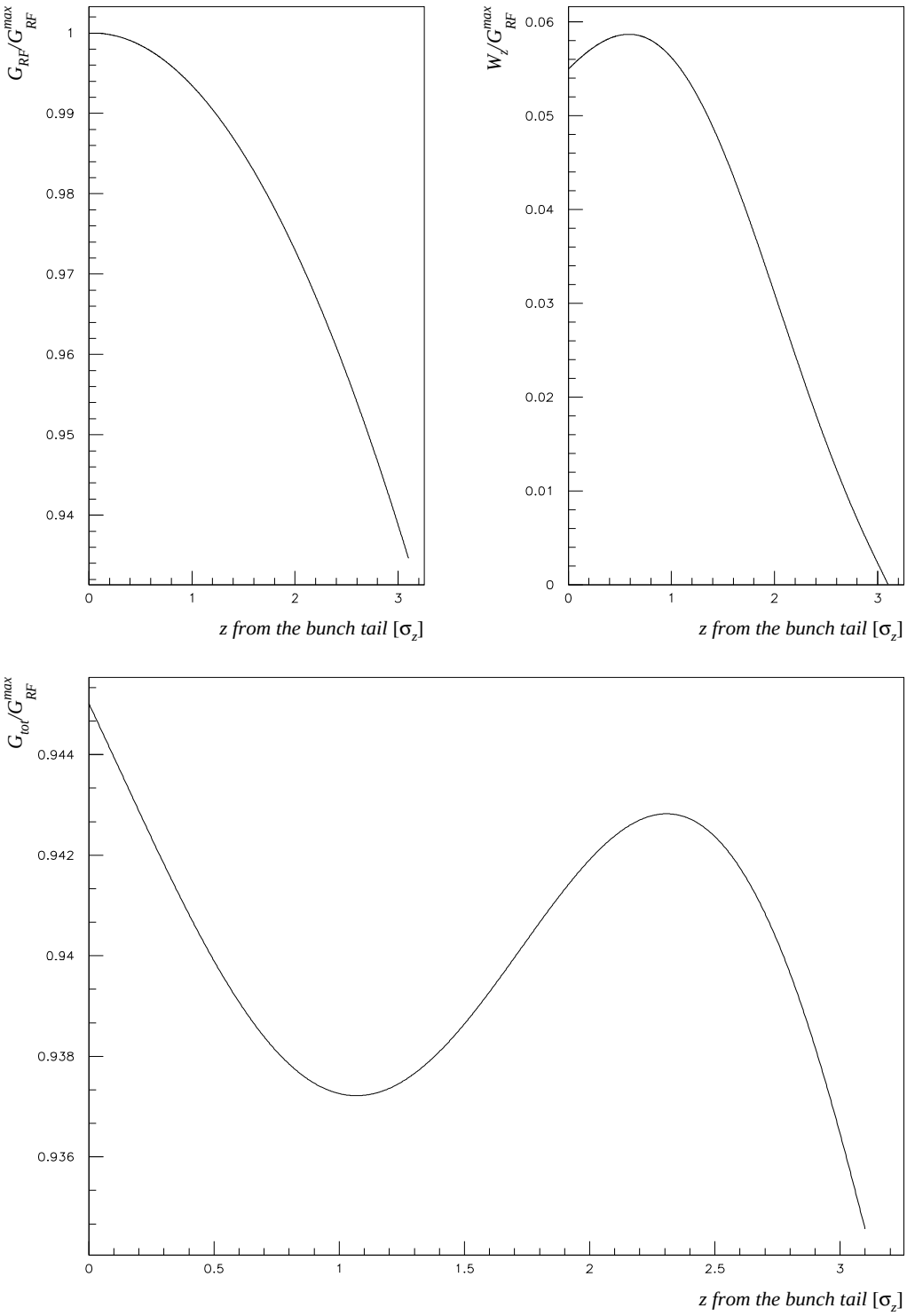

Figure 3.5: RF gradient and longitudinal wakefields in CLIC accelerating structures: old beam parameters (example I)

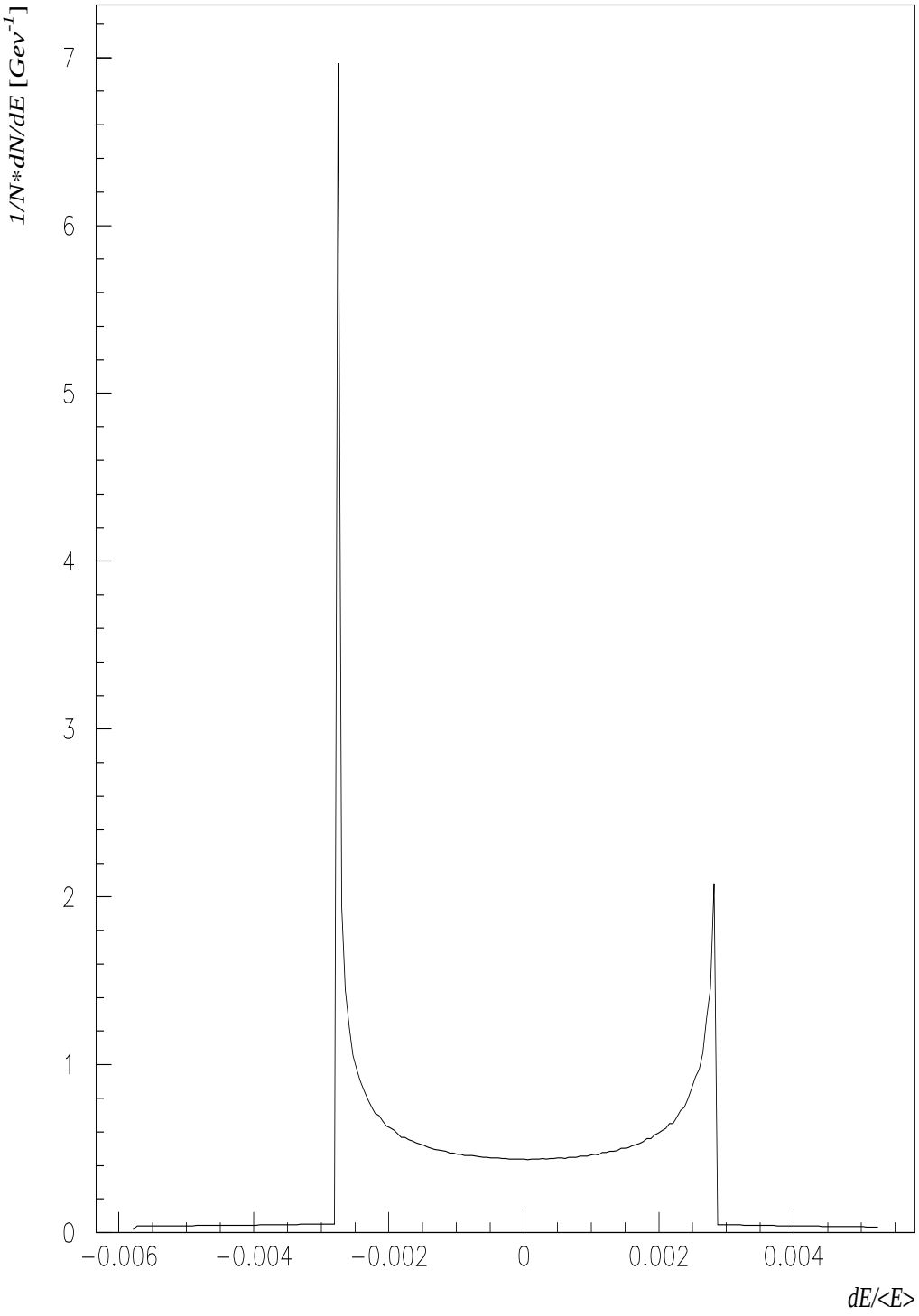

Figure 3.6: Energy spectrum at the end of the linac (example I)

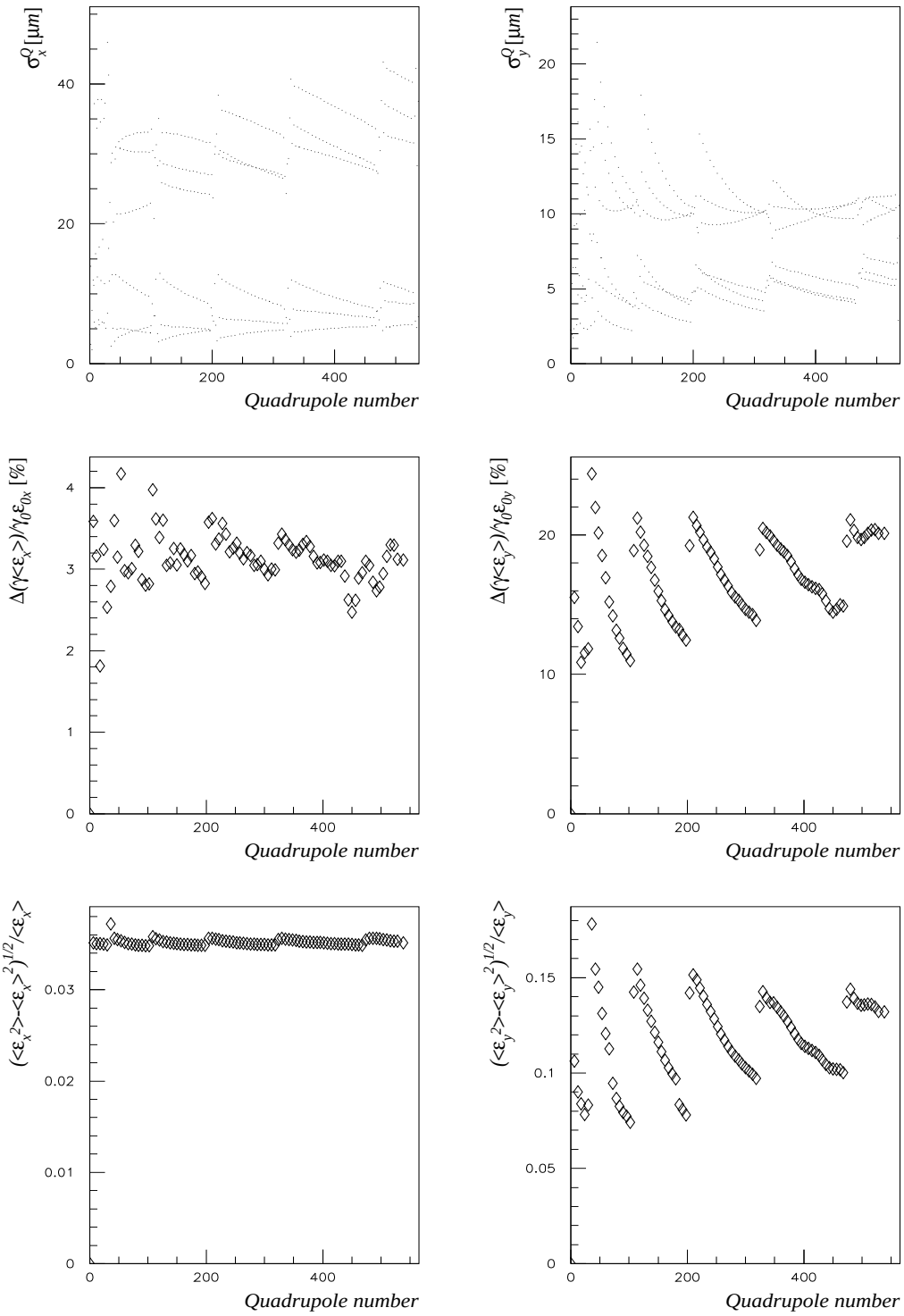

Figure 3.7: Quadrupole displacements and emittance all along the linac, resulting from the WW algorithm (example I)

3.4 Example II : example I but RFQs and quads completely separated

In this second example, we keep exactly the same linac and the same beam parameters as the ones of example I, except that the RFQs are correctly positioned, outside the quadrupoles, and then misaligned in the same way as the other accelerating structures (10 μm RMS). As a result, the final average bunch energy is slightly lower than the one previously obtained[7], $< E_f > = 234.8$ GeV, while the values concerning the energy spread remains almost identical to the ones given in example I: $\triangle E/E = 0.8$ % and $\sigma_{\triangle E/E} = 0.28$ %. However, this supplementary complication remains insignificant compared to the effect that we observe on the final emittance dilution (see Fig. 3.8):

$$\langle \triangle (\gamma\epsilon_x) / (\gamma\epsilon_x)_0 \rangle_{err} = 28\% \text{ and } \langle \triangle (\gamma\epsilon_y) / (\gamma\epsilon_y)_0 \rangle_{err} = 526\% \ .$$

due to the fact that the misaligned microwave quadrupoles behave like RF kickers, the strength of which is randomly distributed all along the linac. The solution should be the elaboration of new correction algorithms by moving in the same time the magnetic quadrupoles and the girders which support the RFQs (global translation of the girder, the girders on each side being at an angle to maintain the chain, or "triangular" displacement of two girders). Nevertheless, due to the presence of more than one RFQ per girder (position scattering) and due to the supplementary misalignments of the accelerating structures laying on the displaced girders, the results that we would obtain will probably not be as good as the ones of example I. Consequently, the possibility of doing BNS damping via a given momentum spread ("energy spread option", Paragraph 2.2.2) has been investigated: examples III and IV in the next two sections.

3.5 Example III: BNS damping with energy spread, with and without spread compensation at the end of the linac

Here, we try to use the "energy spread option" (Paragraph 2.2.2) in order to perform BNS damping, with the same linac and the same beam parameters as the ones of the two previous examples. Using Eq. (2.24) which permits to pass directly from the "RFQ option" to the "energy spread option", and taking the optimised values of the parameters α_{RFQ} given in example I, we obtain the RF phases required in each of the six sectors of the linac (which are of the same order of magnitude as the ones obtained in Ref. [28]):

$$\phi_{RF} = -50^\circ / -30^\circ / -22^\circ / -17^\circ / -14^\circ / -13^\circ \ .$$

[7] The peak effective accelerating gradient is reduced in RFQs, between 16 MV/m and 56 MV/m all along the linac.

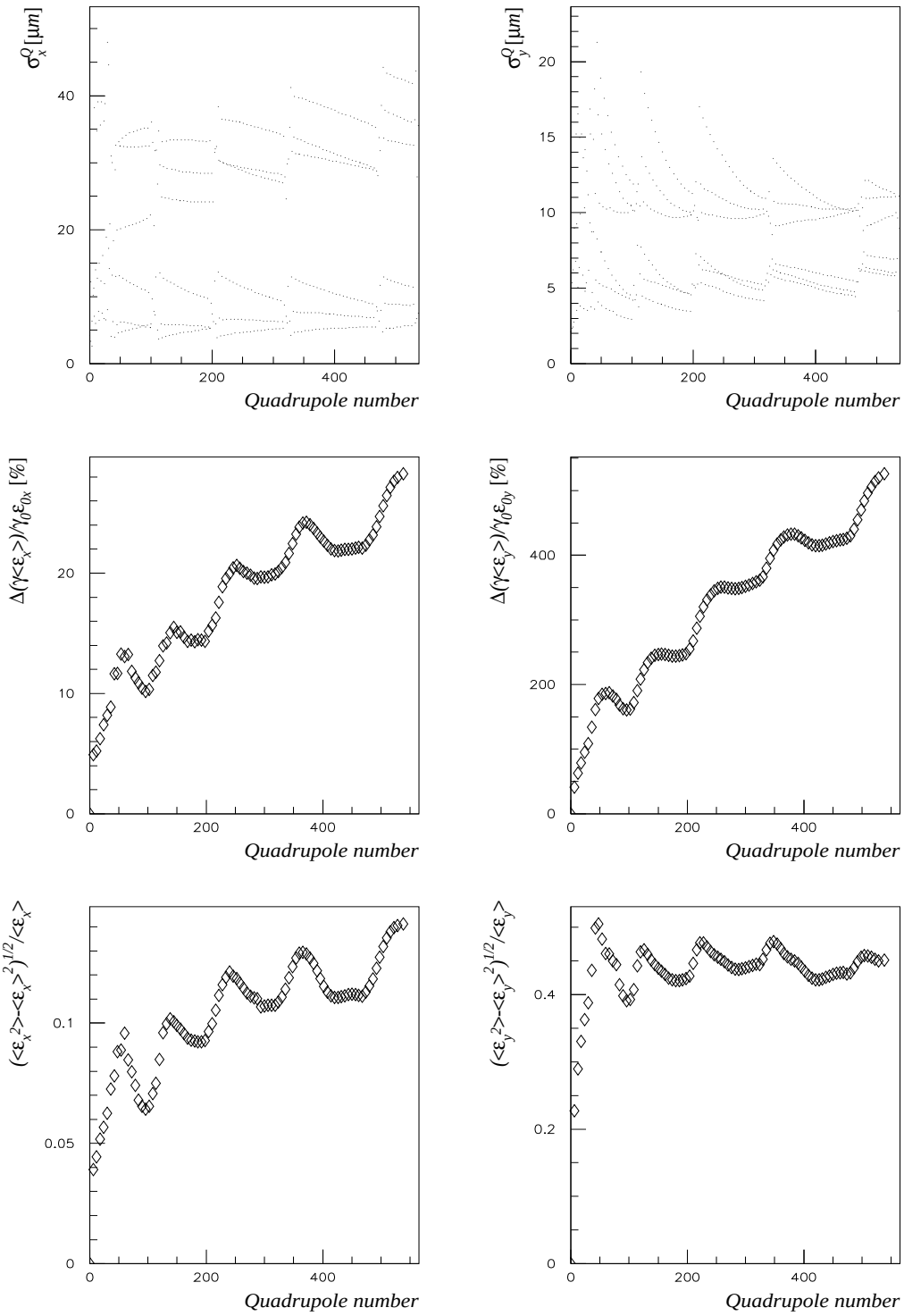

Figure 3.8: Quadrupole displacements and emittance all along the linac resulting from the WW algorithm (example II)

For the moment, we leave the problem of the energy spread minimisation aside. The final average energy of the bunch is then not too much decreased, $< E_f > = 238.5$ GeV, but the energy spread is considerable at the linac output (see Fig. 3.9): $\triangle E/E = 19.1$ % ($E_{f_{max}} \sim 260$ GeV, $E_{f_{min}} \sim 215$ GeV) and $\sigma_{\triangle E/E} = 5.0$ %. On the other hand, the results concerning the emittance dilution at the end of the linac are quasi–identical to the ones obtained in example I (see Fig. 3.10 which is very comparable to Fig. 3.7):

$$\langle \triangle (\gamma\epsilon_x) / (\gamma\epsilon_x)_0 \rangle_{err} = 3\% \text{ and } \langle \triangle (\gamma\epsilon_y) / (\gamma\epsilon_y)_0 \rangle_{err} = 26\% \ .$$

Now, we try to minimise the bunch energy spread at the end of the linac. As explained in Paragraph 2.2.2, we divide the linac into two regions: a first region (sectors I–IV, from $E_0 = 9$ GeV to $< E > \sim 130$ GeV) where the RF phase is chosen negative in order to generate the required energy spread, and a second region where the beam is accelerated with a positive RF phase (sectors V–VI) in order to minimise the final energy spread of the bunch. Then, we keep the values previously given for the RF phase in the first four sectors, and use Eq. (2.22) to compute the RF phase required in the last two sectors; we then obtain from Eq. (2.22), $\phi_{RF} = 56°$, while numerical optimisation gives $\phi_{RF} = 55°$, so:

$$\phi_{RF} = -50°/-30°/-22°/-17°/55°/55° \ .$$

Consequently, on the one hand, the final energy of the bunch is considerably reduced, $< E_f > = 189.9$ GeV, and, on the other hand, the final energy spread is deteriorated compared to example I: $\triangle E/E = 2.0$ % and $\sigma_{\triangle E/E} = 0.32$ %. Lastly, due to the large values required for the RF phases in the first part of the linac, the length of the region of spread compensation cannot be too much reduced otherwise the bunch energy spread could not be controlled anymore at the linac output; therefore, the beam–breakup instability takes place in the second part of the line, deteriorating the final emittance of the bunch (see Fig. 3.11):

$$\langle \triangle (\gamma\epsilon_x) / (\gamma\epsilon_x)_0 \rangle_{err} = 5\% \text{ and } \langle \triangle (\gamma\epsilon_y) / (\gamma\epsilon_y)_0 \rangle_{err} = 75\% \ .$$

With the old focusing lattice, we are then too far from the so–called "self–BNS–damping" condition (Eq. (2.26)), in order to adapt the "energy spread option" to the CLIC main linac: $\alpha_{RFQ} \sim 0.5 \sim 30°$ and $\phi_W = 12°$. Consequently, as explained in Paragraph 2.2.3, we have to consider stronger optics, by multiplying the number of quadrupoles by a factor close to 1.6 [8]: this is done in the next section.

3.6 Example IV : a new linac without RFQs, with stronger focusing and new beam parameters

This last example is then referring to the beam parameters and to the RF parameters given in the second column of Tab. 3.1 (new bunch length and new accelerating gradient leaving

[8] In Ref. [5], the doubling of the total number of quadrupoles had been proposed in order to reduce both single and multibunch instability. Here, the reason why the optics has to be reinforced is then completely different.

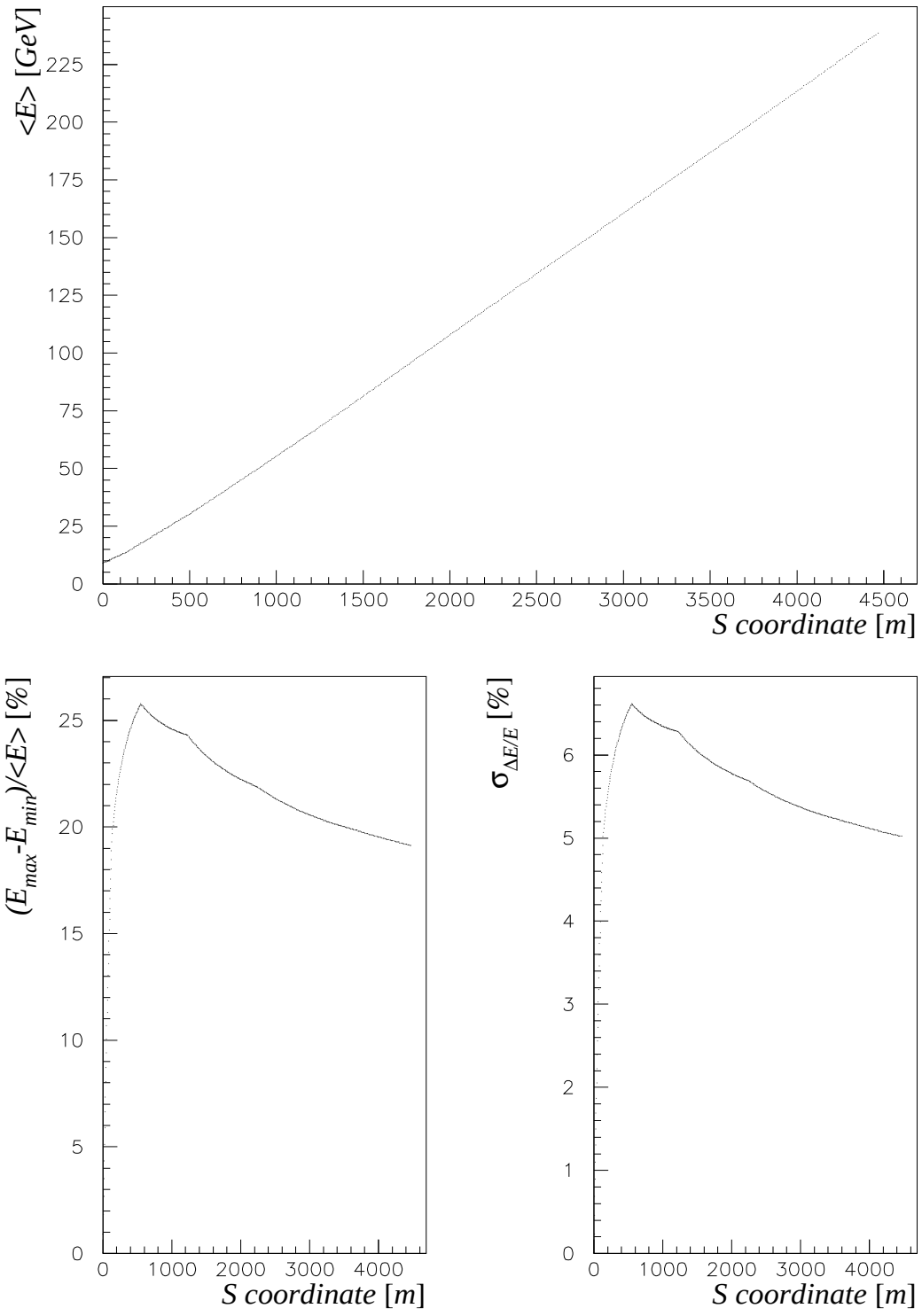

Figure 3.9: Energy and energy spread all along the linac (example III without energy spread compensation at the end of the linac)

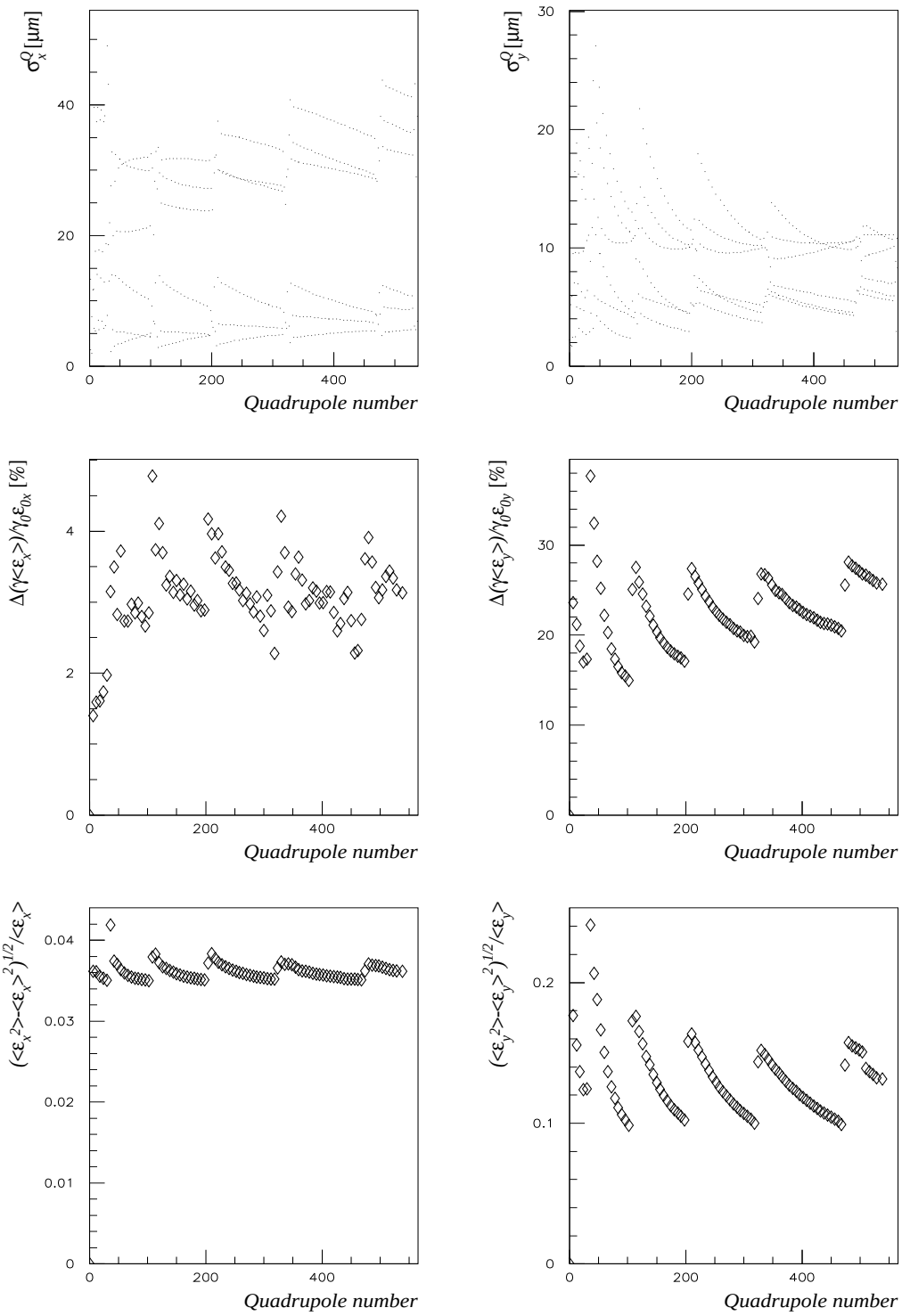

Figure 3.10: Quadrupole displacements and emittance all along the linac resulting from the WW algorithm (example III without energy spread compensation at the linac output)

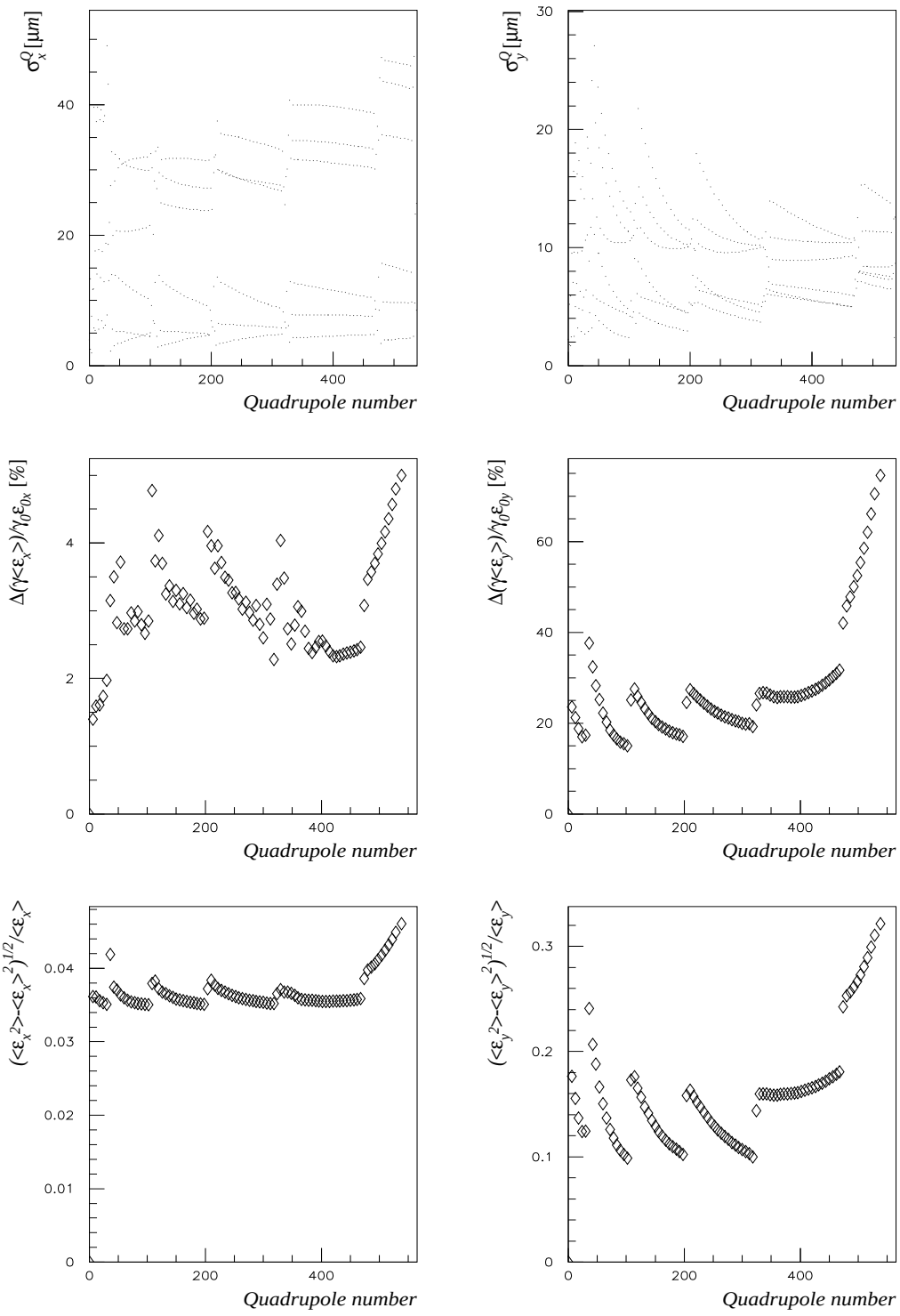

Figure 3.11: Quadrupole displacements and emittance all along the linac resulting from the WW algorithm (example III with energy spread compensation at the linac output)

the value of ϕ_W unchanged [5]). The total number of quadrupoles is now equal to 868, i.e about 1.5 times its old value. Henceforth, the focusing lattice is completely described by Fig. 3.2 and Tab. 3.4 (new linac with 4 sectors).
Now, in order to demonstrate the validity of the "self–BNS–damping" condition in this new linac, we accelerate the beam on–crest in the first three sectors (see Fig. 3.12, showing the effective accelerating field in the RF structures when $\phi_{RF} = 0$, i.e the sum of the longitudinal wakefield and of the RF field), from $E_0 = 9$ GeV to an average energy of about 170 GeV, and minimise the energy spread of the bunch at the linac output by choosing $\phi_{RF} = 37^\circ$ in the sector IV[9]; the choice for the RF phases is then:

$$\phi_{RF} = 0^\circ/0^\circ/0^\circ/37^\circ \ .$$

The final average energy of the bunch is in this case, $< E_f > = 237.7$ GeV[10]; the values relative to the total and RMS energy spread at the end of the linac are $\triangle E/E = 0.8$ % and $\sigma_{\triangle E/E} = 0.19$ %, respectively, better than the ones obtained in example I (see Fig. 3.13 for the evolution of the bunch energy spread all along the line and Fig. 3.14 for the energy spectrum of the bunch at the linac output). Moreover, the values concerning the final emittance of the bunch in both transverse planes are as satisfying as the ones obtained in example I (see Fig. 3.15):

$$\langle \triangle (\gamma\epsilon_x) / (\gamma\epsilon_x)_0 \rangle_{err} = 0.9\% \text{ and } \langle \triangle (\gamma\epsilon_y) / (\gamma\epsilon_y)_0 \rangle_{err} = 22\% \ .$$

Lastly, as announced in Paragraph 1.4.1, we observe in Fig. 3.16 that the butterfly effect is negligible (i.e $< \gamma > \det(\Sigma_0) \sim \gamma_0\epsilon_0$ all along the linac, Σ_0 being defined by Eq. (1.20)), which implies, among other things, that the emittance distribution at the line output ($\rho_{(\triangle\epsilon/\epsilon)}$ given by Eq. (1.31)) takes very rapidly non–zero values: see Fig. 3.17 which plots the distributions $\rho_{(\triangle\epsilon/\epsilon)}$ and $\mathcal{I}_2$ (Eq. (1.32)) in both transverse planes.

3.7 Recapitulation of the main results obtained in examples I–IV

Tab. 3.5 summarises and compares the main results relative to the four examples previously presented. Thus, we easily see that all the performances obtained in example I (emittance and energy spread) are entirely reproduced in the last example, dealing with a more realistic model of linac, without RFQs and with reinforced focusing.

[9] The region of spread generation represents roughly two thirds of the total effective length of the linac (compared to one half in example III), so that, according to Eq. (2.27), we obtain, $\phi_{RF} \sim 3\,\phi_W \sim 36^\circ$, which is checked by simulation.

[10] The relative loss of energy according to a final energy of 250 GeV is then of just 4.9 % $\sim 1 - E_r(1/3) = 0.052$, where the function $E_r(x)$ is defined by Eq. (2.28).

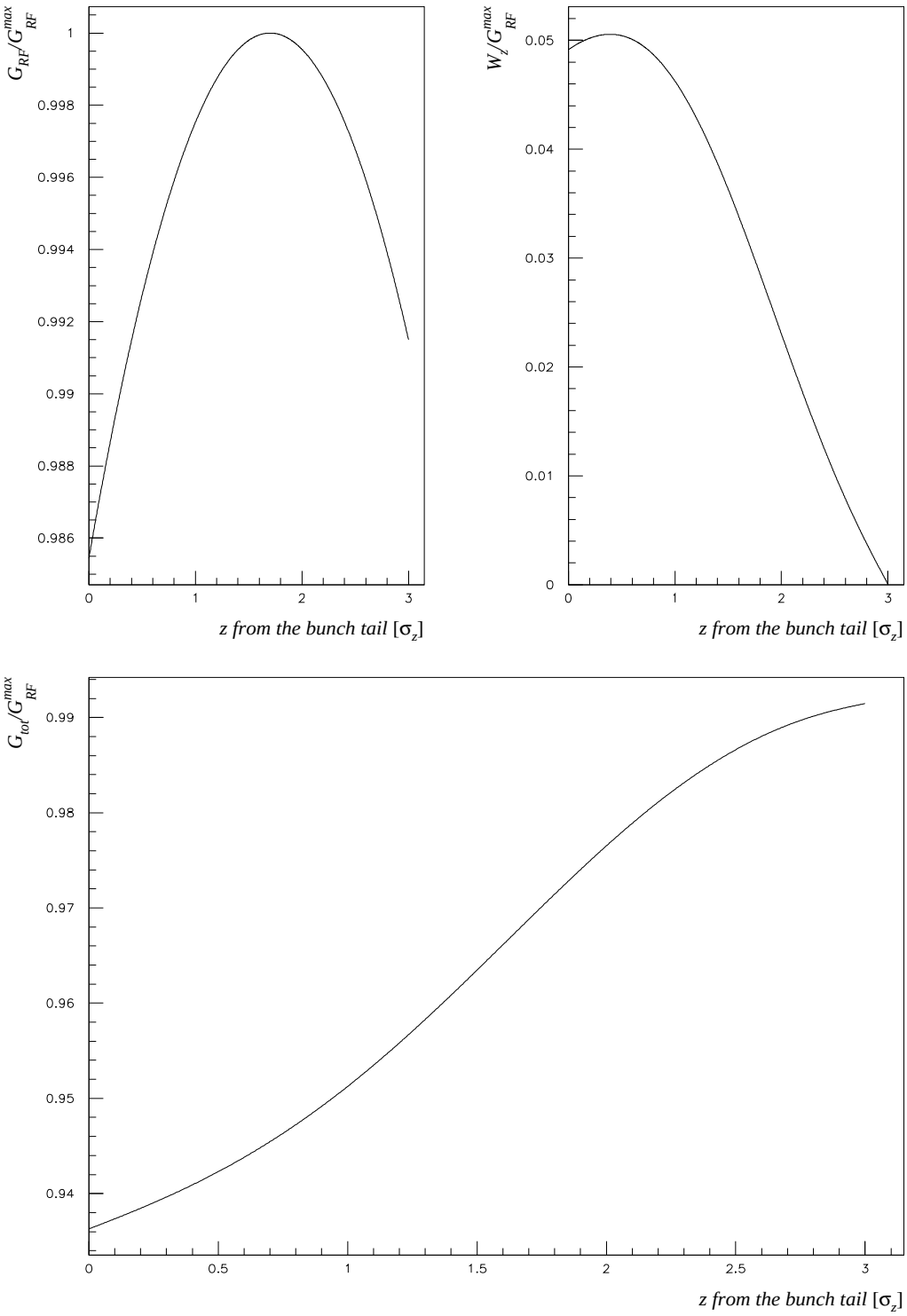

Figure 3.12: RF gradient and longitudinal wakefields in CLIC accelerating structures: new beam parameters (example IV)

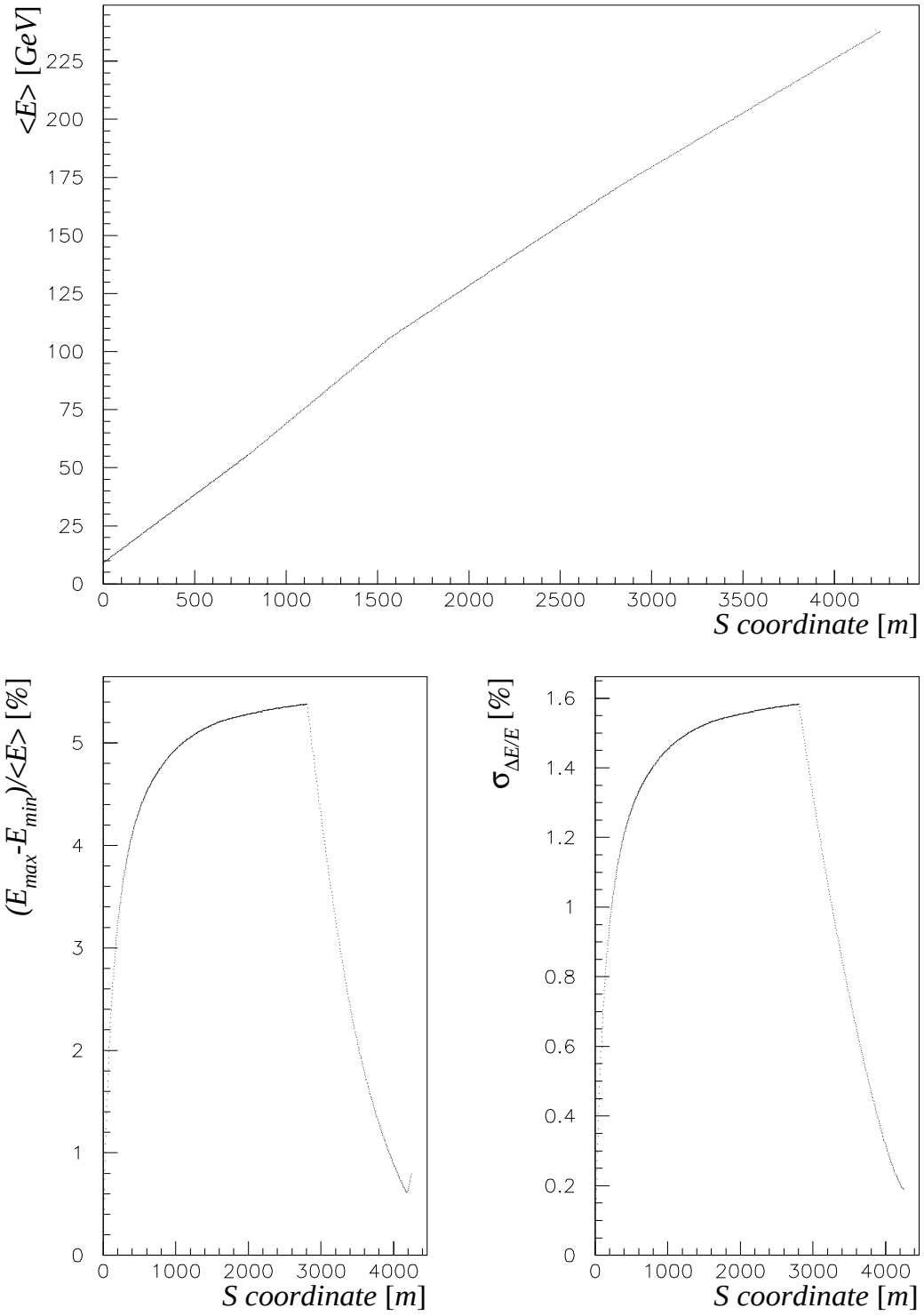

Figure 3.13: Energy and energy spread all along the linac (example IV)

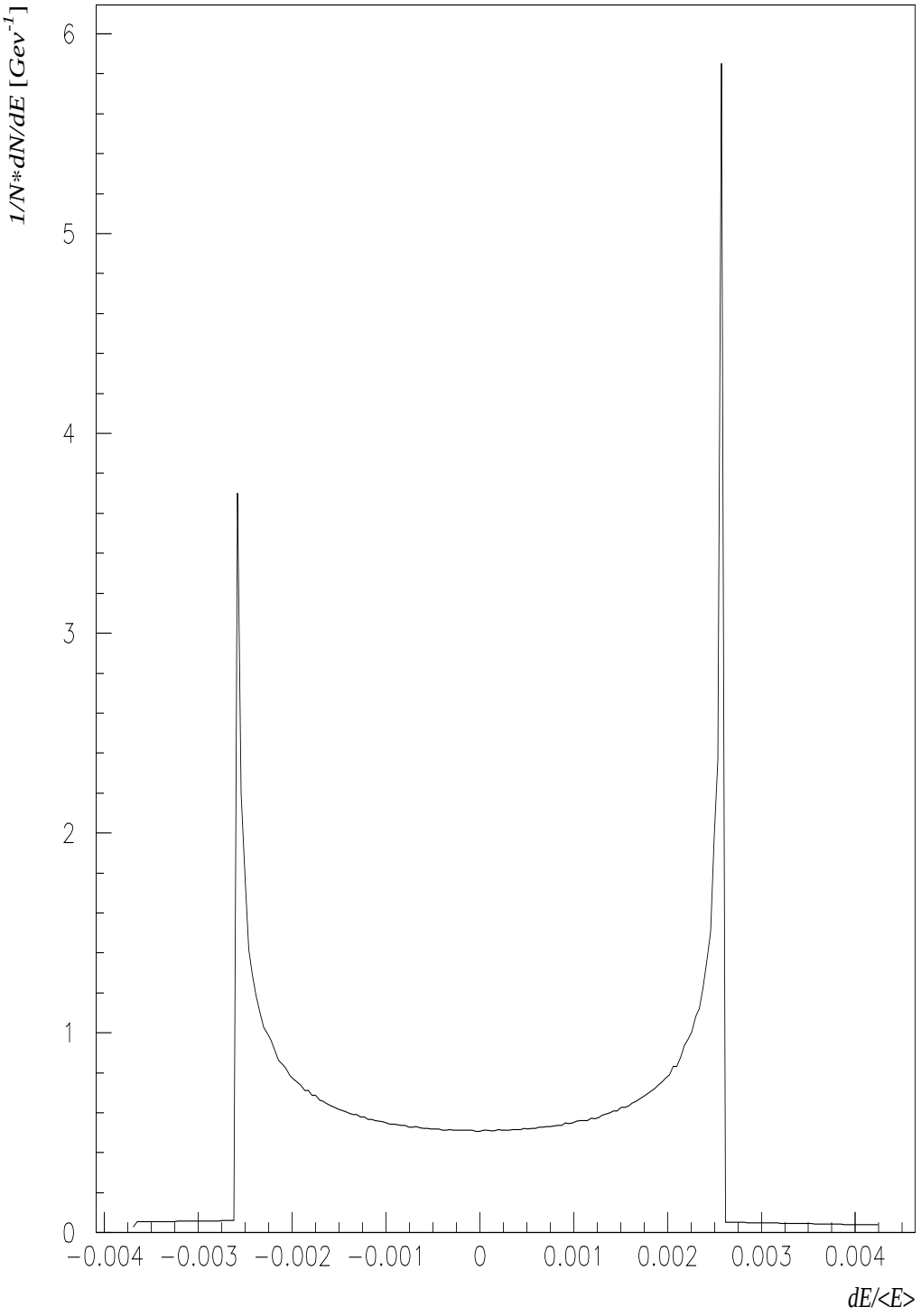

Figure 3.14: Energy spectrum at the end of the linac (example IV)

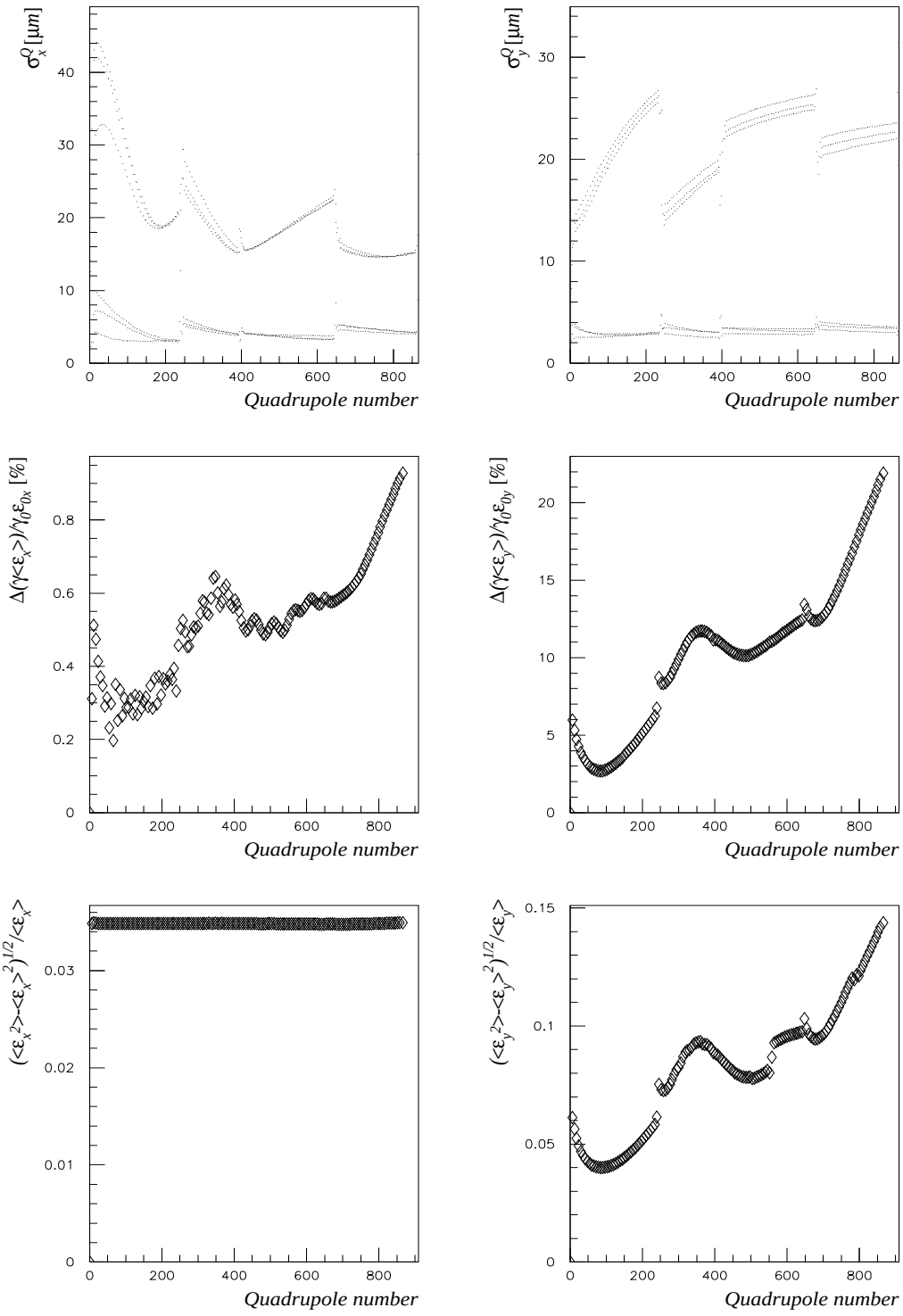

Figure 3.15: Quadrupole displacements and emittance all along the linac resulting from the WW algorithm (example IV)

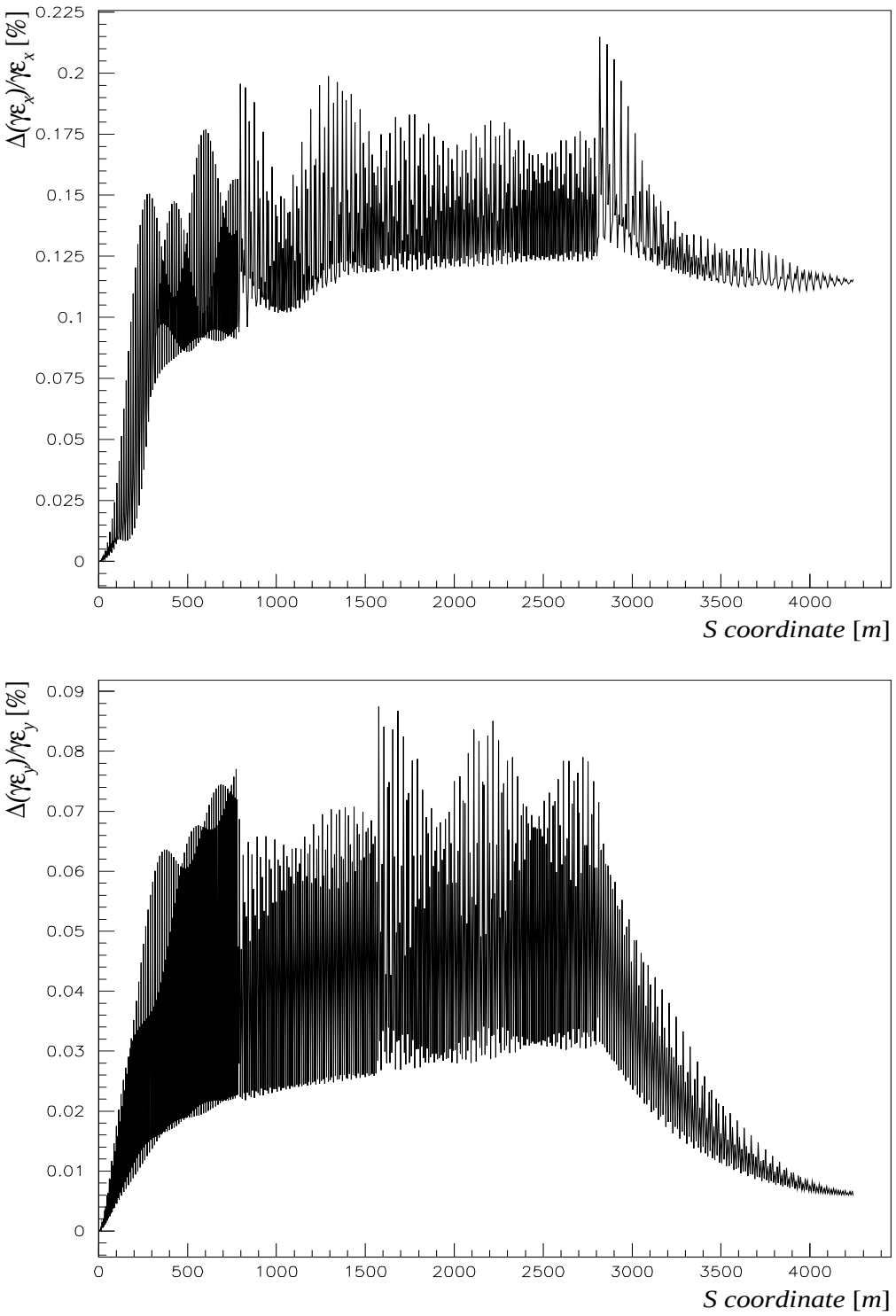

Figure 3.16: Illustration of the butterfly effect all along the linac (example IV)

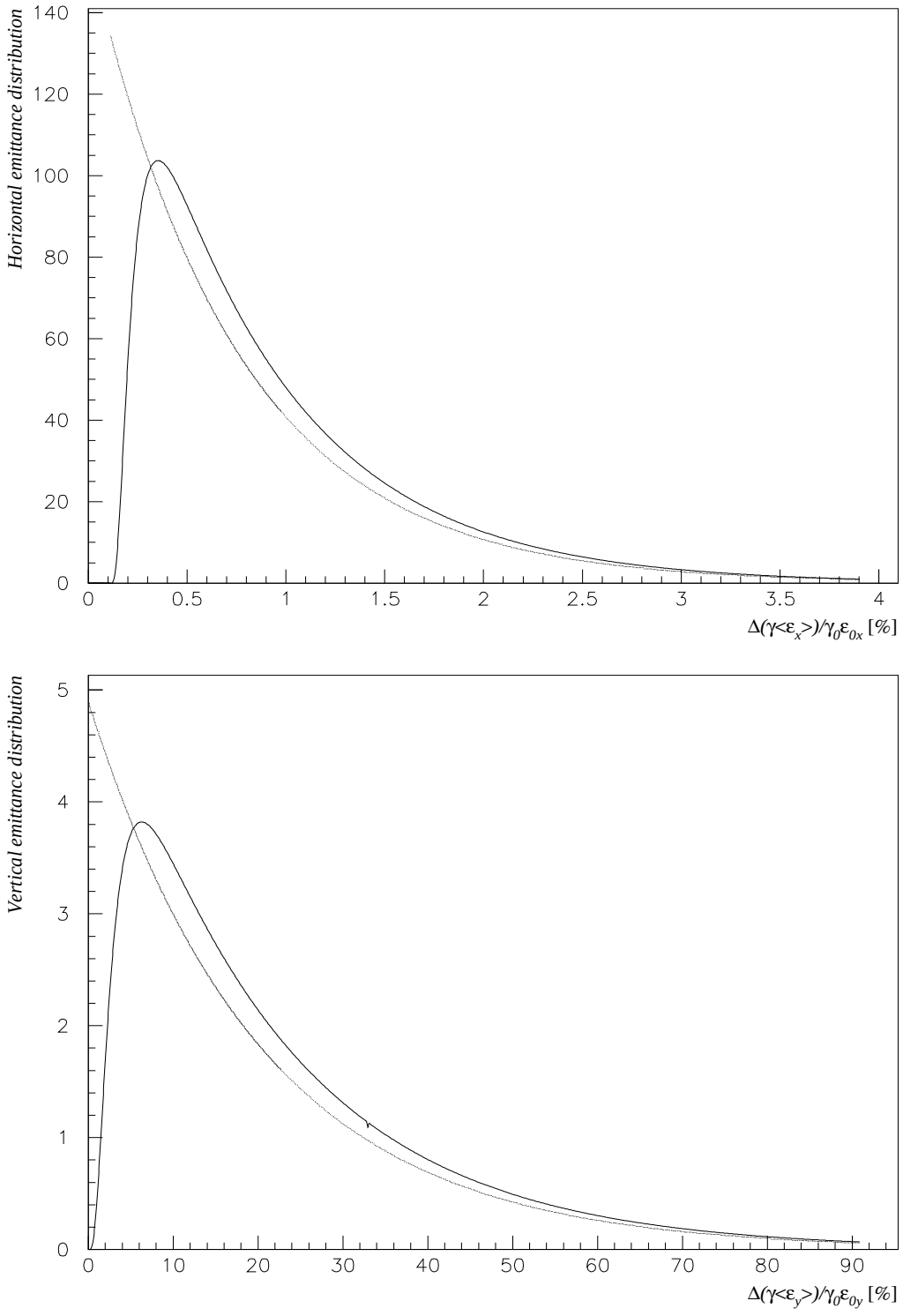

Figure 3.17: Emittance distribution at the end of the linac (example IV)

	Example I	Example II	Example III (no spread compensation)	Example III spread compensation	Example IV
Lattice (old/new)	old	old	old	old	new
RF and beam param. (old/new)	old	old	old	old	new
α_{RFQ} in each sector	.57/.52/.48 .45/.43/.41	.57/.52/.48 .45/.43/.41	no RFQs	no RFQs	no RFQs
ϕ_{RF} in each sector [°]	12/12/12 12/12/12	12/12/12 12/12/12	−50/ − 30/ − 22 −17/ − 14/ − 13	−50/ − 30/ − 22 −17 /55 /55	0/0/0/37
$< E_f >$ [GeV]	249.4	234.8	238.5	189.9	237.7
$\Delta E/E$ [%]	1.1	0.8	19.1	2.0	0.8
$\sigma_{\Delta E/E}$ [%]	0.22	0.28	5.0	0.32	0.19
$\langle \Delta (\gamma\epsilon_{x,y}) / (\gamma\epsilon_{x,y})_0 \rangle_{err}$ [%]	3/20	28/526	3/26	5/75	0.9/22

Table 3.5: Main results obtained in examples I-IV

Conclusion

Although the computation method presented in Chapter 1 has not yet been tested for the study of the "long–range correlation effects", I hope to have convinced the reader about its power and its efficiency. Now, for what concerns the CLIC main linac, considering the second example presented in Chapter 3, it would seem that the "RFQ option" should be left aside[11] and replaced, under good conditions (stronger focusing), by the "energy spread option".

Acknowledgements

I would like to thank all the members of the CLIC study group to have supported this work during the whole period of my military obligations. Especially, I address my thanks to C. Fischer and G. Guignard for numerous and very useful discussions which have permitted me to be rapidly introduced into the subject, and to J. P. Delahaye for pertinent comments concerning the scaling laws presented in this paper.

[11] Moreover, in multi–bunch operation, damped RF structures are required [29], and actually, the construction of damped microwave quadrupoles remains a serious problem.

Appendix A

About wakefields

A.1 Recall about wakefields

When a moving particle of charge q enters into a structure, it interacts with the wall of the structure and radiates electromagnetic field. We will restrict here our study to fully relativistic particles. We note $\vec{r}_0$ the transverse position of the particle according to the longitudinal $\hat{s}$ axis of the structure, and $(\vec{r}, z = ct - s)$ the transverse and longitudinal coordinates in the comoving frame of the driving particle. Now, contrary to a structure possessing a symmetry of translation (as free space), when the structure walls are resistive (case of the resistive–pipe) or present shape discontinuities (case of periodic structures as disk–loaded waveguides), the longitudinal electrical field, $E_L^\delta(\vec{r_0}; \vec{r}, s, t)$, and the transverse Laplace's force $\left[\vec{E}_T^\delta + \vec{v} \wedge \vec{B}^\delta\right](\vec{r_0}; \vec{r}, s, t)$ take non–zero values behind the driving particle. So, the longitudinal and transverse delta–function wake potential per unit length and unit charge, W_L^δ and $\vec{W}_T^\delta$ respectively, are defined in the following way [27]:

$$\begin{aligned} W_L^\delta(\vec{r}_0; \vec{r}, z) &= -\frac{1}{qL}\int_0^L E_L^\delta(\vec{r_0}; \vec{r}, s, t = (z+s)/c)\, ds \\ \vec{W}_T^\delta(\vec{r}_0; \vec{r}, z) &= \frac{1}{qL}\int_0^L \left[\, \vec{E}_T^\delta + c\,\hat{s} \wedge \vec{B}^\delta \,\right](\vec{r_0}; \vec{r}, s, t = (z+s)/c)\, ds \end{aligned} \tag{A.1}$$

The wakefields have two major well known effects:

- The first one, contained in the component W_L^δ is the energy loss of the driving particle itself and of all the particles following it: it is the beam-loading effect.

- The second one, contained in $\vec{W}_\perp^\delta$, is the transverse deflection of all the particles behind the driving particle, or beam–breakup instability.

For cylindrically symmetric structures, we have [27]:

$$\begin{aligned} W_L^{\delta}(\vec{r}_0;\vec{r},z) &= \sum_{m=0}^{\infty}\left(\frac{r_0}{a}\right)^m\left(\frac{r}{a}\right)^m\cos(m\theta)\,w'_m(z) \\ \vec{W}_T^{\delta}(\vec{r}_0;\vec{r},z) &= \sum_{m=1}^{\infty} m\left(\frac{r_0}{a}\right)^m\left(\frac{r}{a}\right)^{m-1}(\cos(m\theta)\vec{e_r}-\sin(m\theta)\vec{e_\theta})\;w_m(z)/a \end{aligned} \tag{A.2}$$

where a is the inner structure aperture. The modes $m = 0,\ 1,\ 2,\ \ldots$, are called respectively the monopole (or longitudinal), dipole (or transverse) and quadrupole modes. For particles close to the structure axis, only the monopole and dipole mode remains of great concern. Then, following Ref. [27], these two modes can be expressed in term of the structure normal modes:

$$\begin{aligned} W_L^{\delta}(\vec{r}_0;\vec{r},z) &\simeq w'_0(z) = \sum_n 2k_{0n}(a)\cos\frac{\omega_{0n}z}{c} \qquad z>0 \\ \vec{W}_T^{\delta}(\vec{r}_0;\vec{r},z) &\simeq \frac{\vec{r}_0}{a}w_1(z)/a = \frac{\vec{r}_0}{a}\sum_n\frac{2k_{1n}(a)}{\omega_{1n}a/c}\sin\frac{\omega_{1n}z}{c} \qquad z>0 \end{aligned}$$

where ω_{0n} and ω_{1n} are the eigenfrequencies of the empty structure, and where $k_{0n}(a)$ and $k_{1n}(a)$ are the loss factors calculated at $r = a$, for the monopole mode and for the dipole mode, respectively. These loss factors are given by:

$$k_n = \frac{\omega_n}{4}\left(\frac{R}{Q}\right)_n \;\propto\; \omega_n^2\ ^{1} \tag{A.3}$$

where $\left(R/Q\right)_n$ is the ratio of the shunt impedance by the quality factor of the mode ω_n. Lastly, due to the linearity of the Maxell's equations, the longitudinal (respectively the transverse) wake potential generated by a longitudinal distribution of particle $\rho(z)$ is just the convolution product of ρ by the longitudinal (respectively transverse) delta-function wake potential:

$$W_{L,T}(z) = \int_{-\infty}^{z}\rho(z^*)\,W_{L,T}^{\delta}(z-z^*) \tag{A.4}$$

A.2 Longitudinal and transverse wake potentials in CLIC accelerating structures

The most recent design of the CLIC main linac accelerating structures (CAS) can be found in Ref. [31]. They are disk–loaded type structures and a simplified geometry (with straight edges) has been used to compute the eigenfrequencies and loss factors associated to the monopole and dipole modes (see Ref. [32]). This geometry has required the following inputs:

[1] $\left(R/Q\right)_n$ is proportional to ω_n (see for instance Ref.[30]).

- a = 2.0 mm : Iris aperture radius
- b = 4.352 mm : Cavity inner radius
- g = 2.782 mm : Cavity gap width
- p = 3.332 mm : Cell length

The longitudinal and transverse wakes have been computed up to the mode number 204 and mode number 218, respectively [32] [2]; the fundamental frequency of the accelerating mode was found to be 29.985 GHz, whereas the fundamental frequency of the dipole mode is a little bit higher, equal to 37.90 GHz.
The short–range shapes of the functions $W_L^\delta(z)$ and $W_T^\delta(z)$ are shown in Fig. A.1, while, in Fig. A.2 are reported $W_L(z)$ and $W_T(z)$ computed for the longitudinal distribution used in example IV of Chapter 3 (i.e Gaussian distribution of $\sigma_z = 0.165$ mm, truncated at the head at 1.3 σ_z, and at 1.7 σ_z at the tail).

A.3 The resistive–pipe wake potentials

As said in the first section, wakefields are also generated in structure with resistive walls, even if these ones possess a translationly invariant geometry. It is the case for a metallic circular pipe with finite conductivity, well–known as one of the few analytically solvable wake–potential problems. The derivation of the solution is given in Ref. [34] and reported hereafter for what concerns the longitudinal and dipole delta–function wake potential:

$$\begin{aligned} W_L^\delta(z) &= \frac{2Z_0 c}{3\pi^2 a^2}\int_{-1}^{\infty} dx \frac{x\sin(\theta_0)+\cos(\theta_0)}{x^2+1} \\ W_T^\delta(z) &= \frac{2^{5/3} Z_0 c}{3\pi^2 a^3}\frac{z_0}{a}\int_{-1}^{\infty} dx \frac{\sin(\theta_1)-x\cos(\theta_1)}{(x^2+1)(x+1)^{2/3}} \\ \text{with} \quad & \theta_0 = \theta_1 = z/z_0\left[\sqrt{2}(x+1)\right]^{2/3} \end{aligned} \tag{A.5}$$

where $Z_0 = \sqrt{\dfrac{\epsilon_0}{\mu_0}} = 120\pi$ is the vacuum impedance, a, the inner radius of the pipe, and where $z_0 = \left(\dfrac{a^2}{Z_0\sigma}\right)^{1/3}$ is a characteristic distance in which σ represents the metal conductivity.
When $z \gg z_0$, we retrieve the asymptotic behaviour of the resistive–pipe wake potential

[2] In order to take into account the high frequency end of the longitudinal wake spectrum, the author of [32] made use of the optical resonator model (see Ref. [33]), not reported here.

(see Ref.[34]):

$$W_L^{\delta}(z) \overset{z \gg z_0}{\sim} -\frac{c}{4\pi a}\sqrt{\frac{Z_0}{\pi\sigma}}\, z^{-3/2} \simeq -1.710^{-5}\ \mathrm{V/pC/m}\ z^{-3/2}$$

$$W_T^{\delta}(z) \overset{z \gg z_0}{\sim} \frac{c}{\pi a^3}\sqrt{\frac{Z_0}{\pi\sigma}}\, z^{-1/2} \simeq 17.02\ \mathrm{V/pC/m^2}\ z^{-1/2}$$

for $a = 2$ mm (CLIC beam pipe radius) and $\sigma = 5.9\,10^7\ \Omega^{-1}\mathrm{m}^{-1}$ (copper conductivity at 300 K), so that $z_0 = 5.644\ \mu$m (see Fig. A.3).
Lastly, compared to Fig. A.2, Fig. A.4 illustrates the longitudinal and transverse wakefields generated in drifts by the truncated Gaussian distribution of particles described in the previous section; thus, we easily see that, for what concerns the CLIC main beam parameters, these wakefields become negligible according to the ones generating in the RF structures.

A.4 Scaling of the wake potentials with the bunch charge, the bunch length and the RF frequency

This last section will be entirely consecrated to the derivation of simple scaling laws concerning the qualitative behaviour of the longitudinal and transverse wakefields, with the RF frequency, the bunch length and the bunch charge.
More precisely, we consider a certain longitudinal charge distribution $\rho(z, \sigma_z)$ of constant charge N_b, and depending on a parameter σ_z (σ_z is typically the RMS value of the distribution), so that:

- Assumption I $\rho(z, \sigma_z) \overset{\sigma_z \to 0}{\longrightarrow} N_b\, \delta(z)$ where $\delta(z)$ is the Dirac's distribution.
- Assumption II $\sigma_z \rho(0, \sigma_z)$ goes to a non–zero constant $N_b \chi_\rho$, characteristic of the type of the distribution, when σ_z goes to zero. For instance, for a Gaussian distribution, we have $\rho(z, \sigma_z) = 1/(\sqrt{2\pi}\sigma_z)\exp(-z^2/2\sigma_z^2)$, leading to $\chi_\rho = 1/\sqrt{2\pi}$, and for a rectangular distribution, $\rho(z, \sigma_z) = 1/(2L)$ (between $-L$ and L with $L = \sigma_z/\sqrt{3}$), giving $\chi_\rho = \sqrt{3}/2$.

Then, we want to study the asymptotic behaviour, when σ_z goes to zero, of the two following quantities: $< \partial W_L/\partial z >_\rho$ and $< \partial W_T/\partial z >_\rho$, where $< \ldots >_\rho$ means average over the distribution ρ and where $W_{L,T}(z)$ are defined by Eq. (A.4). We have:

- $< \partial W_L/\partial z >_\rho = \dfrac{1}{N_b}\displaystyle\int_{-\infty}^{\infty} dz\, \rho(z, \sigma_z)\left(W_L^{\delta}(0)\rho(z, \sigma_z) + \int_{-\infty}^{z} dz^*\, W_L'^{\,\delta}(z - z^*)\rho(z^*, \sigma_z)\right)$

The second term of the integrand has a contribution which goes to zero when σ_z goes to zero (since the function $W_L'^{\,\delta}(z)$ has a sine–like behaviour around $z = 0$), whereas the first

one is equivalent to $W_L^\delta(0)\rho(0,\sigma_z) \sim N_b \chi_\rho W_L^\delta(0)/\sigma_z$ (using successively assumption I and assumption II).

- $$\begin{aligned} < \partial W_T/\partial z >_\rho &= \frac{1}{N_b}\int_{-\infty}^{\infty} dz\, \rho(z,\sigma_z)\left(\int_{-\infty}^{z} dz^*\, W_T'^{\,\delta}(z-z^*)\rho(z^*,\sigma_z)\right) \\ &\sim W_T'^{\,\delta}(0)\frac{1}{N_b}\int_{-\infty}^{\infty} dz\, \rho(z,\sigma_z)\left(\int_{-\infty}^{z} dz^*\, \rho(z^*,\sigma_z)\right) = \frac{N_b\, W_T'^{\,\delta}(0)}{2} \end{aligned}$$

Now, using Eq. (A.3) and considering only the fundamental modes of the longitudinal and transverse wakefields, we have:

$$\begin{aligned} < \partial W_L/\partial z >_\rho &\propto N_b\, \omega_{L,0}^2\, f_L(\omega_{L,0};\sigma_z) \quad \text{where} \quad f_L(\omega_{L,0};\sigma_z) \overset{\sigma_z \ll c/\omega_{L,0}}{\sim} 1/\sigma_z \\ < \partial W_T/\partial z >_\rho &\propto N_b\, \omega_{T,0}^2/a^2\, f_T(\omega_{T,0};\sigma_z) \quad \text{where} \quad f_T(\omega_{T,0};\sigma_z) \overset{\sigma_z \ll c/\omega_{T,0}}{\sim} 1 \end{aligned} \tag{A.6}$$

The asymptotic behaviour of f_L is very well verified, taking the truncated Gaussian distribution relative to the CLIC main beam, whereas f_T continues to vary with σ_z in the range of interest: for σ_z between 100 μm and 400 μm f_T is well approximated by $1/\sqrt{\sigma_z}$ (see Ref.[5]).

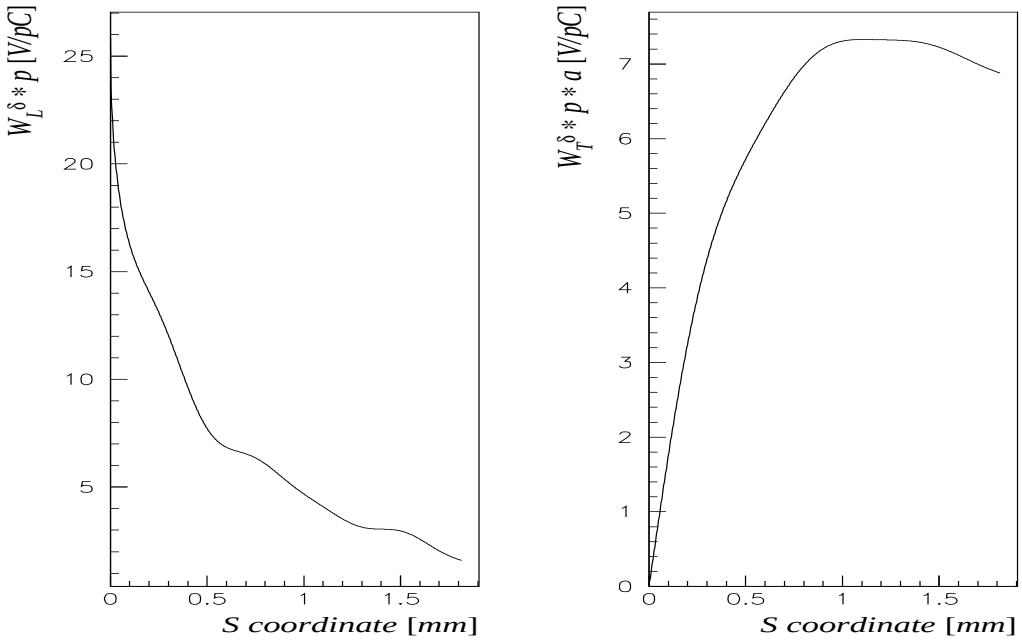

Figure A.1: Longitudinal and transverse delta–function wake potentials in CLIC accelerating structure

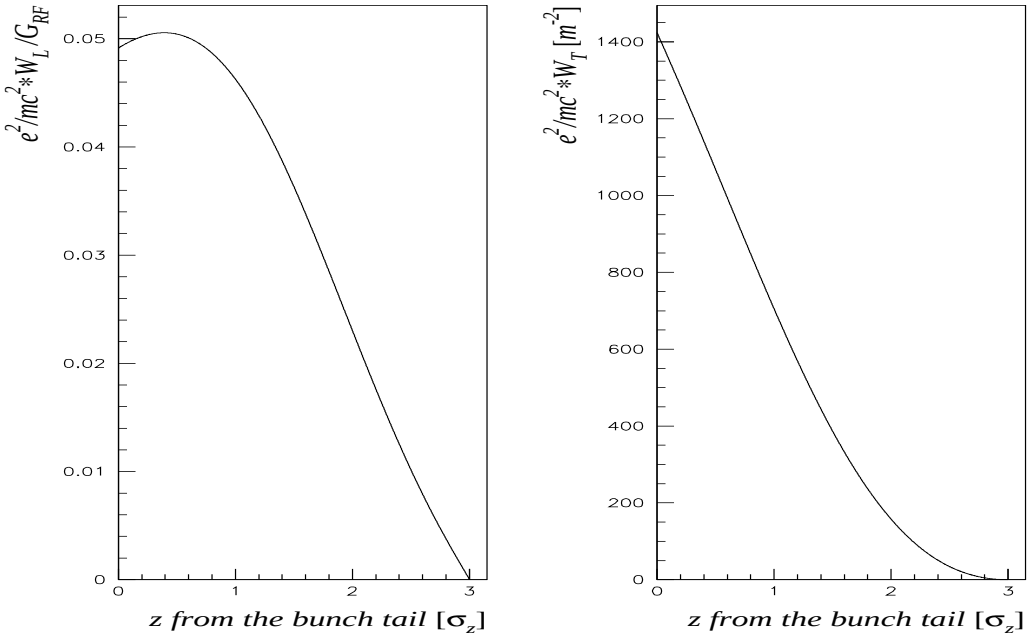

Figure A.2: Longitudinal and transverse wake potentials in CLIC accelerating structure

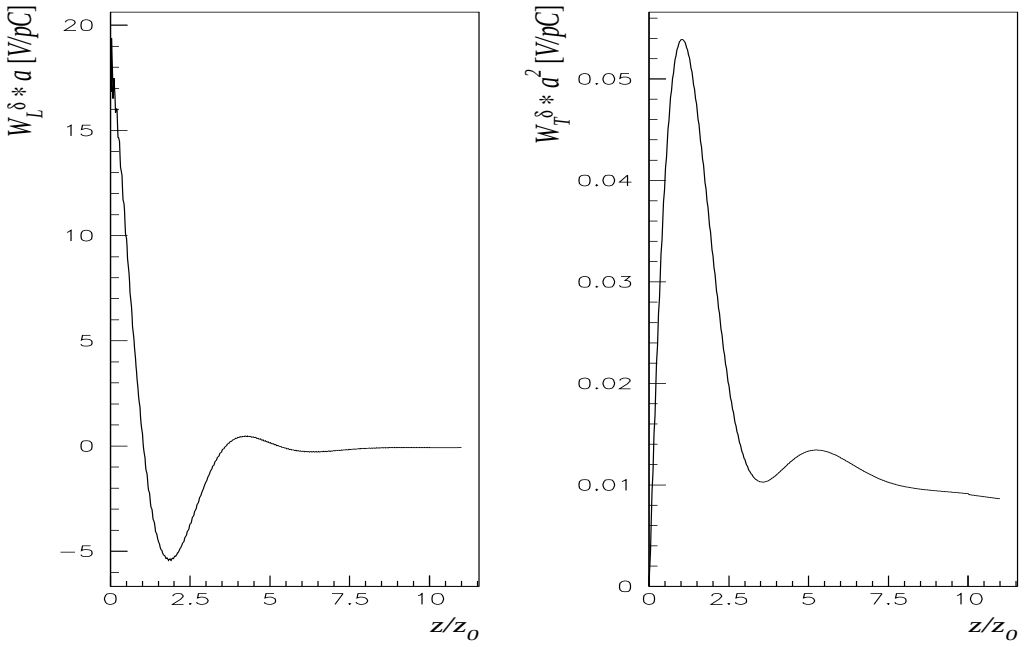

Figure A.3: Longitudinal and transverse delta–function wake potentials in CLIC beam pipe

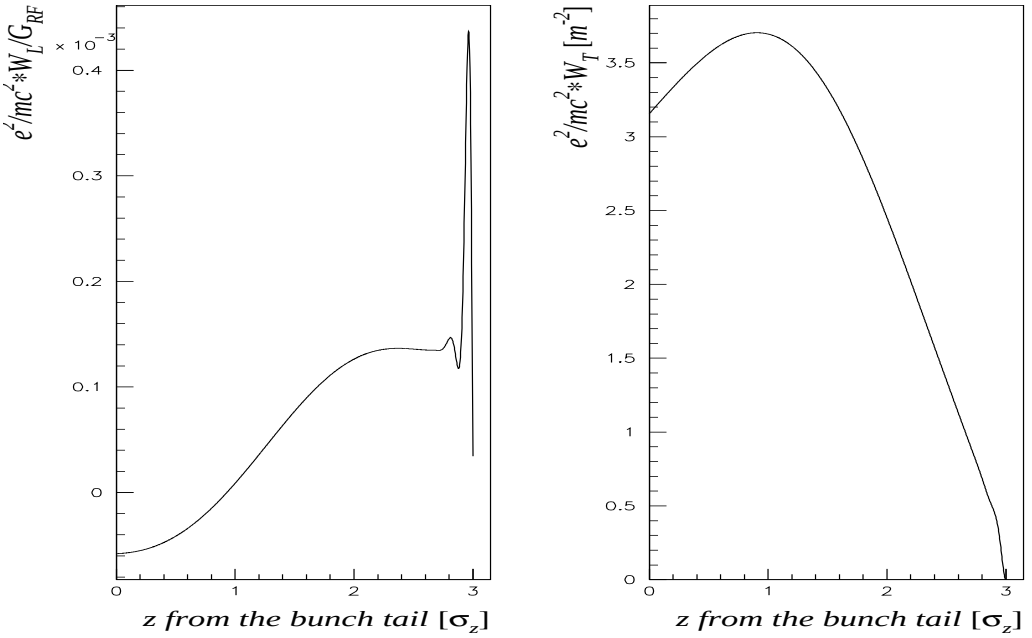

Figure A.4: Longitudinal and transverse wake potentials in CLIC beam pipe

Appendix B

2×2 R–matrix in three particular cases

We consider the Hill equation in the accelerated case [1]:

$$x''(s) + \gamma'(s)/\gamma(s)\, x'(s) + G(s)/\gamma(s)\, x(s) = 0 \tag{B.1}$$

Eq. (B.1) is a linear differential equation of the second order and then, all its solutions are contained in the knowledge of the following 2×2 matrix:

$$R = \begin{pmatrix} c_x & s_x \\ c'_x & s'_x \end{pmatrix}$$

where c_x and s_x are the two independent solutions of the differential equation (B.1) which verify:

$$\begin{cases} c_x(0) = 1 \\ c'_x(0) = 0 \end{cases} \qquad \begin{cases} s_x(0) = 0 \\ s'_x(0) = 1 \end{cases}$$

The R matrix in the two following cases are well known and are reported below without demonstration:

- case $\gamma' = 0 \Rightarrow \gamma(s) \equiv \gamma_0$, and $G(s) = Cst \Rightarrow G(s)/\gamma(s) \equiv K = Cst$:

$$R(L) = \begin{pmatrix} \cos\left(\sqrt{K}L\right) & \sin\left(\sqrt{K}L\right)/\sqrt{K} \\ -\sqrt{K}\,\sin\left(\sqrt{K}L\right) & \cos\left(\sqrt{K}L\right) \end{pmatrix} \text{ if } K > 0$$

$$R(L) = \begin{pmatrix} \cosh\left(\sqrt{-K}L\right) & \sinh\left(\sqrt{-K}L\right)/\sqrt{-K} \\ \sqrt{-K}\,\sinh\left(\sqrt{-K}L\right) & \cosh\left(\sqrt{-K}L\right) \end{pmatrix} \text{ if } K < 0$$

[1] Here the function $G(s)$ is the function $\dfrac{G(s)}{m_e c/e}$ of Paragraph 1.1.1

- case $\gamma'(s) \equiv \gamma'_0 = Cst \Rightarrow \gamma(s) = \gamma_0 + \gamma'_0\, s$, and $G(s) = 0$:

$$R(L) = \begin{pmatrix} 1 & \gamma_0/\gamma'_0\, \ln\!\big(\gamma(L)/\gamma_0\big) \\ 0 & \gamma_0/\gamma(L) \end{pmatrix} \text{ where } \gamma(L) = \gamma_0 + \gamma'_0 L\,.$$

The last case, we will study here, is the one which embraces the two cases mentioned above, i.e $\gamma'(s) = Cst$ and $G(s) = Cst$. The differential equation to solve is then:

$$x''(s) + \gamma'_0/(\gamma_0 + \gamma'_0 s)\, x'(s) + G/(\gamma_0 + \gamma'_0 s)\, x(s) = 0 \tag{B.2}$$

By the change of variable $u = 2/\,|\,\gamma'_0\,|\,\sqrt{\pm G/\,(\gamma_0 + \gamma'_0 s)}$, depending on the sign of G, the equation becomes:

$$\frac{d^2y}{du^2} + \frac{1}{u}\frac{dy}{du} \pm y = 0$$

A basis of solution for this equation is formed by the two Bessel functions of order 0, J_0 and Y_0 in the case $G > 0$, and by the two modified Bessel functions of order 0, I_0 and K_0 in the case $G < 0$. Finally, using some algebraic relations relative to the Bessel functions [35], we are able to derive the analytical form of the R matrix associated with the differential equation (B.2):

$$\text{if } G > 0,\ R(L) = \frac{\pi}{|\,\gamma'_0\,|} \begin{pmatrix} \sqrt{G\gamma_0}\left(J_1^{(0)}Y_0^{(1)} - Y_1^{(0)}J_0^{(1)}\right) & \gamma_0\left(J_0^{(0)}Y_0^{(1)} - Y_0^{(0)}J_0^{(1)}\right) \\ G\sqrt{\dfrac{\gamma_0}{\gamma(L)}}\left(Y_1^{(0)}J_1^{(1)} - J_1^{(0)}Y_1^{(1)}\right) & \gamma_0\sqrt{\dfrac{G}{\gamma(L)}}\left(Y_0^{(0)}J_1^{(1)} - J_0^{(0)}Y_1^{(1)}\right) \end{pmatrix}$$

$$\text{where } \begin{pmatrix} Y_i^{(0)} \\ J_i^{(0)} \end{pmatrix} \stackrel{\text{def}}{=} \begin{pmatrix} Y_i \\ J_i \end{pmatrix} \left(\frac{2\sqrt{G\gamma_0}}{|\,\gamma'_0\,|}\right) \text{ and } \begin{pmatrix} Y_i^{(1)} \\ J_i^{(1)} \end{pmatrix} \stackrel{\text{def}}{=} \begin{pmatrix} Y_i \\ J_i \end{pmatrix} \left(\frac{2\sqrt{G\gamma(L)}}{|\,\gamma'_0\,|}\right)\ i = 0, 1\,.$$

$$\text{if } G < 0,\ R(L) = \frac{2}{|\,\gamma'_0\,|} \begin{pmatrix} \sqrt{-G\gamma_0}\left(K_1^{(0)}I_0^{(1)} + I_1^{(0)}K_0^{(1)}\right) & \gamma_0\left(K_0^{(0)}I_0^{(1)} - I_0^{(0)}K_0^{(1)}\right) \\ -G\sqrt{\dfrac{\gamma_0}{\gamma(L)}}\left(K_1^{(0)}I_1^{(1)} - I_1^{(0)}K_1^{(1)}\right) & \gamma_0\sqrt{\dfrac{-G}{\gamma(L)}}\left(K_0^{(0)}I_1^{(1)} + I_0^{(0)}K_1^{(1)}\right) \end{pmatrix}$$

$$\text{where } \begin{pmatrix} K_i^{(0)} \\ I_i^{(0)} \end{pmatrix} \stackrel{\text{def}}{=} \begin{pmatrix} K_i \\ I_i \end{pmatrix} \left(\frac{2\sqrt{-G\gamma_0}}{|\,\gamma'_0\,|}\right) \text{ and } \begin{pmatrix} K_i^{(1)} \\ I_i^{(1)} \end{pmatrix} \stackrel{\text{def}}{=} \begin{pmatrix} K_i \\ I_i \end{pmatrix} \left(\frac{2\sqrt{-G\gamma(L)}}{|\,\gamma'_0\,|}\right)\ i = 0, 1\,.$$

Appendix C

Analytic computation of two integrals

We consider the two following integrals:

$$\mathcal{I}_1(\lambda;\epsilon) \stackrel{def}{=} \frac{1}{2\pi}\int_{-\infty}^{\infty} \frac{e^{ik\epsilon}\,dk}{\sqrt{1+i\lambda k}} \quad \mathcal{I}_2(\lambda;\mu;\epsilon) \stackrel{def}{=} \frac{1}{2\pi}\int_{-\infty}^{\infty} \frac{e^{ik\epsilon}\,dk}{\sqrt{(1+i\lambda k)(1+i\mu k)}}$$

where λ and μ are two strictly positive real numbers.
Citing Ref. [36], pp. 318, we have:

$$\int_{-\infty}^{\infty} (\beta - ix)^{-\nu} e^{-ipx}\,dx = \begin{cases} \dfrac{2\pi p^{\nu-1}e^{-\beta p}}{\Gamma(\nu)} & \text{for } p > 0 \\ 0 & \text{for } p < 0 \end{cases}$$
$$[\Re(\nu) > 0,\, \Re(\beta) > 0]$$

Using this formula for $\nu = 1/2$, and knowing that $\Gamma(1/2) = \sqrt{\pi}$, the computation of $\mathcal{I}_1$ becomes quite simple:

$$\mathcal{I}_1(\lambda;\epsilon) = \begin{cases} \dfrac{e^{-\epsilon/\lambda}}{\sqrt{\pi\lambda\epsilon}} & \lambda > 0,\, \epsilon > 0 \\ 0 & \lambda > 0,\, \epsilon < 0 \end{cases}$$

The computation of $\mathcal{I}_2$ is more difficult. Citing Ref. [36] pp. 320 and pp. 1059, we have successively:

$$\int_{-\infty}^{\infty} (\beta - ix)^{-\mu}(\gamma - ix)^{-\nu} e^{-ipx}\,dx = \begin{cases} \dfrac{2\pi\, e^{-\beta p}\, p^{\mu+\nu-1}}{\Gamma(\mu+\nu)}\; {}_1F_1(\mu;\, \mu+\nu;\, (\beta-\gamma)p) & \text{for } p > 0 \\ 0 & \text{for } p < 0 \end{cases}$$
$$[\Re(\beta) > 0,\, \Re(\gamma) > 0,\, \Re(\mu+1) > \Re(\nu)]$$

where ${}_1F_1$ is the degenerate hypergeometric function, also noted Φ, and,

$${}_1F_1(\alpha;\, 2\alpha;\, 2z) \stackrel{def}{=} \Phi(\alpha;\, 2\alpha;\, 2z) = 2^{\alpha-\frac{1}{2}} \exp\left[\frac{1}{4}(1-2\alpha)\pi i\right] \Gamma\left(\alpha+\frac{1}{2}\right)\, e^z\, z^{\frac{1}{2}-\alpha} J_{\alpha-\frac{1}{2}}(iz)\,.$$

Using these two last formulae for $\mu = \nu = \alpha = 1/2$, knowing that $\Gamma(1) = 1$ and $J_0(iz) = I_0(z)$ for $(-\pi < \arg z \leq \pi/2)$ (Ref. [35] pp.375), we obtain:

$$\mathcal{I}_2(\lambda;\mu;\epsilon) = \begin{cases} \dfrac{1}{\sqrt{\lambda\mu}} \exp\left[-\epsilon(\dfrac{1}{2\lambda} + \dfrac{1}{2\mu})\right] \; I_0\left[\epsilon(\dfrac{1}{2\lambda} - \dfrac{1}{2\mu})\right] & \lambda > 0,\ \mu > 0,\ \epsilon > 0 \\ 0 & \lambda > 0,\ \mu > 0,\ \epsilon < 0 \end{cases}$$

Appendix D

Direct estimation of the total number of quadrupoles within the line

We note, N_q, the total number of quadrupoles within the line, $\gamma_{in}mc^2$ and $\gamma_{out}mc^2$, the initial and final bunch energy, and $G_{RF} = mc^2/e\,\gamma'_{RF}$, the accelerating field in the structures. If we neglect the physical length of the quadrupole, we have:

$$\sum_{n=1}^{N_q} L_{FODO_n} = \frac{\gamma_{out} - \gamma_{in}}{\gamma'_{RF}} \tag{D.1}$$

where L_{FODO_n} is the distance between the quadrupoles n and $n+1$. We are then looking for an expression for N_q, in the regime, $\gamma_{out} \gg \gamma_{in}$.
We assume a scaling of L_{FODO_n} with the energy, i.e $L_{FODO_n} = L_0(\gamma_n/\gamma_{in})^{\alpha_L}$, where,

$$\gamma_n = \gamma_{in} + \gamma'_{RF} \sum_{m=1}^{n-1} L_{FODO_m} \tag{D.2}$$

is the energy at the location of the quadrupole n.
We note s_n the location of the quadrupole $n+1$. Using Eq. (D.2), s_n verifies the recursion relation:

$$s_n = s_{n-1} + L_{FODO_n} = s_{n-1} + L_0 \left(1 + \frac{\gamma'_{RF}}{\gamma_{in}} s_{n-1}\right)^{\alpha_L} \tag{D.3}$$

Then, we consider the new sequence (u_n), defined by:

$$u_n = \left(\frac{\gamma_{in}}{\gamma'_{RF} L_0}\right)^{\frac{1}{1-\alpha_L}} \left(1 + \frac{\gamma'_{RF}}{\gamma_{in}} s_n\right) \tag{D.4}$$

Using Eq. (D.3), we see that the sequence (u_n) verifies the recursion relation,

$$u_n = u_{n-1} + u_{n-1}^{\alpha_L}, \text{ so that:}$$

$$u_n^{1-\alpha_L} - u_{n-1}^{1-\alpha_L} = u_{n-1}^{1-\alpha_L} \left(\left(1 + u_{n-1}^{\alpha_L - 1}\right)^{1-\alpha_L} - 1\right) \overset{n\to\infty}{\sim} 1 - \alpha_L \tag{D.5}$$

Now, we recall the Cesaro's theorem, which states that, if $(u_n)_{n\in\mathbf{N}}$ is any sequence converging to a limit l, then the sequence $\left(\frac{1}{n}\sum_{m=1}^{n} u_m\right)_{n\in\mathbf{N}}$ converges also to l. Consequently, using Eq. (D.5), we have:

$$\frac{1}{N}\left(u_N^{1-\alpha_L} - u_1^{1-\alpha_L}\right) = \frac{1}{N}\sum_{n=1}^{N-1} u_{n+1}^{1-\alpha_L} - u_n^{1-\alpha_L} \overset{N\to\infty}{\longrightarrow} 1-\alpha_L \text{ and then,}$$

$$\begin{aligned} N_q \overset{\gamma_{out}\gg\gamma_{in}}{\sim} \frac{u_{N_q}^{1-\alpha_L}}{1-\alpha_L} &= \frac{\gamma_{in}}{\gamma'_{RF}L_0\left(1-\alpha_L\right)}\left(1+\frac{\gamma'_{RF}}{\gamma_{in}}s_{N_q}\right)^{1-\alpha_L} \\ &= \frac{\gamma_{in}}{\gamma'_{RF}L_0\left(1-\alpha_L\right)}\left(1+\frac{\gamma_{out}-\gamma_{in}}{\gamma_{in}}\right)^{1-\alpha_L} \end{aligned} \tag{D.6}$$

Appendix E

Matching sections in the new CLIC main linac

Sector	$\delta = -1\%$	$\delta = 0$	$\delta = 1\%$
1	0.669283838	0.662591000	0.656030693
2	0.358857576	0.355269000	0.351751485
3	0.167885859	0.166207000	0.164561386
4	0.116709091	0.115542000	0.114398020

Table E.1: Quadrupole strengths [m^{-2}], at different δ, in the four sectors of the new linac

As said in Paragraph 3.2.2, the matching of two consecutive sectors is achieved by acting on the strengths of five quadrupoles: the last three quads and the first two ones of each sector [4]. Tab. E.1 recalls the nominal values of the quadrupole strengths in the four sectors of the new linac, and Tab. E.2 gives the five quadrupole strengths at each transition between sectors. So, Fig. E.1, E.2 and E.3 illustrate successively the evolution of the β functions at each of the three transitions, while Fig. E.4 plots the values of β_x and β_y (relative to the reference slice, $z = 0$) at the middle of each quadrupole of the line[1].
Now, when the correction algorithms DF, WF, DW or WW (see Paragraph 1.2.1) are considered, we have just to apply a scaling factor $1 \pm \delta$ to the nominal strength of the quadrupoles (see Tab. E.1), without forgetting that this is not true any more for what concerns the matching quadrupoles, since the matching conditions are not linear (see Tab. E.3, E.4, E.5 and E.6, for the values of the matching quadrupole strengths in the four momentum configurations, $\delta = -1\%$, $\delta = +1\%$, $\delta = \mp 1\%$ and $\delta = \pm 1\%$).

[1] The slight fluctuations that we observed in Fig. E.4 can be explained by a imperfect matching between sectors, but also and mainly, by the RF structures which breaks the periodicity of the focusing lattice within each sector (term γ'/γ in the equation of motion). But, as we see it , this effect is small at high energy.

Transition	k_1	k_2	k_3	k_4	k_5
1-2	0.582423697	0.517833758	0.481115412	0.416685494	0.364951308
2-3	0.339622597	0.356832516	0.334151078	0.168259297	0.166800850
3-4	0.154858645	0.142003633	0.142952394	0.131806160	0.118986461

Table E.2: Quadrupole strengths [m^{-2}] at the transition for $\delta = 0$

Transition	k_1	k_2	k_3	k_4	k_5
1-2	0.588517327	0.522996720	0.485293236	0.418981962	0.368469035
2-3	0.342985410	0.360964671	0.337249800	0.170128763	0.168543177
3-4	0.156624532	0.143595428	0.144439302	0.132829667	0.120161122

Table E.3: Quadrupole strengths [m^{-2}] at the transition for $\delta = -1\%$

Transition	k_1	k_2	k_3	k_4	k_5
1-2	0.576365548	0.512705890	0.476982444	0.414395687	0.361495285
2-3	0.336323449	0.352840101	0.331128292	0.166455403	0.165102724
3-4	0.153122187	0.140435028	0.141501220	0.130801699	0.117834948

Table E.4: Quadrupole strengths [m^{-2}] at the transition for $\delta = +1\%$

Transition	k_1	k_2	k_3	k_4	k_5
1-2	0.578477698	0.522353784	0.477703405	0.417568921	0.361148688
2-3	0.337239460	0.362523321	0.332757848	0.170759373	0.165406502
3-4	0.153578265	0.143417228	0.141616237	0.132436201	0.117772310

Table E.5: Quadrupole strengths [m^{-2}] at the transition for $\delta = \mp 1\%$

Transition	k_1	k_2	k_3	k_4	k_5
1-2	0.586181019	0.513110971	0.484258824	0.415737139	0.368797734
2-3	0.342079883	0.351478927	0.335711888	0.165952281	0.168282011
3-4	0.156123248	0.140555266	0.144255872	0.131176023	0.120217660

Table E.6: Quadrupole strengths [m^{-2}] at the transition for $\delta = \pm 1\%$

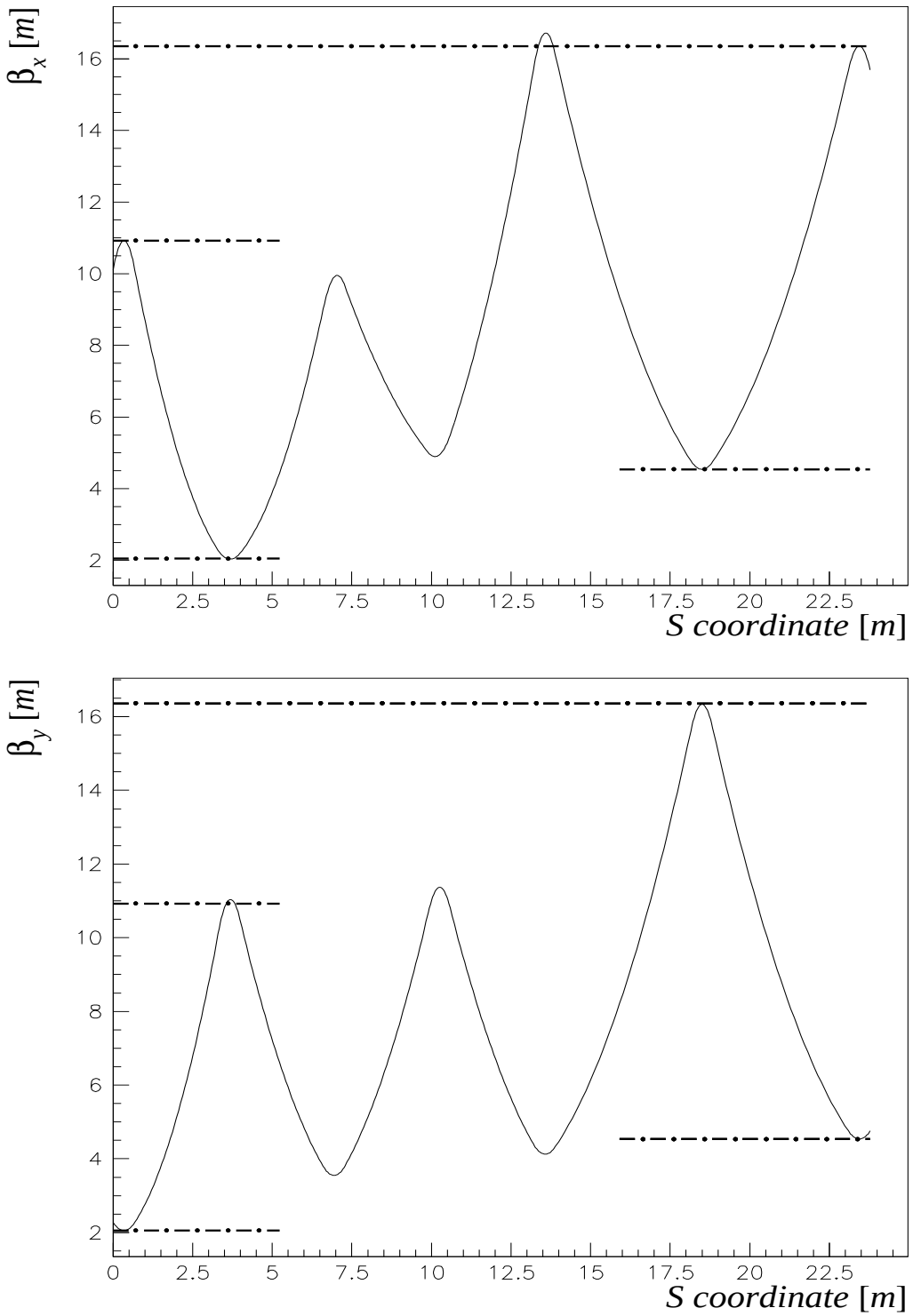

Figure E.1: β functions in both transverse planes at the transition between sector I and sector II

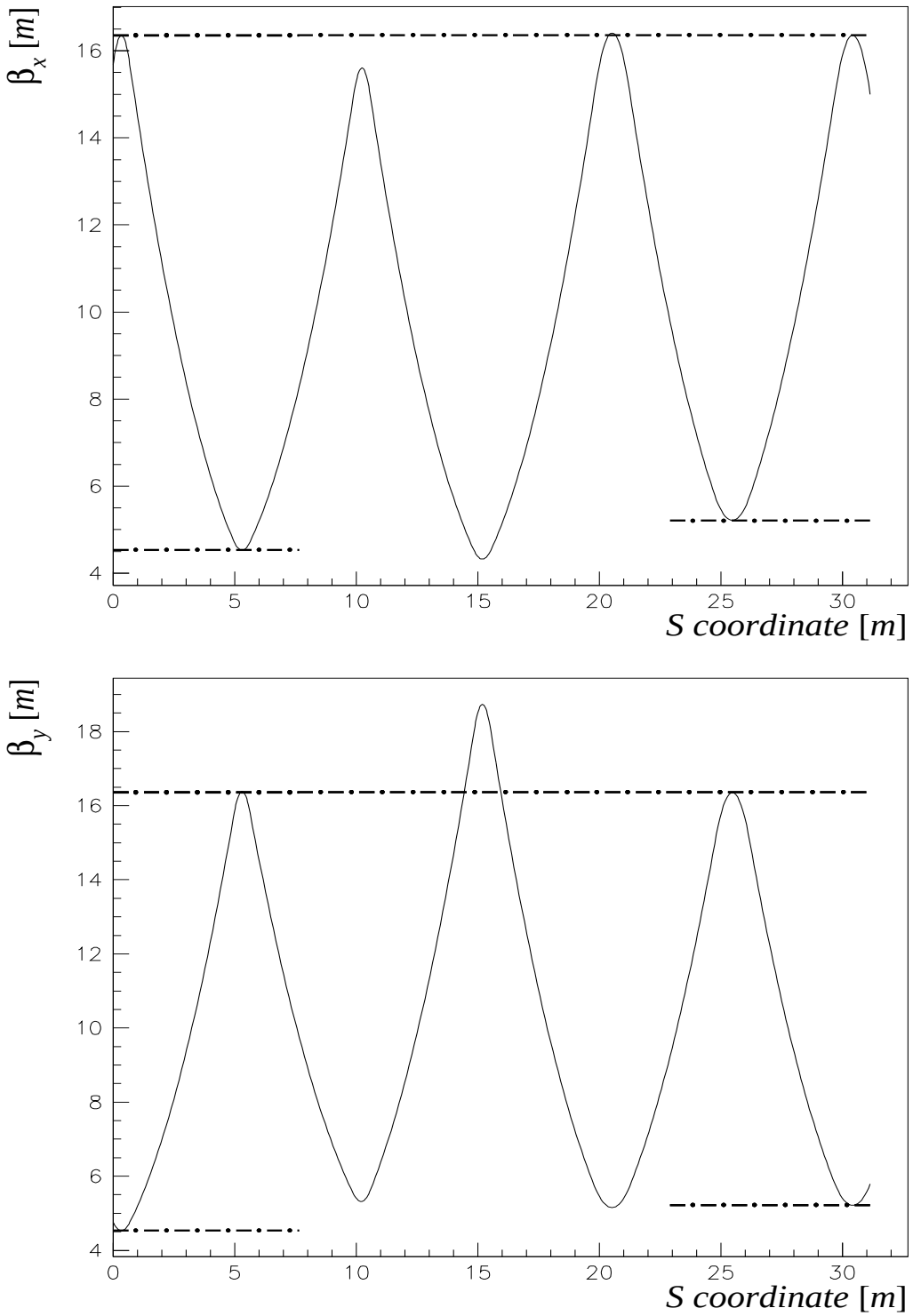

Figure E.2: β functions in both transverse planes at the transition between sector II and sector III

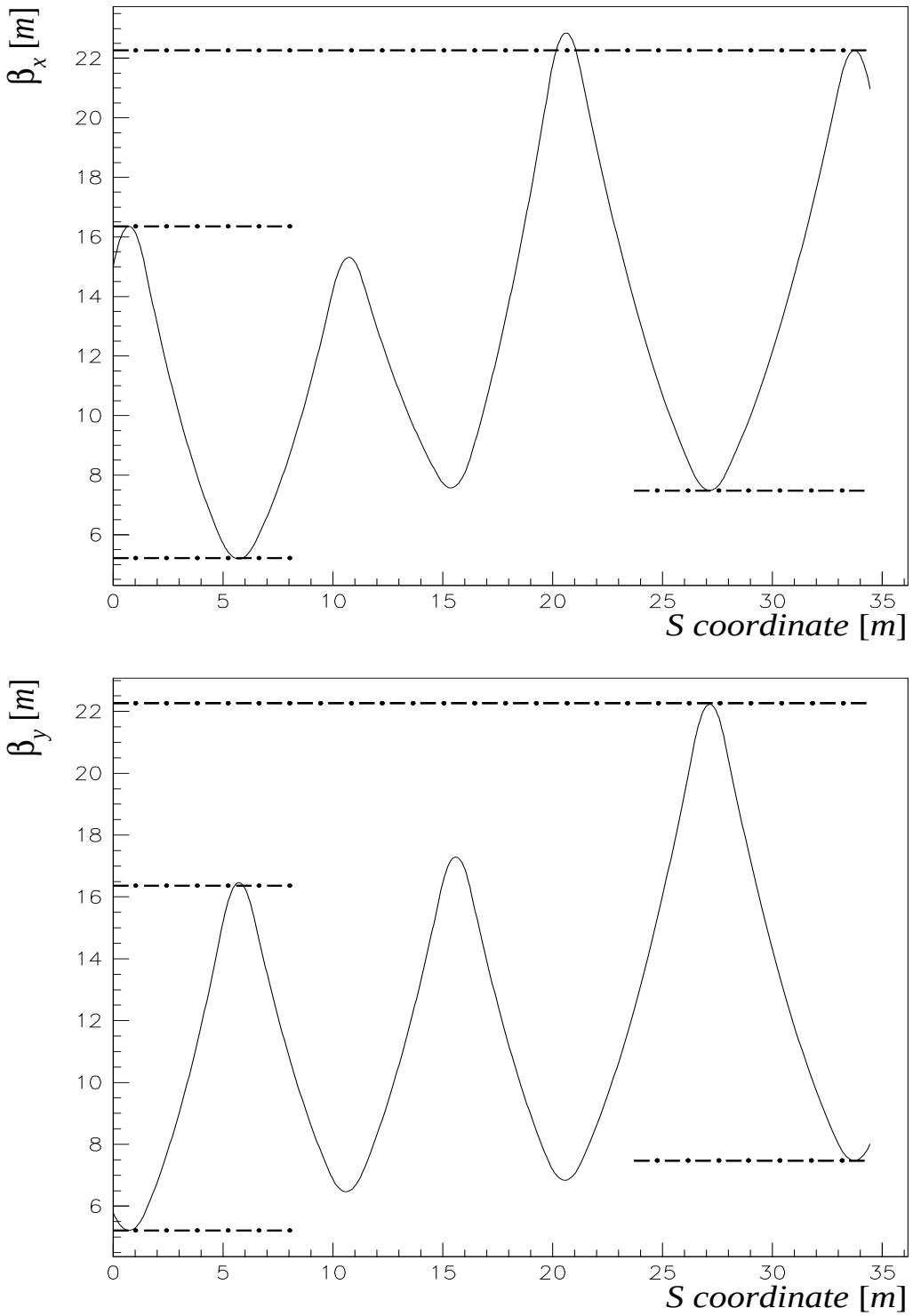

Figure E.3: β functions in both transverse planes at the transition between sector III and sector IV

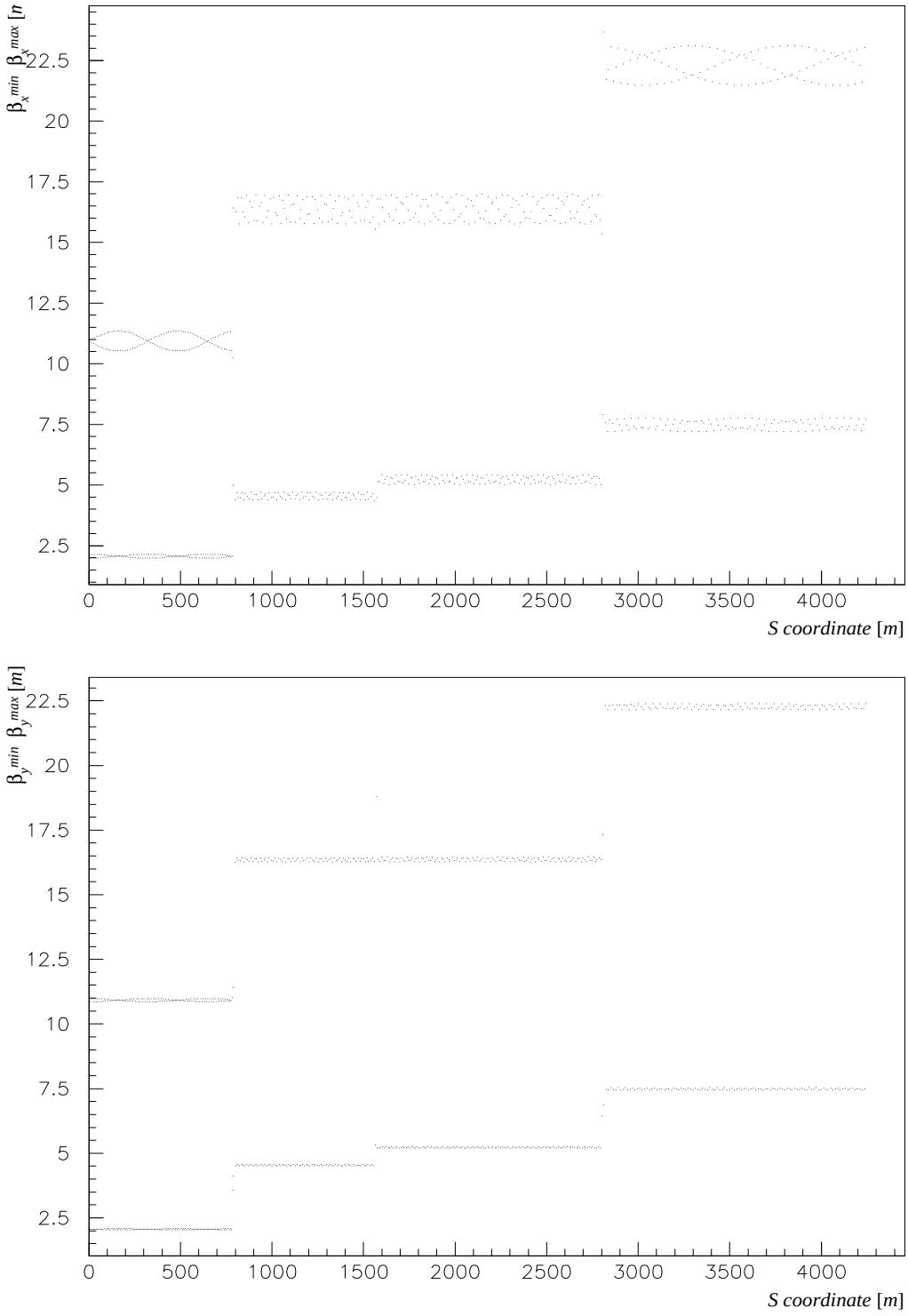

Figure E.4: β functions in both transverse planes at the middle of each quadrupoles all along the linac

Bibliography

[1] International Linear Collider Technical Review Committee Report. SLAC–R–95–471. 1995.

[2] G. Guignard. Stability studies for the CLIC main linac. Report CERN/SL 91-19 (AP), also available in XV Int. Conf. on H. E. Acc., Hamburg, 1992.

[3] G. Parisi. CALICO User's Guide (version 1.0). CLIC Note 302.

[4] G. Parisi. Arrangement in sectors of CLIC main linac focusing. CLIC Note 221.

[5] G. Guignard. Beam Dynamics Issues and the CLIC Target Parameters. CLIC Note 320.

[6] S. Fartoukh. A Statistical Method To Analyse Wakefield Effects in Linacs With Application To The CTF2 Drive Beam. CLIC Note 321, also available in Report CERN/PS 96-42(LP).

[7] W. Schnell and I. Wilson. Microwave quadrupole structures for the CERN Linear Collider. CLIC Note 143 also available in Proc. PAC 91.

[8] A. Chao, B. Richter, C.–Y. Yao, Nucl. Inst. and Meth. 178 (1980) pp. 1.

[9] D. Chernin, A. Mondelli, Part. Accel. 24 (1989) pp.177.

[10] T. Raubenheimer. SLAC Report 387 (1991).

[11] K. Kubo and T.O Raubenheimer. Proc. 17th Int. Linac Conf., Tsukuba, Japan, 1994.

[12] C. Fischer. Improved CLIC performances using the beam response for correcting alignment errors. CLIC Note 281 & CERN/SL 95–19(BI).

[13] V. Balakin, A. Novokhatsky, V. Smirnov, Proc. 12th Int. Conf. on High Energy Accelerators, Fermilab, 1983.

[14] H. Henke and W. Schnell. An analytical criterion for the onset of transverse damping due to wakefields in a linear accelerator. CERN–LEP–RF/86–18 & CLIC Note 22.

[15] Own simulations & MTRACK simulations: G. Guignard, private communication (1996).

[16] G. A. Loew and J. W. Wang. Minimizing the energy spread within a single bunch by shaping its charge distribution. PAC 85 pp. 3228–3230.

[17] G. Guignard. Small and Large Emittances in the CLIC Main Linac. CLIC Note 235 also available in Proc. EPAC 94.

[18] J. P. Delahaye. Design Issues of TeV Linear Colliders. CLIC Note 308 & CERN/PS 96–30 (LP), also available in Proc. EPAC 96.

[19] G. Guignard and E. T. d'Amico. Preliminary Design of a Bunch Compressor for CLIC. CLIC Note 236 & CERN/SL 96–30 (AP), also available in Proc. EPAC 94.

[20] G. E. Fisher. Iron dominated magnets. SLAC PUB 3726 (1985).

[21] G. Guignard. Lattice Scaling and Emittance Control in the CLIC main Linac. CLIC Note 193 and CERN/SL 93–20 (DI).

[22] W. Coosemans, H. Mainaud. Métrologie linéaire: Ecartométrie biaxiale et fil tendu. CLIC Note 316.

[23] W. Coosemans, H. Mainaud. To be published. 1997.

[24] J. P. H. Sladen, I. Wilson, W. Wuensch. CLIC Beam Position Monitor Tests. CLIC Note 305, also available in Proc. EPAC 96.

[25] H. Mainaud. Private communication. 1996. The correction resolution is related to the step of the micro-movers supporting the quadrupoles, $\sim 0.2\,\mu$m, and to mechanical constraints.

[26] Confirmation by C. Fischer using the code MTRACK9. Private communication. 1996.

[27] K. Bane, T. Weiland and P. Wilson. AIP Conf. Proc. 127 (AIP. New York 1985), pp. 875–928.

[28] G. Guignard. Stability Studies for the CLIC Main Linac Beam. CLIC Note 140 & CERN SL/91-19 (AP).

[29] G. Guignard and J. Hagel. Multibunch BNS Damping and Wakefield Attenuation in High Frequency Linacs. CLIC Note 312 & CERN/SL 96–60 (AP).

[30] P. Wilson. AIP Conf. Proc. 87 (AIP, New York 1982), pp. 450 563. Also available as SLAC–PUB–2884 (1982).

[31] I. Wilson, W. Wuensch. CLIC Note 120.

[32] A. Millich. Computation of wakefields for the CLIC disk–loaded waveguide (DLWG). CLIC Note 137 & CERN SL/91-27(CO).

[33] D. Brandt , B. Zotter. Calculation of the wakefield with the optical resonator model. CERN-ISR/TH/82-13 & LEP Note 388 (1982).

[34] O. Henry, O. Napoly. The resistive–pipe wake potentials for short bunches. CLIC Note 142.

[35] M. Abramowitz and I. Stegun, Handbook of mathematical functions, Dover publications, INC., New York, 1970.

[36] I.S. Gradshteyn and I.M. Ryznhik. Table of integrals, series and products. Corrected and enlarged edition (1980).